Dissertation

Extracellular Matrix Components in Idiopathic Pulmonary Arterial Hypertension: a Non-coding Perspective

Submitted by
Helene Thekkekara Puthenparampil, MSc.

for the Academic Degree of
Doctor of Philosophy (PhD)

at the

Medical University of Graz

Ludwig Boltzmann Institute for Lung Vascular Research

under the Supervision of

Assoc. Prof. Grazyna KWAPISZEWSKA

2022

Statutory Declaration

I hereby declare that this thesis is my own original work and that I have fully acknowledged by name all individuals and organizations that have contributed to the research for this thesis. Due acknowledgement has been made in the text to all other material used. Written permission was obtained to reproduce or reprint figures published elsewhere and submitted together with this thesis. Throughout this thesis and in all related publications I followed the “Standards of Good Scientific Practice and Ombuds Committee at the Medical University of Graz“.

Date: 06.04.2022

Name: Helene Thekkekara Puthenparampil

Disclosures

Most data presented in this dissertation have been previously published in the following peer-reviewed original research articles or public presentations:

Research Articles:

The Journal of pathology, 2019, *247*(3), 357–370. https://doi.org/10.1002/path.5195

Long non-coding RNAs influence the transcriptome in pulmonary arterial hypertension: the role of PAXIP1-AS1.

Katharina Jandl *[,1], Helene Thekkekara Puthenparampil*[,1], Leigh M Marsh[1], Julia Hoffmann[1], Jochen Wilhelm[2], Christine Veith[3], Katharina Sinn[4], Walter Klepetko[4], Horst Olschewski[1,5], Andrea Olschewski[1,6], Matthias Brock[7] and Grazyna Kwapiszewska[1,6]

*contributed equally

[1] Ludwig Boltzmann Institute for Lung Vascular Research, Graz Austria

[2] Department of Internal Medicine, Justus-Liebig-University Giessen, Universities of Giessen and Marburg Lung Center, German Center for Lung Research, Giessen Germany

[3] Excellence Cluster Cardio-Pulmonary System, Justus-Liebig-University Giessen, Universities of Giessen and Marburg Lung Center, German Center for Lung Lung Research, Giessen Germany

[4] Division of Thoracic Surgery, Department of Surgery, Medical University of Vienna, Vienna Austria

[5] Division of Pulmonology, Department of Internal Medicine, Medical University of Graz, Graz Austria

[6] Otto Loewi Research Center, Chair of Physiology, Medical University of Graz, Graz Austria

[7] Division of Pulmonology, University Hospital Zürich, University of Zürich, Zürich Switzerland

American journal of respiratory cell and molecular biology, 2020, *63*(1), 104–117. https://doi.org/10.1165/rcmb.2019-0303OC

Basement Membrane Remodeling Controls Endothelial Function in Idiopathic Pulmonary Arterial Hypertension

Katharina Jandl[1,2], Leigh M Marsh[1], Julia Hoffmann[1], Ayse Ceren Mutgan[3], Oliver Baum[4], Wilhelm Bloch[5], Helene Thekkekara-Puthenparampil[1], Dagmar Kolb[6], Katharina Sinn[1,7], Walter Klepetko[7], Akos Heinemann[2], Andrea Olschewski[1,8], Horst Olschewski[1,9], Grazyna Kwapiszewska[1,3]

[1] Ludwig Boltzmann Institute for Lung Vascular Research, Graz, Austria.

[2] Division of Pharmacology, Otto Loewi Research Center, Medical University of Graz, Graz Austria

[3] Division of Physiology, Otto Loewi Research Center, Medical University of Graz, Graz Austria

[4] Institute of Physiology, Charité-Universitätsmedizin Berlin, Berlin, Germany.

[5] German Sports University Cologne, Cologne, Germany.

[6] Gottfried Schatz Research Center, Medical University of Graz, Graz, Austria.

[7] Division of Thoracic Surgery, Department of Surgery, Medical University of Vienna, Vienna, Austria.

[8] Experimental Anaesthesiology, Department of Anaesthesiology and Intensive Care Medicine, Medical University of Graz, Graz, Austria.

[9] Division of Pulmonology, Department of Internal Medicine, Medical University of Graz, Graz, Austria.

Presentations:

Transcriptomic Profiling Reveals Pivotal Involvement of lncRNAs in the Pathogenesis of IPAH: the Role of PAXIP1-AS1 – Helene Thekkekara Puthenparampil, Katharina Jandl, Jochen Wilhelm, Julia Hoffmann, Leigh M. Marsh, Walter Klepetko, Andrea Olschewski, Matthias Brock, Grazyna Kwapiszewska
(FEBS 2018 International Meeting; Extracellular Matrix: Cell Regulation, Epigenetics and Modeling; 27 September – 2 October, 2018 I Patras, Greece) (poster and oral presentation)

Differentially expressed lncRNAs in IPAH: the impact of PAXIP1-AS1 on human PASMC function – Helene Thekkekara Puthenparampil, Katharina Jandl, Jochen Wilhelm, Julia Hoffmann, Leigh M. Marsh, Walter Klepetko, Andrea Olschewski, Matthias Brock, Grazyna Kwapiszewska
(Annual Meeting 2017 of the ÖGP, „Österreichische Gesellschaft für Pneumologie“, 06.10.2017, Innsbruck, Austria) (poster and oral presentation)

Foreword

I want to express my gratitude to my supervisors Assoc. Prof. Dr. Grazyna Kwapiszewska-Marsh and Dr. Katharina Jandl, and members of my thesis committee Univ.-Prof. Dr.med.univ. Akos Heinemann and Univ.-Prof. Dr.med. Andrea Olschewski for their continuous support, encouragement and scientific inputs.

A special thanks belongs to Grazyna and Kathi for always encouraging me to achieve more and believing in me. I want to thank the whole group of LBI, who immediately accepted me as part of the group and was always helpful and supportive as a collective in numerous occasions throughout the PhD. A special thank also goes to all the technical experts in the group who never hesitated to help with their expertise, regardless of time pressure.

I would also like to thank Assoz. Prof. Priv.-Doz. Dr.rer.nat. Andelko Hrzenjak, Priv.-Doz. Dr. Leigh Marsh, Dr. Valentina Biasin and Dr. Bence M. Nagy for their scientific advises and moral support. I owe a big thank you to my dear PhD-mates Dr. Neha Sharma, Dr. Davor Skofic-Maurer, Dr. Anna Birnhuber and Ceren Mutgan. I want to thank all colleagues and collaborators from diverse institutes for their invaluable contributions to this study.

I am extremely grateful to my family for their endless love, care and prayers, and for reminding me there is more to life than work. A big thank you goes to my husband Gillsu George Thekkekara Puthenparampil, who has supported me throughout each step of the process and was always there for me, no matter what.

Finally, I want to thank God for all His endless blessings and for giving me the opportunity to grow.

Acknowledgements

This work was conducted at the Ludwig Boltzmann Institute for Lung Vascular Research and the Center for Medical Research (ZMF I and II) of the Medical University of Graz. The Ph.D. study was supported by the Austria Research Promotion Agency (FFG; grant number 858308) and the Medical University of Graz, Graz, Austria through the Ph.D. Program DK-MOLIN.

The micro array gene expression analysis was performed in collaboration with Dr. Jochen Wilhelm at the Justus-Liebig-Universität Gießen and Dr. Matthias Brock, University of Zürich. The isolation of the pulmonary arteries via laser capture-microdissection was performed by Dr. Julia Hoffmann, Ludwig Boltzmann Institute for Lung Vascular Research, Graz. The proteomic analysis was performed in collaboration with Assoc.Prof. Ruth Birner-Gruenberger from the Diagnostic and Research Institute of Pathology, Medical University of Graz.

I would like to thank Eva Grasmann and Alexandra Treitler for their excellent technical assistance.

Table of Content

Abbreviations and Definitions

μm	Micrometer
6MWD	6-min walk distance
AAV	Adeno-associated virus
Abb	Abbreviation
AE	Acute exacerbation
ALI	Acute lung injury
ANOVA	Analysis of variance
ARDS	Acute respiratory distress syndrome
AU	Arbitrary unit
bGH	Bovine growth hormone
BM	Basement membrane
BMPR2	Bone morphogenetic protein receptor type II
cAMP	Cyclic adenosine monophosphate
cDNA	complementary DNA
CF	Cystic fibrosis
cGMP	Cyclic guanosine monophosphate
CIAP	Calf intestinal alkaline phosphatase
circRNA	circular RNAs
CMV	Cytomegalovirus
CO_2	Carbon dioxide
COPD	Chronic obstructive pulmonary disease
Ctrl	Control
DIC	Differential interference contrast
DMSO	Dimethyl sulfoxide
ECM	Extracellular matrix
EDTA	Ethylenediaminetetraacetic acid
EdU	5-ethynyl-2′-deoxyuridine
EGFP	Enhanced green fluorescent protein
ELISA	Enzyme-linked immunosorbent assay
endo-siRNA	endogenous small interfering RNAs
ES	Endostatin
ET-1	Endothelin-1

FACS	Fluorescence activated cell sorting
FBS	Fetal bovine serum
FGF	Fibroblast growth factor
GAPDH	Glyceraldehyde-3-Phosphate Dehydrogenase
GO	Gene ontology
GSEA	Gene set enrichment analysis
HIS-tag	Polyhistidin-Tag
HR	Heart rate
HRP	Horseradish peroxidase
IL-1β	Interleukin 1 beta
IPAH	Idiopathic pulmonary arterial hypertension
IPF	Idiopathic pulmonary fibrosis
KEGG	Kyoto encyclopedia of genes and genomes
LB	Lysogeny broth
LC	Liquid chromatography
LFC	Log_2(fold change)
lncRNA	Long non-coding RNAs
M	Molar mass
MAPK	Mitogen-activated protein kinase
Min	Minute
miRNA	microRNAs
ml	milliliter
MMP	Matrix metalloproteinase
moRNA	microRNA-offset-RNAs
mPAP	Mean pulmonary arterial pressure
mRNA	Messenger RNA
MS	Mass spectrometry
NaCL	Sodium chloride
ncRNA	Non-coding RNAs
NF-κB	Nuclear factor 'kappa-light-chain-enhancer' of activated B-cells
NO	Nitric oxide
OE	Overexpression
ORA	Over representation analysis
ORF	Open redeaing frame
P	Probability

PA	Pulmonary artery
PAAdFB	Pulmonary artery adventitial fibroblast
PAEC	Pulmonary Artery Endothelial Cell
PASMC	Pulmonary Artery Smooth Muscle Cell
PAXIP1-AS1	PAX-interacting protein 1 Antisense 1
PBS	Phosphate buffered saline
PDE-5	Phosphodiesterase type 5
PDGF	Platelet derived growth factor
pFB	Parenchymal fibroblasts
pg	picograms
PGP	proline, glycine and proline
PH	Pulmonary hypertension
pH	potential of hydrogen
piRNA	piwi-interacting RNAs
qRT-PCR	Quantitative real-time polymerase chain reaction
rRNA	ribosomal RNAs
scaRNA	small Cajal body RNAs
Scr	Scrambled (control)
sdRNA	sno-derived RNAs
SDS	Sodium dodecyl sulfate
sGC	Soluble guanylate cyclase
siRNA	small interfering RNAs
snoRNA	small nucleolar RNAs
TBS-T	Tris-buffered saline with Tween20
TGF-β	Transforming growth factor β
TIMP	Tissue inhibitors of metalloproteinase
tiRNA	transcription initiation RNAs
Tris-HCL	Tris hydrochloride
tRNA	transfer RNAs
t-SNE	t-distributed stochastic neighbor embedding
TSP	Thrombospondin
VEGF	Vascular endothelial growth factor
VIP	Vasoactive intestinal peptide
vtRNA	vault RNAs
WB	Western blotting

Abstract (German)

Ein Kernaspekt der pathologischen Entwicklung von idiopathischer pulmonal-arterieller Hypertonie (IPAH) ist die charakteristische Gefäßveränderung oder „Vascular Remodelling“ der distalen Pulmonalarterien, die zu einer erhöhten Ablagerungsrate von extrazellulären Matrixproteinen (EZM) führt. Dies ermöglicht eine permissive Umgebung, die die Zellproliferation, Zellmigration und die Resistenz gegen Apoptose begünstigt und dadurch stark zur Gefäßsteifigkeit bei IPAH beiträgt. Die Rolle von langen nichtkodierenden RNAs („long non-coding RNAs“, lncRNAs) in diesem Zusammenhang in IPAH ist wenig erforscht. Durch Transkriptionsanalysen an kleinen, mittels Lasermikrodissektion gewonnenen Pulmonalarterien konnten wir das Genexpressionsprofil in IPAH charakterisieren, das sowohl durch kodierende als auch durch nicht-kodierende Gene geprägt ist. Unsere Ergebnisse zeigten gestörte metabolische, zytoskelettale, apoptotische und proliferative Signalwege in IPAH. Die EZM identifizierten wir als die zentrale zelluläre Komponente, die von IPAH betroffen ist, und folglich beschrieben wir die Expression von EZM-Komponenten in IPAH. Wir berichteten über die Bedeutung von lncRNAs bei IPAH und zeigten die Hochregulierung der lncRNAs TUSC8 und PAXIP1-AS1 in IPAH. Im Detail gingen wir auf die funktionelle Beteiligung von PAXIP1-AS1 und intrinsische molekulare Mechanismen in glatten Muskelzellen der Pulmonalarterien ein. Wir berichteten über die deutlich reduzierte Proliferation und Migration und über das erhöhte pro-apoptotische Verhalten bei PASMC nach PAXIP1-AS1-Knockdown. Die Transkriptomanalyse zeigte, dass die Basalmembran die am stärksten betroffene Zellkomponente ist nach dem PAXIP1-AS1-Knockdown, und führte zu der Enthüllung des Regulationsmechanismus dieses lncRNAs über die fokale Adhäsionsmaschinerie, wobei PAXIP1-AS1 über das nachgeschaltete Signalmolekül Paxillin agiert. Wir zeigten die Hochregulierung des Basalmembrankollagens COL18A1 bei IPAH und bestätigen die antiproliferativen Wirkungen seines proteolytischen Produkts Endostatin. Schließlich fanden wir in unserem experimentellen Aufbau erste Hinweise darauf, dass die Überexpression von PAXIP1-AS1 keinen Einfluss auf die Freisetzung von Endostatin in pulmonale Endothelzellen hat. Zusammengefasst konnten wir eine starke Verflechtung der lncRNAs mit der EZM zeigen im Rahmen von IPAH und enthüllten PAXIP1-AS1 als einen potenten Regulator der Zellfunktion der glatten Muskulatur, der über sein nachgeschaltetes Effektorprotein Paxillin wirkt.

Abstract (English)

Extracellular matrix (ECM) remodelling of the distal pulmonary arteries occurs early in idiopathic pulmonary arterial hypertension (IPAH) and is a core aspect of its pathologic development. The resulting increased ECM turnover provides a permissive environment that favours cell proliferation, migration and resistance to apoptosis, and thereby strongly contributes to the vascular stiffness in IPAH. The rather newly identified players in IPAH are the long non-coding RNAs (lncRNAs). Central biologic importance has been attributed to the lncRNAs recently, while less is known about them in the context of ECM remodelling in IPAH. By applying transcriptomic analysis on laser-capture microdissected small pulmonary arteries, we characterized the differential gene expression profile in IPAH that is shaped by coding as well non-coding genes. Our findings identifed metabolic, cytoskeletal, apoptotic and proliferative processes as key signalling pathways perturbed in IPAH, and identifed the ECM as the core cellular component that is affected in the disease. Focusing further on the ECM, we described the expression of ECM related components in IPAH. Demonstrating the significance of lncRNAs in IPAH, we validated the upregulation of the lncRNAs TUSC8 and PAXIP1-AS1 in IPAH and detailed the functional involvement of PAXIP1-AS1 and intrinsic molecular mechanisms in pulmonary artery smooth muscle cells (PASMC) by applying a siRNA-mediated knockdown approach. We reported the markedly reduced proliferative and migrative behaviour, and elevated pro-apoptotic events in PASMC after PAXIP1-AS1 knockdown. Transcriptomic analysis identified the basement membrane as the most affected cellular component after PAXIP1-AS1 knockdown and revealed a regulatory mechanism of the lncRNA via the focal adhesion machinery where PAXIP1-AS1 acts via its downstream target paxillin. Our results showed the upregulation of the prominent basement membrane collagen COL18A1 in IPAH and confirmed the anti-proliferative effects of its proteolytic product endostatin. Finally, we found first indications that suggest PAXIP1-AS1 overexpression does not influence endostatin release in pulmonary artery endothelial cells in our experimental setup. Taken together, we were able to identify an entanglement of the lncRNAs with the ECM in the setting of IPAH and revealed PAXIP1-AS1 as a potent regulator of smooth-muscle cell function acting via its downstream effector protein paxillin.

1. Introduction

1.1 Idiopathic Pulmonary Arterial Hypertension

Pulmonary Arterial Hypertension (PAH) is a form of Pulmonary Hypertension (PH), which is a condition where the pressure of the pulmonary circulation is abnormally high (resting mean pulmonary arterial pressure of >20 mmHg). In contrast to other, more common forms of PH associated with left heart or lung disease, PAH is a more severe form that is marked by a vasculopathy of the pulmonary arterial circulation (1). Substantially, PAH is a disease of the small pulmonary arteries characterized by vascular remodelling and an increase in vascular stiffness and resistance, which ultimately results in right ventricular hypertrophy and right heart failure (1-3). It is an incurable, rare condition with an estimated prevalence of 15 per million, and occurs more than twice as often in women than in men (1). With the currently available therapy options, PAH patients still face poor prognosis with an estimated 3-year survival rate just above 50% (54.9% in incident cases, and 58.2% if incident and prevalent cases combined) (4).

PAH can be subdivided into the several subtypes, including idiopathic PAH, familial PAH, or as PAH associated with other diseases or as PAH resulting from drug or toxin exposure (1, 4) Table 1.

Table 1. **Classification of PAH (5, 6)**

1.1	Idiopathic PAH
1.2	Heritable PAH
1.3	Drug and toxin induced PAH
1.4	PAH associated with:
	Connective tissue disease
	HIV infection
	Congenital heart disease
	Portal hypertension
	Schistosomiasis
1.5	PAH long-term responders to CCBs
1.6	PAH with overt features of PVOD/PCH
1.7	Persistent PH of the newborn

Idiopathic PAH (IPAH) is a form of PAH that is diagnosed when no cause or known risk factor can be identified (2) and accounts for ~52.6% if all PAH cases (7).

1.1 Pathophysiology and Genetics of PAH

Several risk factors and sources of vascular injury, such as environmental factors, genetic predisposition or dysfunctional immune response can contribute to the pathologic development of this disease (8). Central features of the multifaceted pathobiology of PAH include endothelial dysfunction, increased smooth muscle cell proliferation, migration, resistance to apoptosis and deposition of extracellular matrix (9, 10). This vasculopathy mainly affects the distal pulmonary arteries and is hallmarked by vascular remodelling (1, 11).

The pulmonary vessel wall has a three-layered structure (Figure 1). The innermost layer of the pulmonary artery is called tunica intima. Its main cellular component is the single layered vascular endothelium. The medial layer of the vessel wall, the tunica media, mainly consists of concentric layers of smooth muscle cells. The main cellular component of the outermost layer, tunica adventitia, are adventitial fibroblasts.

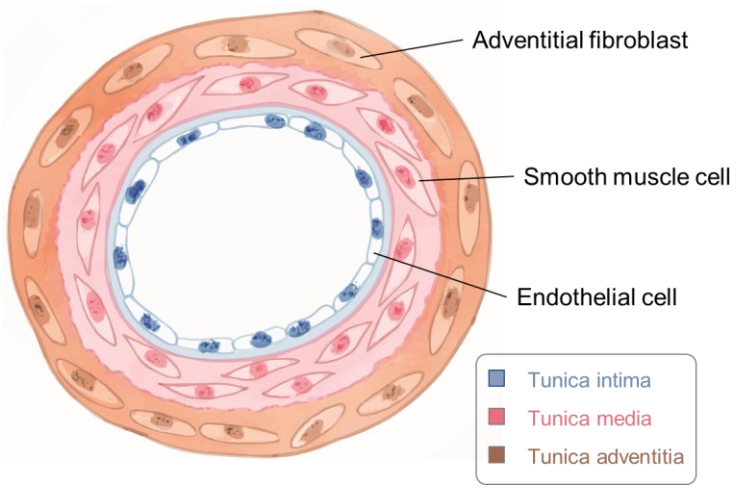

Figure 1. **Structure of the pulmonary artery.** The basic, three-layered structure of the pulmonary artery, that consists of the tunica intima, tunica media and tunica adventitia.

The process of vascular remodelling leading to luminal narrowing happens in all three layers of the pulmonary artery while affecting the intimal and medial layers the most, and the adventitia to a comparatively smaller extent (12). Remodelling of the adventitial layer is marked by the enhanced proliferative and migrative capacities of the adventitial fibroblasts as well as the elevated synthesis of matrix proteins (11). Hypertrophy and hyperplasia of vascular smooth muscle cells and an increased production of connective tissue and elastic fibers are characteristics of the medial thickening process (13). Furthermore, an occlusive neointima arises from migrating and reorienting vascular smooth muscle cells that undergo clonal

expansion and accumulate beneath the endothelial layer (14). Endothelial dysfunction leading to the acquisition of a pro-proliferative, apoptosis-resistant (15), and pro-inflammatory (16) endothelial phenotype is thought to be one of the first triggers of PAH development. An abnormal, disorganized endothelial proliferation and an increased matrix production characterizes the intimal thickening. In severe cases, this can lead to the formation of plexiform lesions (13, 17, 18). Here, anti-apoptotic endothelial cells, originating from the remodelled pulmonary arteries, proliferate to form complex capillary-like vascular structures that sometimes connect with the bronchial circulation or build spherical structures at the abrupt ends of distal pulmonary arteries (19).

Dysfunctional inflammatory responses (16, 17), thrombotic lesions (20) and platelet dysfunction (21) are further characteristics of this vasculopathy. Endothelial dysfunction also causes an imbalance in several endothelial cell specific factors (e.g. growth factors, pro-thrombotic factors, vasoactive factors) resulting in an altered cell signalling (22). The chronically impaired production of vasodilators such as nitric oxide (NO), vasoactive intestinal peptide (VIP) and prostacyclin, and an overexpression of vasoconstrictors such as endothelin (ET-1) (8, 11) not only affects the vascular tone, but promotes the remodelling (Figure 2).

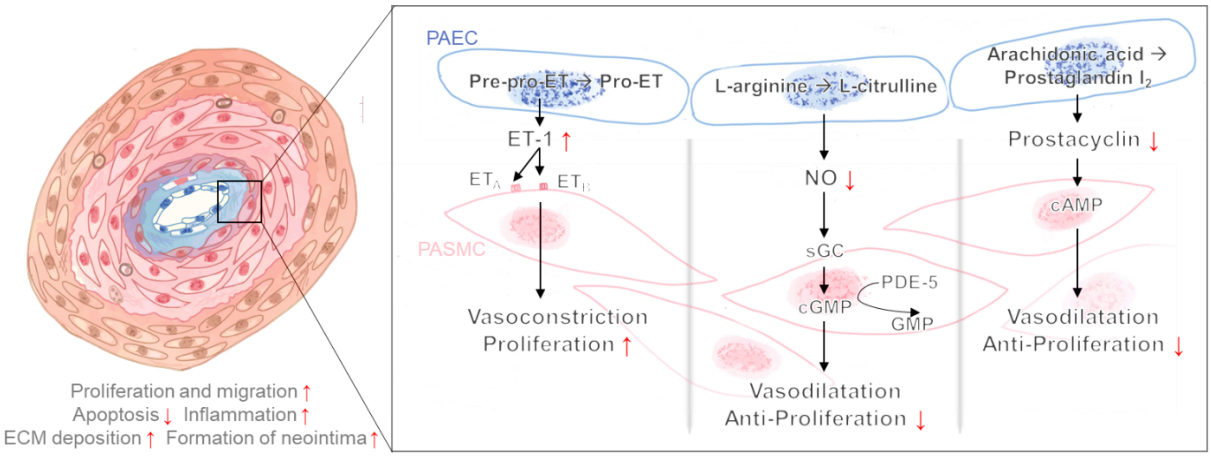

Figure 2. **Endothelial dysfunction caused imbalance of vasoactive factors in IPAH.** Dysfunctional pulmonary artery endothelial cells (PAEC) produce more vasoconstrictive endothelin-1 (ET-1) and less vasodilative nitric oxide (NO) and prostacyclin, promoting vasoconstriction and pulmonary artery smooth muscle cell (PASMC) proliferation in IPAH. ET_A/ET_B, Endothelin receptor A/B; sGC, soluble guanylate cyclase; cGMP, cyclic guanosine monophosphate; PDE-5, Phosphodiesterase type 5; cAMP, cyclic adenosine monophosphate. Information adapted from (11).

The currently available therapy for PAH aims exactly at these three signalling pathways targeting vascular tone and consequently the remodelling process in PAH: Prostacyclin analogues and prostacyclin receptor agonists are applied to work against the decreased prostacyclin levels in PAH patients. Prostacyclin is an effective vasodilator that works via cyclic adenosine monophosphate (cAMP), and additionally inhibits PASMC proliferation and decreases platelet aggregation (23). Endothelin receptor antagonists are applied to block the vasoconstriction caused by the increased ET-1 production in PAH. To counteract the impaired vasodilation caused by the decreased NO availability in PAH patients soluble guanylate cyclase (sGC) simulators or activators are used (1). NO increases vasodilation by activating sGC to synthesize cGMP. Another approach aims at increasing sGC levels by inhibiting the conversion of cGMP to GMP mediated by phosphodiesterase type 5 (11).

Recent technologic advancement has opened new possibilities to explore the underlying pathophysiologic processes driving the disease and have led to an increasing molecular understanding of PAH development (24). Several signalling pathways, in particular pathways involving several different growth factors (e.g. TGF-β, PDGF-BB, FGF, VEGF) are recognized to be affected in the complex pathobiology of PAH, by perturbating central cellular functions such as proliferation, migration, differentiation, extracellular matrix secretion and deposition (11, 25, 26). An increased release of the platelet-derived growth factor PDGF-AA and PDGF-BB has been reported in the pulmonary artery endothelial cells of PAH patients, and an elevation of its receptors (mainly PDGFRα) in pulmonary artery smooth muscle cells of PAH patients (27-29). An increased TGF-β receptor activity as well as higher TGF-β1 levels has been shown in plasma and pulmonary artery smooth muscle cells of PAH patients (29, 30),

Prominent signalling pathways further altered in PAH include mitogen-activated protein kinase (MAPK), Wnt signalling, oestrogen signalling, hedgehog signalling, YAP-TAZ and Notch signalling (25, 31-33), as well as apoptotic pathways and hypoxia triggered signalling (34, 35). From the genetic aspect, mutations in the BMPR2 gene were the first identified. Today, it is well recognized that 70–80% of familial PAH and 10–20% of IPAH cases are caused by mutations in the BMPR2 gene (13). BMPR2 gene encodes for a cell surface receptor for bone morphogenetic protein (BMP) ligands, that are members of the TGF-β superfamily. BMPR2 exerts an anti-proliferative effect on PASMC and promotes PAEC survival (36, 37).

1.2 Extracellular matrix in PAH

The extracellular matrix (ECM) of the pulmonary artery is a complex meshwork of finely orchestrated matrix molecules that contribute to structural and functional integrity of the vasculature. The complex micro-environment of the ECM influences the cell-cell and cell-ECM crosstalk and thereby regulate cell migration, proliferation and differentiation, cellular processes that are highly affected in the pathogenesis of PAH (38).

The tunica intima, the innermost layer of the pulmonary artery that mainly consists of vascular endothelial cells has a specialized ECM: the basement membrane (BM). Main components of the BM include laminins, type IV collagens and proteogylcans. Main ECM components of the tunica media, the medial layer of the vessel wall, are elastin fibers, fibrillar collagens (type I, II, V), elastins, fibronectins, laminins and proteoglycans. Main adventitial ECM components include collagens types I and II (38). Structural and mechanical changes in the ECM have an immense influence on the vascular remodelling process in PAH. The disbalance in ECM metabolism manifests early in PAH development (39), even before any changes in the pulmonary arterial pressure or vascular resistance can be observed. Several processes are involved in this ECM remodelling process that leads to vascular stiffness that is associated with increased mortality in PAH patients (40-43).

All three layers of the pulmonary arteries are affected by the ECM remodelling causing the stiffening and reduced compliance. Here, most increase in deposition and cross-linkage is observed in the neo-intima, that is followed by the media (12, 44, 45), and then the adventitia with a weaker involvement (12). Next to this increased collagen expression (e.g. COL14A1, COL4A5, COL18A1) in PAH patients (12), an increased breakdown of elastin (46, 47) as well as accumulation of tenascin and fibronectin (48) have been observed. The increase in osteopontin expression (49) and elevated calcification also contribute to the progression of ECM remodelling (50, 51). Endothelial injury, alterations in the structure and function of pulmonary artery endothelial cells, is widely appreciated as the initiating event for this ECM remodelling (50). Endothelial cells not only regulate the vascular tone and the proliferative function of the pulmonary artery smooth muscle cells, but also contribute greatly to the integrity and stability of the vascular wall by building a tightly controlled barrier (52). An injury leading to increased permeability of the vessel wall allows factors to enter the vessel that can stimulate protease production and activation. Endothelial injury disturbs the proteolytic balance of the ECM that demands a tight interplay between several matrix metalloproteinases (MMPs), metalloproteases, serine elastases, lysyl oxidases (LOX) and tissue inhibitors of

metalloproteinases (TIMPs) (38, 50). Exemplarily, a decreased expression of MMP10 and TIMP-1 in IPAH has been shown in all three layers of the PA, while MMP19 expression is elevated in the intimal and medial layers, and TIMP3 was shown to be decreased in the adventitia (12). Furthermore, it was shown that cytokines, such as TNFα that is known to drive PAH by suppressing BMPR-II (53), enhances the production of MMPs in endothelial cells (54, 55). Consequently, ECM turnover is increased, growth factors and bioactive proteolytic fragments are released that further drive the proliferative vasculopathy, ECM deposition, and further release of ECM proteases (12, 50, 56).

Structural changes in the ECM can trigger mechanosensitive signalling, where the altered mechanical cues are transduced to the cell interior. This ECM-Cell interaction is mediated by transmembrane proteins with mechano-sensing capacities (mainly integrins) (57) and the assembly of focal adhesions. Focal adhesions are dynamic protein complexes built through interactions of the intracellular integrin tails with adaptor proteins such as talin, paxillin, vinculin or tensin that bind the actin cytoskeleton (57-59). Altered focal adhesion associated protein levels (e.g. of integrins, focal adhesion kinases, paxillin) (59-61) and consequent changes in the integrin-ECM communication has been implemented in PAH disease progression (61). Integrins undergo conformational changes when extracellularly activated by a stiff matrix. It triggers the assembly of the focal adhesion complex, leading to cytoskeletal rearrangements and downstream signalling further promoting the stiffening process (57, 60).

One central molecular mechanism that has been proposed to play a role in the vascular stiffening is the activated YAP/TAZ signalling in PAH. It could be demonstrated that ECM remodelling induces microRNA-130/301 expression via activation of the transcription factors YAP/TAZ (Yes-associated protein/transcriptional coactivator with PDZ-binding motif) (41). Collagen deposition and LOX-dependent collagen cross-linking is activated here via the microRNA-130/301 family, which results in a mechanosensitive positive feed-back loop (31). YAP/TAZ activation also leads to metabolic reprogramming of the pulmonary artery endothelial cells, smooth muscle cells and adventitial fibroblasts, driving increased proliferation of all three pulmonary vascular cell types (50).

1.3 The basement membrane

Basement membranes (BM) are specialized extracellular matrix structures containing of 60-200 proteins. They underlie epithelial and endothelial cells, provide structural support, are involved in cellular signalling and influence cell behaviour (62). While major components of the

BM remain type IV collagens, laminins, nidogens, and sulfated proteoglycans (like perlecans, agrins or type XVIII collagens) (63, 64), each BM composition is finetuned and matched to its individual local importance (62). The thickness of a BM can vary between 50 and 500 nm (65). The vascular BM is relevant for blood vessel robustness and integrity. Its components are mainly produced by the endothelial cells that line the lumen of the vessel and the pericytes that wrap around the endothelial cells (65).

The BM is composed of two interconnected insoluble polymer networks made of collagen IV and laminins that build the two layers of the BM: lamina lucida and lamina densa (64). Type IV collagens (COL4A1-A6) mainly occur in BM and is its most abundant component, comprising of six distinct alpha (α)-chains (α1-α6). These chains form only three distinct heterotrimers: α1α1α2, α3α4α5, and α5α5α6 (66). Type IV collagens can regulate proliferative and migrative pathways by directly interacting with cell surface receptors (64). Laminins are heterotrimeric proteins that consist of intercoiled α-, β- and γ-chains. Appearing in several genetically distinct isoforms, laminins can build at least 16 different types of heterodimers that exert cell-type specific functions (65, 67). Laminins play a vital role in cell differentiation and morphogenesis (67).

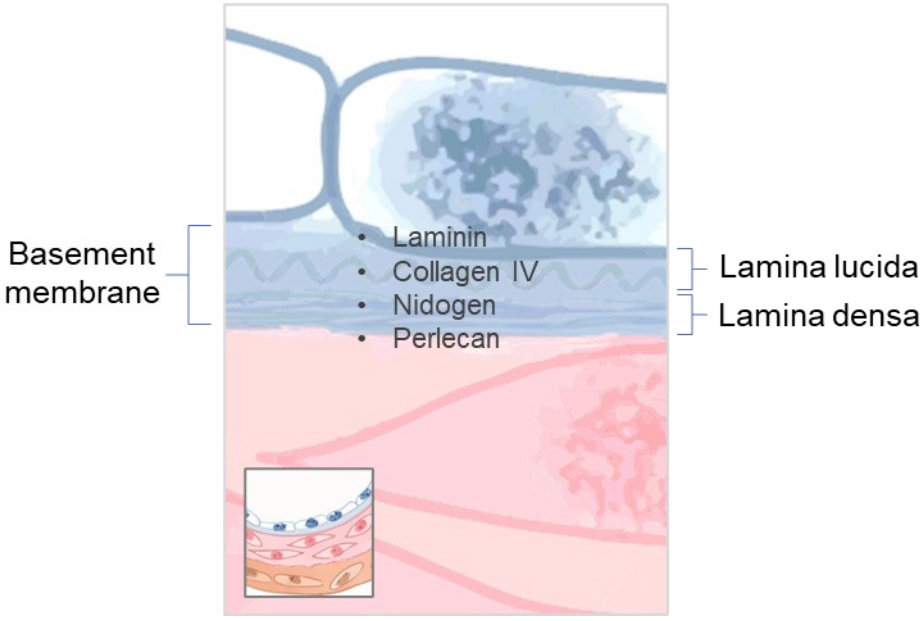

Figure 3. **Basement membrane of the pulmonary artery.**

The lamina lucida and lamina densa are stabilized by nidogens that crosslink type IV collagens and laminins. The ubiquitously expressed nidogen has two isoforms and is a glycoprotein that is essential for BM stability (65). Nidogens are also bound by perlecans that further strengthens

the crosslinking. Proteoglycans with their hygroscopic properties also contribute to BM volume and serve as growth factor reservoirs by binding them (64, 65, 67).
A disbalance in BM components often leads to increased BM degradation, directly influencing endothelial barrier integrity and facilitating trans-endothelial immune cell migration – processes that are of central importance in the progression of IPAH (64, 65).

1.4 Matrikines and their role in lung pathology

Dynamic remodelling, that is accomplished by finely orchestrated proteolytic enzymes of the ECM, is required to maintain the metabolic balance of the ECM – even in physiological conditions. The ECM serves as a reservoir for bioactive molecules, including growth factors and morphogens such as VEGF, bFGF, insulin-like growth factor-1, TGF-β, that can be released on need (38, 64). Enzymatic cleavage of ECM can release proteolytic bioactive matrix fragments, called matrikines, that exert biologic activities which are different to the biological activities of their native full-length molecules. The unmasked bioactive sites of the matrikines can contribute to major cellular processes such as cell survival, migration, proliferation and angiogenesis, and drive inflammatory processes. Common sources in the ECM for such bioactive peptides are collagens, proteoglycans, elastin and laminins (10, 68).

A variety of proteolytic enzymes of the ECM are involved in this process that liberates matrikines from the ECM. MMPs play a central role here (38), and many MMPs have been shown to be dysregulated in PAH, where MMP-1, -2, -3, -7, -9, or -10 are only exemplary for them (38, 69, 70). Being the most abundant ECM molecule in the lung, collagen serves as a significant source for matrikine liberation/activation.

Most of the collagen-derived matrikines arise from fibrillar collagens (e.g. collagen I, II or III).
An increasingly large number of matrikines with central roles in lung pathology have been identified today. While a lot more is left to explore about their role in lung pathobiology, Table 2 lists several matrikines with known contributions to lung pathology. The most prevalent matrikine originating from lung collagen is PGP that consists of tri-peptide fragments, with 3-5 proline, glycine and proline (PGP) repeats. PGP has mainly been shown to act as a chemoattractant to neutrophils (71) and has been associated with Chronic Obstructive Pulmonary Disease (COPD) and cystic fibrosis (72, 73).

Similarly high importance in lung pathology has also been shown for non-fibrillar collagen-derived matrikines, for which the specialized ECM of the tunica intima, the BM, serves as the main source (71). Interestingly, several of the source components for these matrikines (Table 2) are also implicated in the pathology of PAH: Collagen IV, Collagen XVIII, versican and elastin have been shown to be upregulated in PAH (12, 74, 75).

Endostatin, a 20 kDa matrikine resulting from C-terminal fragmentation of the non-fibrillar Collagen COL18A1, counts to the most studied matrikines today, a matrikine that has an anti-proliferative effect on endothelial cells and inhibits angiogenesis and tumour growth (10, 76). Recently, endostatin could be validated as a robust, independent risk predictor of PAH mortality (12, 77, 78).

Table 2. **Matrikines in lung diseases**

Source Molecule	**Matrikine**	**Associated Disease**
Collagen[1]	Proline-Glycine-Proline (PGP), N-terminal acetylated PGP (N-α-P)	COPD, CF (72, 73)
Collagen IV	7S Collagen	ARDS (79)
Collagen IV α1	P4NP 7S C4M2	COPD-AE (80) (81)
Collagen IV α3	C4Ma3	COPD, IPF-AE, IIP-AE (82, 83)
	Tumstatin	Asthma (84)
Collagen XVIII α1	Endostatin	ALI, Asthma, IPF, COPD, PH (12, 77, 85-88)
Versican	VCANM	COPD-AE, IIP-AE (80, 89)
Elastin	VGVAPG	COPD (90)

[1] PGP can be liberated from a variety of collagen types as it is a prevalent sequence within collagen molecules (e.g., 28x in type I, 43x in type III and 25x in type IV collagen) (91).

Abbreviations: ARDS: Acute Respiratory Distress Syndrome; COPD: Chronic Obstructive Pulmonary Disease; CF: Cystic Fibrosis; COPD-AE: Chronic Obstructive Pulmonary Disease with Acute Exacerbation; IPF-AE: Idiopathic Pulmonary Fibrosis with Acute Exacerbation; IIP-AE: Idiopathic Interstitial Pneumonia with Acute Exacerbation; ALI: Acute Lung Injury; IPF: Idiopathic Pulmonary Fibrosis; PH: Pulmonary Hypertension.

1.5 Endostatin and its origins

Type XVIII collagen (COL18A1) is a core component of the pulmonary vascular basement membrane crucial for tissue architecture and membrane integrity, and consists of three α1 chains (homotrimeric structure). This collagen generally has three known isoforms (short, medium and long). The isoforms have differentiating spatial expression profiles, of which the short isoform is most abundant in the vasculature. The common functional domains characteristic of all collagen XVIII isoforms include the thrombospondin (TSP) 1-like domain, the triple-helical domain consisting of 10 collagenous and 11 non-collagenous regions, and a NC1 domain that consists of a trimerization domain, a hinge region and the C-terminal endostatin domain. The N-terminal DUF959 (Domain of Unknown Function) is characteristic for the medium and long isoforms, while the long isoform additionally possesses a frizzled domain between the DUF959 and the TSP 1-like domain (92).

Endostatin arises from the C-terminal region of collagen XVIII consisting of 184 amino acids that is present in all three isoforms of the protein (93). It is released from its parent protein through various proteolytic mechanisms via elastases, cathepsins and MMPs (92). This 20 kDa proteolytic fragment endostatin has a compact globular structure consisting of β-sheets, loops, α helices, disulfide bridges, heparin binding sites and a Zn(II)-binding sites, facilitating various possible interactions and complex signalling (93). Besides endostatin, additional matrikines resulting from the NC1 domain of collagen XVIII include neostatin-7 (contains 60 amino acids additional to endostatin) and neostatin-14 (contains 14 additional amino acids than endostatin).

The human endostatin (hES) shows high structural similarities among different species, with about 86% identity and >90% similarity with mouse endostatin (93); thereby facilitating applicability of animal models for research purposes. A challenge for the clinical applicability on the other hand is its short half-life in circulation (94) and the huge amounts of purified endostatin required in order to achieve the desired biological activity (93). In an effort to overcome these challenges, studies could prove that a modified mutant endostatin, hES-P125A, is more potent in its biological function than the native endostatin. hES-P125A is a human endostatin molecule with a point mutation at position 125 where proline is substituted with alanine, resulting in an enhanced endothelial cell binding capability of the molecule (95).

Endostatin is an anti-proliferative, anti-migratory matrikine that also inhibits angiogenesis, a key process for lung vessel homeostasis (96). Angiogenesis is mainly controlled by the growth

factor VEGF (vascular endothelial growth factor) (97). Studies show that endostatin antagonizes VEGF signalling by directly binding to VEGF receptor 2 (VEGFR2) (98). Though far less studied than endostatin, first studies indicate that neostatin-fragments also have anti-angiogenic potential (99). In fact, endostatin has been shown to induce apoptosis, stop cell cycle and suppress cell proliferation and migration of endothelial cells through a variety of signalling mechanisms (93, 100), including e.g. involvement in caspase activation (101), Bcl-2 signalling (102), Wnt/b-catenin signalling (103, 104), FGF- and VEGF-mediated signalling (105) as well as proteolytic pathways acting via metalloproteinases (106). Notable here is a study by Goyanes at al., where it was demonstrated that endostatin inhibits proliferation, migration of human PAEC and promotes PAEC apoptosis by interacting with inhibitor of differentiation 1 (ID1), a downstream effector of BMPR2 signalling (100), thereby emphasizing its role in PAH pathobiology. Specifically, it was shown that this effect of endostatin on PAEC was mediated by the suppression of ID-1 expression, leading to the increased expression of thrombospondin 1 (TSP-1), which in turn inhibits PAEC proliferation and migration via CD36/CD47 (100).

With its versatile involvement in central pathways relevant for PAH and being a proven, robust disease prognosis marker for PAH (12, 77, 78), endostatin presents a promising matrikine of which the signalling mechanism, especially its non-coding aspect, is yet insufficiently explored.

1.6 Long non-coding RNAs (LncRNAs)

The non-coding genome has been extensively studied over the last two decades, even though, initially, not much importance was given to the non-protein coding parts of the genome. Several functionally important classes of non-coding RNAs are abundantly present in our body. Meanwhile, the current GENCODE statistics (version 39; GRCh38.p13 (107)) counts more than twice the amount of non-coding genes (including small, long and pseudogenes) than coding genes (Figure 4).

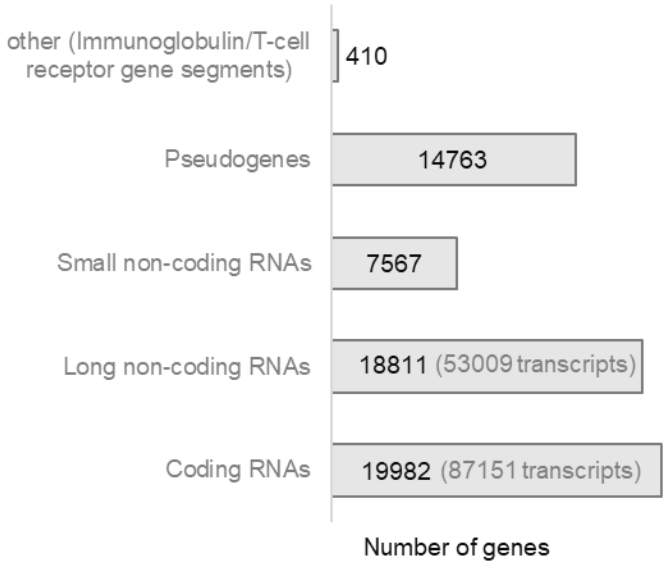

Figure 4. **Total number of genes – current GENCODE statistics** GRCh38.p13 (107).

The exponentially growing number of identified ncRNA has led to a growing catalogue of ncRNA types, that is currently being shaped with gained knowledge from ongoing research. Table 3 gives a comprehensible overview of currently described non-coding RNA classes.

Table 3. **Classification of ncRNA**

tRNA	transfer RNAs
rRNA	ribosomal RNAs
sdRNA	sno-derived RNAs
tiRNA	transcription initiation RNAs
miRNA	microRNAs
moRNA	microRNA-offset-RNAs
vtRNA	vault RNAs
siRNA	small interfering RNAs
endo-siRNA	endogenous small interfering RNAs
snoRNA	small nucleolar RNAs
scaRNA	small Cajal body RNAs
piRNA	piwi-interacting RNAs
lncRNA	long non-coding RNAs
circRNA	circular RNAs

Data adapted from (107, 108)

While most of our non-coding understanding is based on micro RNAs (miRNA), the involvement of a different RNA species, that of long non-coding RNAs (lncRNAs), have proven to be of central importance lately (109). In contrast to miRNA that belong to the small non-coding RNA (<200nt in length), long non-coding RNAs are defined as RNAs that are above 200 nucleotides in length. They can comprise of one or several exons that are spliced together undergoing the same transcriptional process as protein coding messenger RNAs (mRNAs). LncRNAs have no translated open reading frames (ORF) with proper transcription start/stop sites in comparison to mRNA, but are biochemically identical to the mRNAs (109). LncRNAs are ubiquitously present in our body, but their abundance can be very low. Contrary to the assumption that low-abundance transcripts may have less functional influence, several low-abundance lncRNAs have shown that it is the process of transcription itself that gives the lncRNA its functionality rather than the transcript (110).

The involvement of lncRNA in human biology is versatile with various gene regulatory functions including roles as decoy, guide, signal- and scaffold-molecules (111). Based on their subcellular localization, that can be cytoplasmic, nucleic or both, cis- as well as trans-regulatory activities has been described for the lncRNAs. They can regulate the expression of neighboring genes (acting in cis) by binding to transcription factors or control the gene expression from a distance (acting in trans) by influencing protein structure or altering chromatin state. In fact, many lncRNAs harbor huge regulatory potential given by their ability to interact with the chromatin-modifying machinery.

Exemplarily, NRON represses the transcription factor NFAT, nuclear factor of activated T cells and interfers with interleukin-2 receptor activation (112, 113). Another example is the interaction of the lncRNA PVT1, plasmacytoma variant translocation 1, with the oncogenic transcription factor MYC that considerably contributes to tumorigenesis (114). Of note, PVT1 also has been shown to possess circular RNA (circRNA) transcripts with importance in various biological settings including lung pathology (115, 116). The heart-enriched lncRNA Chaer (cardiac-hypertrophy-associated epigenetic regulator) interacts with polycomb repressor complex 2 (PRC2) inhibiting histone H3 lysine 27 methylation of gene regions involved in cardiac dysfunction (117). HOTAIR is another example for a lncRNA that regulates chromatin dynamics. By interacting with PRC2 it promotes trimethylation and silencing of its target locus HOXD (118).

LncRNA interactions with DNA that lead to the formation of RNA-DNA triplex structures have also been reported to modulate central functional pathways (e.g. TGF-β signalling (119)).
One of the main lncRNA functions that was discovered very early was the ability of the lncRNAs to sponge off miRNAs from their mRNA targets. Micro RNAs that belong to the group of small non-coding RNAs, exhibit their function in the posttranscriptional regulation by mRNA cleavage, direct translational repression and/or mRNA destabilization (120). Many lncRNAs harbor miRNA binding sites that interacts with the respective miRNAs, keeping them from exhibiting their inhibitory effect on their targets (120). An example for such interaction is miR372 (121) that interacts with lncRNA FER1L4 leading to elevated proliferation in glioma cells (122). Similarly, the lncRNA H19 modulates miRNA family let-7 availability by acting as molecular sponge (123). Adding an extra layer of complexity to the lncRNA-miRNA-mRNA regulatory axis, the involved lncRNAs can also carry embedded miRNA sequences and can serve as the origin for miRNA, as e.g. in the case of MEG3 (110, 124).

The primary structure of lncRNAs generally is poorly conserved between species, only showing “patches” of conserved bases within a longer stretch of transcript. But, lncRNA molecules can form evolutionarily more conserved compact elements consisting of complex higher order structures, that enables interactions with proteins, small regulatory RNAs or translation initiation or splice site machineries (110).

1.7 LncRNAs in PAH

Recent findings suggest key contribution of lncRNAs to the remodelling of the pulmonary arteries in PAH, modulating proliferative, migrative and apoptotic processes (111). Examples for lncRNAs that exert pro-proliferative and pro-migratory effects in pulmonary artery smooth muscle cells (PASMCs) include lncRNA H19, MALAT1 or lnc-Ang362:
Following PDGF-BB stimulation, the lncRNA H19 upregulates Angiotensin II receptor Type 1 (AT1R), while silencing H19 prevents pulmonary artery remodelling in PAH animal models (125). MALAT1, or metastasis-associated lung adenocarcinoma transcript 1, was shown to indirectly upregulate the transcription factor Krupple-like factor 5 (KLF5) by sponging off miR-124-3p.1, causing enhanced proliferation and migration of PASMC (126, 127). The expression of the lncRNA lnc-Ang362 was reported to enhance expression of its proximal miRNAs miR-221 and miR-222, thereby promoting proliferation and migration of PASMCs via activation of NF-KB signalling (128).

Using pericytes and PASMC from IPAH patients, hypoxia exposed cells modelling IPAH and precision-cut lung slices from PAH patients, Zehendner et al. shows the TYKRIL knockdown reverses the proproliferative and antiapoptotic phenotype in hypoxic and PAH cells. Furthermore, they show that the lncRNA TYKRIL exerts its function via the p53/PDGFRβ signalling axis (129).

Hoxa cluster antisense RNA 3 (HOXA-AS3) (130), Tug1 (131) and maternally expressed gene 3 (MEG3) (132) are examples for lncRNAs that reacts to hypoxia signalling in PAH models. Tug1 (131), TCONS_00034812 (133) and urothelial cancer-associated 1 (UCA1) (134) are lncRNAs that have been shown to demote apoptosis in PAH models, again contributing to the remodelling process of pulmonary arteries in PAH.

The versatile signalling mechanisms of the few listed lncRNAs here already highlight the huge therapeutic and diagnostic potential any new discovery would add to the rudimentarily explored field of lncRNAs in PAH (111). However, how and whether lncRNAs can influence ECM-cytoskeletal axis has not been thoroughly investigated so far.

1.8 Rationale of the study

Central biologic importance has been attributed to matrikines and lncRNAs recently: matrikines as well as lncRNA can influence cell behaviour and have been shown to be involved in the pathology of various respiratory diseases (71, 72, 91, 127, 128, 130, 131, 133, 135-138). In this study, we hypothesized that lncRNA have functional importance in IPAH pathogenesis, and that they act by exerting a regulatory function over ECM remodelling and matrikine production.

The specific aims of the current study were:

- to characterize donor and IPAH pulmonary arteries by identifying and analyzing differentially regulated proteins and genes, thereby especially focusing on the ECM components,
- to explore the importance of lncRNAs in IPAH, especially the role of the lncRNA PAXIP1-AS1,
- and to find the regulatory link between ECM/matrikines and the lncRNA PAXIP1-AS1.

2. Materials and Methods

2.1 Patient samples

All human lung tissue samples were preserved from IPAH patients who underwent lung transplantation at the Department of Surgery, Division of Thoracic Surgery, Medical University of Vienna, Austria. The institutional ethics committee approved the protocol and tissue usage (976/2010), and patient consent was obtained before lung transplantation. All approvals were obtained per national law and the Good Clinical Practice/International Conference on Harmonization guidelines. Downsized non-tumorous non-transplanted donor lungs served as controls. The patients' characteristics are listed in Table 4. The diagnoses of the lungs were reviewed using chest computer tomography scans and confirmed by pneumologists and pathologists. A detailed description on how the explanted lungs were sampled and stored can be found in (9).

Table 4. **Patient characteristics.**

	IPAH (n = 25)	**Donors (n = 32)**	**P Value**
Sex, F/M	16/9	15/17	—
Age at Ltx	32.43 ± 10.5	41.68 ± 15.64	0.01
6MWD	308.5 ± 166.38	—	—
HR, bpm	83.04 ± 13.96	—	—
mPAP, mm Hg	68.64 ± 21.55	—	—
NT-proBNP, pg/ml	3536.7 ± 2585.48	—	—

2.2 Cell culture

Cell isolation and culturing – PAEC, PASMC and PAAdFB

Primary pulmonary artery endothelial cells (PAEC) were bought from Lonza (Switzerland) and cultured in Lonza endothelial cell growth medium EBM^{TM}-2 that was supplemented with EGM^{TM}-2 Endothelial SingleQuotsTM Kit that contains growth factors, heparin, cytokines and other supplements and a 2% fetal bovine serum (FBS) solution (=complete medium). Starvation of the PAEC was performed in basal EBM^{TM}-2 medium that was supplemented with 0.5%FBS, but no other additives or antibiotics/antimycotics. Before culturing the flasks were precoated with 1% gelatin for 1 hour at 37°C. See Table 5 for detailed ID number of used cells.

Primary human pulmonary artery smooth muscle cells (PASMC) and pulmonary artery adventitial fibroblasts (PAAdFB) were isolated from pulmonary arteries from non-transplanted donor lungs or IPAH lungs. The isolation was performed according to Stulnig et al. (139): First,

the endothelial layer was removed, the media then separated from the underlying adventitial layer and collected separately. The medial layer was then cut into small sections. After centrifugation the collected pieces were resuspended in VascuLife Complete SMC Medium (Cellsystems, Germany) supplemented with growth factors, 20% FBS and 0.2% gentamycin/streptomycin, and cultured in T_{75} flasks. Reaching confluency, the cells were then trypsinized to be cultured further, or are stored deep frozen in liquid nitrogen in VascuLife Complete SMC Medium containing 15% FBS and 10% DMSO until further use. For starvation purposes, a basal medium supplemented with 0.2% antibiotics was used. Quality stainings were performed using immunofluorescent antibodies for smooth muscle-specific isoforms of *α*-actin in order to confirm the purity of the isolated PASMCs (minimum 95% of cells stained positive).

The previously separated adventitial layer was used to outgrow pulmonary arterial adventitial fibroblasts. The isolated cells were cultured in FibroLife Serum Free Fibroblast Complete Medium containing (Cellsystems, Germany) growth factors and associated supplements. The complete medium was supplemented with 15% FBS and 10% DMSO for deep-freezing purposes, and basal medium without any additives, but 0.2% antibiotics/antimycotics was used as starvation medium.

All cells were incubated in a humidified atmosphere at 37°C and 5% CO_2. To determine the appropriate cell number for the respective assays before seeding, cell numbers were determined using trypan blue and the Neubauer cell counting chamber. In case of all primary cells used, passage numbers between 2 and 10 were taken for the respective experiments.

Table 5. **PAEC from Lonza.**

Cell ID	Age (yr)	Sex (M/F)
28032	51	M
28074	67	F
21292	21	M
21304	45	F
35049	33	F
18664	63	M
27930	21	M

Transfection of the primary cells

Electroporation and transfection agent-based methods were tested during the study setup. Amaxa® Nucleofector® Technology from Lonza (Switzerland) was used for nucleofection of

the PAEC/PASMC as described in the manufacturers protocol. The program A-033 and the Amaxa™ Basic Nucleofector™ Kit for Primary Mammalian Smooth Muscle Cells was used for PASMC, and in the case of PAEC, the Basic NucleofectorTM Kit for Primary Mammalian Endothelial Cells and the program S-005 was used. For transfection reagent-based transfection, either Lipofectamine 2000 (L2000) transfection reagent (Thermo Fisher Scientific, Switzerland), Effectene (Qiagen, Germany) or JetPRIME (Polyplus Transfection, France) were tested using the respective manufacturers' protocols.

Following oligonucleotides and plasmids (Table 6) were used for the functional assays after knock-down and overexpression in PAEC, PASMC and PAAdFB:

Table 6. **GapmeRs, siRNAs and overexpression plasmids.**

Type	Target / Purpose	Supplier / Ref. ID	Applied amounts
GapmeR	PAXIP1-AS1 / Knock Down	custom LNA oligonucleotide, Design ID: 657824; Exiqon, Vedbaek, Denmark; 25 nM	25 nM
GapmeR	Scrambled/ non-gene-targeting / Control	custom LNA oligonucleotide, Design ID: 657823; Exiqon; 25 nM	25 nM
siRNA	PAXIP1-AS1 / Knock Down	Lincode Human PAXIP1-AS1 siRNA, N-184835-05-0005; Dharmacon, Vienna, Austria; 50 nM	50 nM
siRNA	Scrambled/ non-gene-targeting	ON-TARGETplus non-targeting siRNA #1, D-001810-01-05; Dharmacon	50 nM
Plasmid	Paxillin in pcDNA3.1 backbone / Overexpression	Overexpression plasmid created as part of a previous study (140); Cloned and provided by Dr. Julia Hoffmann.	2 µg DNA / 250k cells
Plasmid	PAXIP1-AS1 in pcDNA3.1 backbone / Overexpression	Cloning process of the overexpression plasmid detailed in section 2.15.	2 µg DNA / 250k cells
Plasmid	pcDNA3.1 / Control	Backbone plasmid from Invitrogen (Germany)	2 µg DNA / 250k cells
Plasmid	pmaxGFP™ / Control	GFP expressing control plasmid provided by Lonza (Switzerland) in Amaxa® Nucleofector® Kits for tracking transfection efficiency	1 µg DNA / 250k cells

JetPRIME based transfection was performed for all overexpression experiments with plasmids on PAAdFB, PASMC and PAEC, as well as for all siRNA mediated silencing in PASMC. GapmeR mediated silencing of PAXIP1-AS1 in PASMC was performed with Lipofectamine 2000. PAXIP1-AS1 GapmeR mediated silencing of PAEC was performed via unassisted uptake. For the delivery of GapmeRs via unassisted uptake, the cells were seeded at a density of 100 – 250 k cells/well in a six-well plate (or at a density of 5k cells/well in 96-well plates) using complete growth media. The next day the oligonucleotides dissolved in PBS were added to the well to reach 1 µM per well. Cells were harvested after 48 hours before further processing.

Cell stimulation

To investigate the changes in PAXIP1-AS1 expression in response to various stimuli, PASMC grown on 12-well plates were starved overnight in VascuLife Basal Medium, and then treated with PDGF-BB (Sigma-Aldrich, Austria), TNF-α (eBioscience, Austria), IL1-β (PeproTech, Austria) and TGF-β (Immunotools, Germany) and Endothelin-1 (Sigma-Aldrich, Austria). An end concentration of 10 ng/ml, or 500 nM in the case of Endothelin-1, was applied respectively, and total RNA was collected 2, 4, 8 and 24 hours post treatment and of an untreated control sample. The expressional changes were then measured via qRT-PCR (141).

2.3 Protein isolation

peqGOLD TriFast™ (PeqLab, Germany) was used to isolate proteins from cell or tissue samples according to the manufacturer's suggestions. In short, the tissue samples were pulverized using mortar, pestle and liquid nitrogen, and then further homogenized in TriFast solution using ceramic beads and an electric homogenizer (MagNA Lyser, Roche Diagnostics, Austria)). In case of cells, the Trifast was directly added without previous homogenization. Further steps of phase separation included 10min incubation on ice, centrifugation, 10min further incubation at 4°C, addition of chloroform, vortexting, 10min incubation at room temperature, and a final centrifugation at 1300 rpm and 15min at 4°C.

The aqueous was used for RNA isolation. The organic phase was then supplemented with acetone (4x the amount of the sample), incubated at -20°C, then centrifuged. A 90min incubation at 65°C with the RIPA buffer (with phosphatase and proteinase inhibitors, and 1% SDS) was then performed to lyse the dried pellets. The first fraction of protein lysate resulted from the following centrifugation step. The remaining pellet was then dissolved and incubated for 30min at 55°C in a Urea buffer (8M Urea in 0.05M Tris – pH8.5), homogenized using the MagNA Lyser and centrifuged. The supernatant was then added to the first fraction and used for further analysis.

2.4 RNA isolation, cDNA synthesis and qRT PCR

peqGOLD Total RNA isolation kit (PeqLab, Germany) was used to isolate total RNA from cell or tissue samples. The isolation was performed according to the manufacturer's protocol. In case of tissue samples, the aqueous phase from the peqGOLD TriFast™ protocol was used. The concentration and purity of the isolated RNA was assessed by spectrophotometric analysis (Nanodrop). The total RNA was then reverse transcribed using the iScript cDNA

Synthesis Kit (BioRad, Austria). SYBR Green qRT-PCR was then performed with the CFX384 Touch™ Real-Time PCR Detection System (Biorad, Austria) or the Light cycler 480 System (Roche Applied Science, Austria). Sequences of primers used for gene expression analysis are shown in Table 7. Before usage, the specificity of the primers was verified running agarose gels and comparison of detected and expected band sizes. Specific amplification was also verified by melt curve analysis. The expression of β2-microglobulin (B2M) was used to normalise the obtained expression levels of genes of interest. Differential gene expression was calculated using the threshold cycle (Ct) method (142).

Table 7. **List of used primers.**

Gene Abb.	Forward primer 5´- 3´	Reverse primer 5´- 3´
ACAN	TCTTCAAGGTGAACTATGACCAVT	TTGGGGGATGCTGACACTCA
ACTB	TCAAGATCATTGCTCCTCCTGAG	TCCTGCTTGCTGATCCACATC
AGRN	TGTGGAAGATAAACCCGGGAC	TCTTCTTGCAGACGCAGGAC
B2M	CCTGGAGGCTATCCAGCGTACTCC	TGTCGGATGGATGAAACCCAGACA
BGN	CTGGCATCCCCAAAGACCTC	CCAGTTCGATGGCCTGGATT
COL14A1	GTCGGGACCACACTTGAGAG?	TACCCGCAGGCTAGAAGTAGT
COL18A1	TCAGTGCCACCACCATCTTCA	GCATCTGGCCCAAAGACGTAG
COL4A1	CCCAAAGGTGTTGACGGCT	TGAGTCCCGGTAGACCAACT
COL4A2	CTTTCCTGGACTGAGGGGTT	CATCAGGCCCTTGATAGCCA
COL4A4	GATGGCCAGAAAGGACCAGT	GGGATTCGGGGACAGTCATC
COL4A5	GAACCAAGGGAGAACGTGGAT	CTTTGGTCCTGGCAGTGATGA
CTSB	AGAGTTATGTTTACCGAGGACCT	GCAGATCCGGTCAGAGAT
CTSK	CAGTTTTACAGCAAAGGTGTGT	TTTCCCCAGTTTTCTCCCCAG
CTSL	GCTAATGACACCGGCTTTGT	TTTCAAATCCGTAGCCAACC
DCN	GCATTCCTCAAGGTCTTCCTCC	AGCCATTGTCAACAGCAGAG
ELN	ACCTCTTAAGCCAGTTCCCG	CTAAGCCACCAACTCCTGGG
EMILIN1	CCTGCGTCTTCCACACCA	CTCTGCACCTGTTCCTCCAG
FBLN1	CGCAACTGCCAAGACATTGA	TCCCGATTCTCATGGCAAGG
FBLN2	CTGCAAAGACAATGGACCCT	ACAATCGTGAGCACCCATCA
FBLN5	GGAATAAAACACCCGCGAGC	ATTCGTGCACTGTGCCTGT
FBN1	GGCGAGGACAGCAGGAC	TGATATTTGCCCACTGGAACA
HSPG2	CCCGTCAACCAGGAGATTGT	AAGAGCCGTCAGCACATTCA
ITGA1	TCCTCACTGTTGTTCTACGCTG	ACGGAGAACCAATAAGCACC
ITGA5	AAGGGAACCTCACTTACGGC	TAGGAGGCCATCTGTTCCCC
ITGA6	CGGTCTCGGGAGTTGCTAAA	TGCCGAGGTTTGTAAGAGGT
ITGA8	GCTGCTGGGGAGTTTACTGG	GATGCCATCTGTTCTCCCGTG
ITGA9	CAAAGGCATCGGCAAGGTTT	TCCCCATTCAGGTCAACTGC
ITGAV	ACAAATGCTCCTAGGCACCC	TCTCTATTGCCTGTTGCATCAAA
ITGB6	ACGTACAAGGTGGCTGTGC	GGGTATCACACCTTTCGCCA
JARID1-AS1	CCTCAACGAGGTCCGGAATG	CAGAGGGCTGGGTAGAATGC

LAMA3	CCTGGCGACATGGTTCTTCT	TGAAGTTTCCCTCGACCACG
LAMB1	CTACTGCAAGCGTCTGGTGA	TGACTCCGCAAAGCAACTGT
LAMB2	AGACCGTTCACCTCCCCTTA	GCCAGCACGCTTAGCAGTAG
LAMC1	GCCAATGTGTCAGTCACTCAG	GCTGTCTTTGCCACTCGAAC
LINC00877	CGAGAAGGAAAGCCGGTGAT	TCCATGTGTCTGCTTTGCCT
LINC01214	CAGAGGGACTTTCAGTTTTTCAC	CAAGTGCCCAAGTAACAAAAGG
LINC01398	CCTCGGTTTCTGAGGGTCTG	ACCATGGAGGGTTTGGTTGG
MMP1	ACAACTGCCAAATGGGCTTG	TGTCCTTGGGGTATCCGTGT
MMP14	GAGCATTCCAGTGACCCCTC	ACCCTGACTCACCCCCATAA
NID1	CTGCCAAGATGTAGATGAATGCCA	CACCGGGTTTTCTCCACCT
NID2	GGTGAACCAGAGGAGGCATT	GGTGGAAGATTCCTCTAAAGGCT
PAXIP1-AS1	ACAAACCGGAGTCCAGGAAC	CAATGCTCCACAGTTTTACGAC
PAXIP1 (Ex2-3)	CATCGACCCGCAGGTTATTC	CTGAGATTATGTGTGAGGCTAG
PAXIP1 (Ex17-18)	CTGTTTCAGCTTGGAAGAATCC	AATTTTGCCTTAAAGAGTGGAGAAAC
PTK2	GAGTCCAGAAGACAGGCCAC	CCAGGGTAGCCAGAAACCTG
PXN	TGGACAGCCCTACTGTGAAA	AGAAGTGTTCAGGGTGCCA
SNHG16	AGTAATCGCCATGCGTTCTTTG	GGTTTTCCAGAATAATCTCAGTTG
SRC	GGAGTGACCACCTTTGTGGC	CGCCTTTCTTGAAGGACAGGTC
TLN1	CGTAAGATCTTCCAGGGCACA	AGAGAACGGGCTAGCTTCAC
TNS1	AGGATGTCGGCCATTTCTCC	CGATGGTGATGCAGACGCTA
TUSC8	ACTGGCCTTCCCAGAAACAG	GTTCACCTCCACCGGAAGG
VCAN	TGTTAATCGTGTGGGCCATGA	AGAAGCTGTCTGGCTGGTTG
VCL	CTGAACCAGGCCAAAGGTTG	CCCAGAATCTCCCTGCGTTC

2.5 Western Blot analysis

Protein lysates from cells or tissues won through the previously described peqGOLD TriFast™ protocol were used for western blotting. A 2x Laemmli buffer was used for sample preparation before running the samples in 10-15% sodium dodecyl sulfate (SDS) polyacrylamide gel (adapted to target protein size) and being transferred to 0.45 µm PVDF membrane (Immobilon-P, Millipore Corporation, Austria). Blocking was performed with 2.5, 3 or 5% bovine serum albumin (BSA) (in Phosphate Buffered Saline (PBS) or Tris Buffered Saline Buffer with Tween 20 (TBST)), and the membrane was then incubated over night at 4°C with the respective antibodies as listed in Table 8, diluted in 2.5, 3 or 5% BSA in PBS or TBST. Goat anti-Rabbit and goat anti-Mouse IgG (H+L) Secondary Antibodies, HRP (Thermo Fisher Scientific, Austria; 1:5000) were used as secondary antibodies. The Amersham ECL Plus Western Blotting Detection System (GE Healthcare, Germany) was used for the detection of the proteins. Bio-Rad ImageLab software (Bio-Rad, Austria) was used for the quantitative analysis of the blots and the values were normalized to GAPDH or α-tubulin.

Table 8. **List of primary antibodies used for western blotting.**

Antigen	Supplier	Catalogue number	Dilution
GAPDH	Cloud Clone Corp	CAB932Hu22	1:2000
Collagen I	Southern Biotech	1310-01	1:500
α-tubulin	Cell Signaling Technology	#2125S	1:5000
pPaxillin	Cell Signaling Technology	#2541	1:1000

2.6 Protein isolation with ECM enrichment

The ECM enrichment protocol was performed as previously described by Herbert B Schiller et al. (143). In brief, isolated and frozen donor and IPAH pulmonary arteries were crushed and homogenized using ceramic beads and an electric homogenizer using the extraction buffer (buffer 1: containing sodium chloride (NaCL), tris-hydrochlorid (Tris-HCL), glycerol, sodium deoxycholate, sodium dodecyl sulfate (SDS) and IGEPAL). After centrifugation, the soluble proteins were collected and proteins were extracted from the insoluble pellet in three steps using buffers with increasing stringency (buffer 2: 50 mM Tris-HCL (pH 7.5), 5% glycerol, 150 mM NaCL, fresh protease inhibitor tablet (+Ethylenediaminetetraacetic acid (EDTA)), 1.0% IGEPAL CA-630, 0.5% sodium deoxycholate, 0.1% SDS, 1% benzonase (#70746-3; Merck, Austria); and buffer 3: 50 mM Tris–HCl (pH 7.5), 5% glycerol, 500 mM NaCL, protease inhibitor tablet (+EDTA), 1.0% IGEPAL CA-630, 2% sodium deoxycholate, 1% SDS, 1% benzonase (#70746-3; Merck, Austria). The pooled samples containing the two soluble fractions resulting from buffers 1 and 2 and an insoluble pellet was subjected to LC-MS/MS analysis. The adapted protein reduction, alkylation and subsequent protein digestion steps are described in detail in (143).

2.7 Immunofluorescence staining

Immunofluorescence staining on PASMC was performed in an eight-well chamber format. PASMC were fixed in 4% paraformaldehyde 48 hours post transfection. After rinsing 3x in PBS, the cells were blocked for 1 hour with 5% BSA (Sigma-Aldrich, Austria) in PBS and then incubated overnight at 4°C with Anti pPaxillin (Tyr118, #2541, 1:50; Cell Signaling, Germany) antibody dilution in 3% BSA and 0.02% Triton. Cells were then washed with PBS, incubated for 60 minutes with corresponding fluorescent-labeled secondary antibody (Donkey anti-rabbit 488, 1:500). Thereafter, the staining for F-actin was performed with the labelled antibody Alexa Fluor 555-Phalloidin (A34055, 1:80; Invitrogen, Austria). Then the slides were mounted with fluorescence Vectashield mounting medium including DAPI (Vector Laboratories, United Kingdom) and sealed with nail polish. The microscopic detection was performed on Nikon’s

A1+ confocal laser microscope system. Fluorescent intensity per area was determined for quantification (141).

2.8 Fluorescence *in situ* hybridisation

The ViewRNA® Cell Plus Assay (Thermo Fisher Scientific, Austria) was used for PAXIP1-AS1 *in situ* hybridisation (ISH) in PASMC (8-well chamber format; 30 000 cells/well) or frozen lung sections (5 µm). The manufacturer's instructions were followed 1:1 for ISH on the cells. When using cryosections, the manufacturer's protocol was followed upto the digestion step. For digestion, the tissue sections were incubated for 10 min at room temperature in proteinase K (1 mg/ml in PBS; 04-1070, Peqlab, Germany) and in 0.3% Triton X-100 (T8787, Sigma-Aldrich, Austria). Target probe hybridisation and signal amplification steps were proceeded with according to the ViewRNA® Cell Plus Assay protocol. The probe sets for PAXIP1-AS1 (VA1-3015586, Type I, Thermo Fisher Scientific, Austria) and ACTA2 (VA6-13283, Type 6, Thermo Fisher Scientific, Austria) were applied at a dilution of 1:10. Cells were stained with DAPI before mounting with the Dako Fluorescence Mounting Medium (Agilent Technologies, Austria). The imaging was performed on Nikon's A1+ confocal laser microscope system (141).

2.9 Immunohistochemical staining

Immunohistochemical staining was performed on donor and IPAH paraffin lung sections (2.5 µm). The deparaffinization that was performed overnight at 60°C is followed by the rehydration sequence of 2x 10min xylol, then 100%, 90%, 80%, 70% and 50% ethanol, and finally distilled water. An antigen retrieval step using DAKO retrieval solution PH=6 (DAKO, California, USA) followed, and then the staining was performed with Anti-PAXIP1 (Atlas Antibodies, HPA016950; 1:500) over night at 4°C. ImmPRESS (Peroxidase) Polymer Anti-Rabbit IgG Reagent (Vector laboratories, United Kingdom) was used as secondary antibody to then develop the staining using ImmPACT® NovaRED® Substrate, Peroxidase (HRP) (Vector laboratories, United Kingdom). Nuclear counter stain was performed using a haemalaun solution for 45 seconds following the dehydration steps (96%, 100% ethanol, and xylol) before mounting with mount media (Thermo Fisher Scientific, Austria). Images were obtained using the Olympus VS120 slide scanning microscope (Olympus, Austria) at 40× magnification.

2.10 Apoptosis

Apoptosis measuring was performed by flow cytometry using annexin V (FITC) and propidium iodide (Thermo Fisher Scientific, Austria) double staining. In all cases, Staurosporin (3 µM in well, 24 hours) served as a positive control for apoptotic cells.

For the Annexin V/PI assay, PASMC were grown in 6-well plates (150 000-200 000 cells/well), transfected with siRNA the following day and kept in the appropriate starvation medium for 48 hours before trypsinising and starting the staining with Annexin V FITC (Thermo Fisher Scientific, Austria) or Annexin V APC (eBioscience, Austria) and PI (Thermo Fisher Scientific, Austria). The flow cytometric analysis was then performed on LSRII flow cytometer (BD, Biosciences, Austria) or cytoFLEX-SII (Beckman Coulter, Austria).

2.11 Proliferation

The cell proliferation rate was either determined by Click-iT™ EdU Cell Proliferation Kit for Imaging, Alexa Fluor™ 647 dye (Thermo Fisher Scientific, Austria), [3H]-thymidine (BIOTREND Chemikalien GmbH, Germany) incorporation assay or by Cell Counting Kit – 8 (CCK-8, Sigma Aldrich) for colorimetric quantitation of viable cell number in proliferation.
PAEC or PASMC were seeded in a 96-well plate at a density of 5000 cells per well and transfected with GapmeRs the following day. [3H]-thymidine was added after 24 hours and again incubated for 24 hours before readout. The [3H]-thymidine incorporation was determined by measuring radioactivity using a scintillation counter (Wallac 1450 MicroBetaTriLux Liquid Scintillation Counter & Luminometer). The experiments were performed in quadruplicates.

When performing the EdU incorporation assay an 8-well chamber format was chosen (40 000 PAEC/well). Cells were treated/labelled with EdU (10 μM in well) alongside with the respective endostatin and/or cytokine treatment on day 1 after seeding in PAEC culturing medium as indicated. The manufacturer's protocol that includes the labelling, fixation and permeabilization steps, and the EdU detection step involving a reaction-cocktail (Click-iT® reaction cocktail) preparation was strictly followed. The the slides were counterstained with Hoechst 33342 and mounted. The imaging was performed on Nikon's A1+ confocal laser microscope system and the image analysis on ImageJ 1.46r.

The CCK-8 assay was performed in at 96-well-plate format and in quadruplicates; 5000 cells per well were seeded, the treatments were performed the following day and the readout performed 24 hours after. The assay was performed according to the manufacturer's instructions. The colorimetric signal was measured on a luminescence microplate reader (LUMIstar Omega, Austria) 4 hours after adding CCK-8 solution (10μl in 100μl total volume).

2.12 Migration

An *in vitro* wound-healing assay was employed to assess the migration capacity of PASMC. In short, 30 000 - 40 000 cells were seeded on each side of an Ibidi culture insert µ-dish (Ibidi, Munich, Germany) and transfected with siRNA. The inserts were removed 48 hours post transfection to create a gap of ~500 µm. Followingly, the migration rate of PASMC was quantitatively assessed at various time points after being photographed at 4x magnification (Olympus CKX41). The area of the initial gap was compared to the area of the healing wound at three different time points (3, 5 and 7 hours) using image analysing software (ImageJ 1.46r) (141).

2.13 Endostatin treatment

PAEC were either treated with recombinant human native endostatin (150-01, PeproTech, Austria), or adeno-associated virus (AAV) were used to overexpress endostatin-P125A (mutant endostatin (144) in the respective cell type. Native endostatin treatment was performed at a concentration of 1 µg/ml in well and was cultured for 24 hours in treatment before performing the respective readouts. Before start of treatment, the PAEC were starved for 2.5 hours in basal medium. PBS was used as a vehicle control.

The vector for AAV mediated endostatin expression was designed using VectorBuilder's online vector construction tool (https://en.vectorbuilder.com/design.html). Endostatin (P125A) expressing AAVs (Vector ID: VB190116-1076wee) and controls (Vector ID: VB150925-10026) were bought from VectorBuilder. An AAV vector that expresses enhanced green fluorescent protein (EGFP) was used as the control. A MOI of 200 000 was used for the transductions, and functional assays were performed 48 hours after the transduction.

2.14 Endostatin ELISA

Endostatin levels were measured using an Endostatin Human ELISA Kit (Abcam, Austria; ab100508) following manufacturer's instructions. The measurements were performed using a micro-plate reader (SpectraMax Plus 384 spectrophotometer, Molecular Devices, Austria). All the unknown protein concentrations (ng/ml) were calculated using an equation derived from standard curves.

2.15 Cloning of PAXIP1-AS1 overexpression plasmid

For the construction of PAXIP1-AS1 overexpressing plasmid, first the full length PAXIP1-AS1 gene was amplified by PCR using Phusion High-Fidelity DNA Polymerase (Sigma Aldrich, Austria) and the following primers with NheI and HindIII overhangs:

F: 5′-GCTGGCTAGCGCGCGCGGCGGAGGG-3′

R: 5′-GCTGAAGCTTTAAAAAGGCAGCATGATCTGTATTTGG-3′

The correct size of the PAXIP1-AS1 amplicon was verified running a 1% agarose gel. The amplified product was then extracted from the cut-out band using the MiniElute Gel extraction Kit (Qiagen, Germany), and restricted with NheI and HindIII (Promega, Switzerland) together with the pcDNA3.1 vector backbone. Following the plasmid was dephosphorylated using Calf Intestinal Alkaline Phosphatase (CIAP), before initiating the ligation at a molar ration of 1:3 of vector to insert using the Quick Ligation™ Kit (NEB New England, Austria) according to the manufacturer's instructions. The ligation mix was then used to transform JM109 chemically competent E. coli before plating them on LB-Agar plates (+50 µg/ml Ampicillin) for selection of positively transformed cells. Overnight cultures of resulting colonies were used to isolate the constructed plasmid. The successful construction was verified by colony PCR and agarose gel analysis, and later Sanger sequencing of the isolated product using BGHrev and PAXIP1AS1 primers (performed at Eurofins Genomics Lab, Austria).

2.16 Proteomic analysis

The protocol for protein isolation with ECM enrichment (see section 2.6) was followed to prepare protein samples from pulmonary arteries that was used for the proteomic analysis by liquid chromatography (LC) coupled with tandem-mass spectrometry (MS/MS). The analysis was performed as previously described in (143). After determining the protein content using the Lowry procedure (145), protein digestion of 200 ng protein was performed using LysC-Trypsin. The digested solution was then separated by nano-HPLC and further analyzed by tandem mass spectrometry using the Orbitrap Velos Pro mass spectrometer (Thermo Fisher Scientific, Austria). MS raw data files were analyzed by the MaxQuant software (146) (version 1.6.0.16), and peak lists were searched against the human UniProt FASTA database (version Aug 2018). For label-free quantification in MaxQuant, the minimum ratio count was set to two. For matching between runs, the retention time alignment window was set to 20 min and the match time window was 1 min. The analyses was adapted from the protocol previously described in (143).

2.17 Genome-wide expression profiling

While genome expression profiling was either performed on total RNA isolated using RNeasy Mini kit (Peqlab, Germany) from PAXIP1-AS1 GapmeR treated, non-targeting GapmeR treated or untreated PASMC, or on material obtained from laser capture microdissected (LCM) small pulmonary arteries of donor and IPAH patients. Purified RNA was from the LCM material was

amplified using the Ovation PicoSL WTA System V2 kit (NuGEN Technologies, Bemmel, The Netherlands) before proceeding with labelling of the 2 µg of the amplified product. In case of PASMC, 150–200 ng of RNA per sample were directly taken for labelling. The SureTag DNA labelling kit (Agilent, Waldbronn, Germany) was used to Cy5- and Cy3-label the samples which were subsequently hybridised to 8 x 60K 60mer oligonucleotide spotted microarray slides (SurePrint G3 Human GE v3 8 x 60K Microarray; Agilent Technologies, Germany, design IDs: 072363 and 039494). Details on the procedure were previously described in (141).

2.18 Functional enrichment, network analysis and functional/structural predictions

Gene Set Enrichment Analysis (GSEA) and Over- Representation analysis (ORA) of transcriptomics and proteomics data was performed by using GO dataset (147, 148), KEGG (149) or Reactome (150) and applying the indicated significance and LFC cutoffs. The STRING (Version 11.0) Protein-Protein Interaction Networks/Functional Enrichment Analysis database (151) was used to retrieve data on gene/protein interactions and examine the connections between genes. The gene-list enrichment tool Enrichr (152) was utilized to compare functional results. The open-source software platform Cytoscape (Version 3.7.2) (153) was used for visualizing complex networks and representation of pathway terms with root nodes. Potential functional RNA motifs and binding sites in PAXIP1-AS1 were studied using an integrated web server RegRNA 2.0 (154). The web-based interfaces of CPC and CPAT were used to calculate the coding potentials of the lncRNAs (155, 156). The Vienna RNA Websuite was used for nucleic acid folding and thermodynamic ensemble prediction of PAXIP1-AS1 (157). For sequence similarity search, we ran BLAST, version 2.7.1 (158, 159) and relied on the NCBI nonredundant database (160). Transcription factor analysis was performed using ConTra v3 (161) and RegRNA 2.0 (154).

2.19 Statistics

Mean differences were tested using the two-sided independent-sample t-test, the paired-sample t-test or Mann-Whitney U test. For comparing more than two sample groups, the one-way analysis of variance (ANOVA) with Tukey or Dunnett's post hoc test. In all statistical analyses, two-sided tests were applied. Values of $p<0.05$ were considered statistically significant (* = $p<0.05$). The n number indicates independent experiments. Microarray data was analysed using R (3.3.2) and the limma package (3.30.13) from BioConductor (162, 163). The Rtsne package (0.13) implemented in R (with perplexity parameter set to 7) was used to perform dimensional reductions based on t-SNE. PerseusStatistics 1.6.1.1 was used for the

analysis of the proteomics data. Other statistical analyses were performed on GraphPad Prism 8 statistical analysis software (GraphPad Software, CA).

3. Results

3.1 Expressional changes in IPAH – the coding profile

Transcriptional platforms offer powerful, relatively unbiased solutions for studying the global gene expression in healthy and diseased subjects (164). To better understand the gene expression in the diseased setting of IPAH, we performed a study of the pulmonary transcriptome using oligonucleotide spotted microarray slides (Agilent Technologies, design ID: 039494). Considering that IPAH is mainly a disease of the distal pulmonary arteries (13), we chose to perform the comparative analysis on laser capture-microdissected small pulmonary arteries (50-500 µm) of idiopathic PAH patients (n=18) and healthy controls (n=17). The isolation of the arteries was performed by Dr. Julia Hoffmann at our institute. The microarray experiment was performed at the Justus-Liebig-University, Giessen with the help of Dr. Jochen Wilhelm.

Passing the quality control and image processing steps that are integrated in the microarray analysis pipeline, we further proceeded with an in-depth analysis of the gained data. To put the expression values resulting from the translated microarray signal intensities in biological context, we first analyzed the similarity between the individual samples via t-distributed stochastic neighbor embedding (t-SNE). We found that the transcriptome of pulmonary arteries of healthy lungs clearly differ from the one of IPAH lungs (Figure 5). Further analyzing this data, we found that the heatmap and clustering as presented in Figure 5B also supports the clear distinction between the sample groups. The global distribution of all detected genes with their respective $\log_2$(fold changes) (LFC) and significances ($-\log_{10}$(P)) is captured by the volcano plot in Figure 5C. A list of the top 15 most strongly regulated protein coding genes with the highest calculated LFC is summarized in Table 9.

Around half of all detected RNA in our study were protein coding RNA (47%). Additional to the protein-coding transcriptome, we found that a significant part of the IPAH-characteristic transcriptome (13% of all detected genes) consists of non-coding RNAs (Figure 5D). The RNA subtype long non-coding RNAs (lncRNA) accounted for the major subtype represented in this non-coding fraction (our screening focuses on longer transcripts; chosen microarray platform and RNA isolation procedure not optimized for miRNA detection).

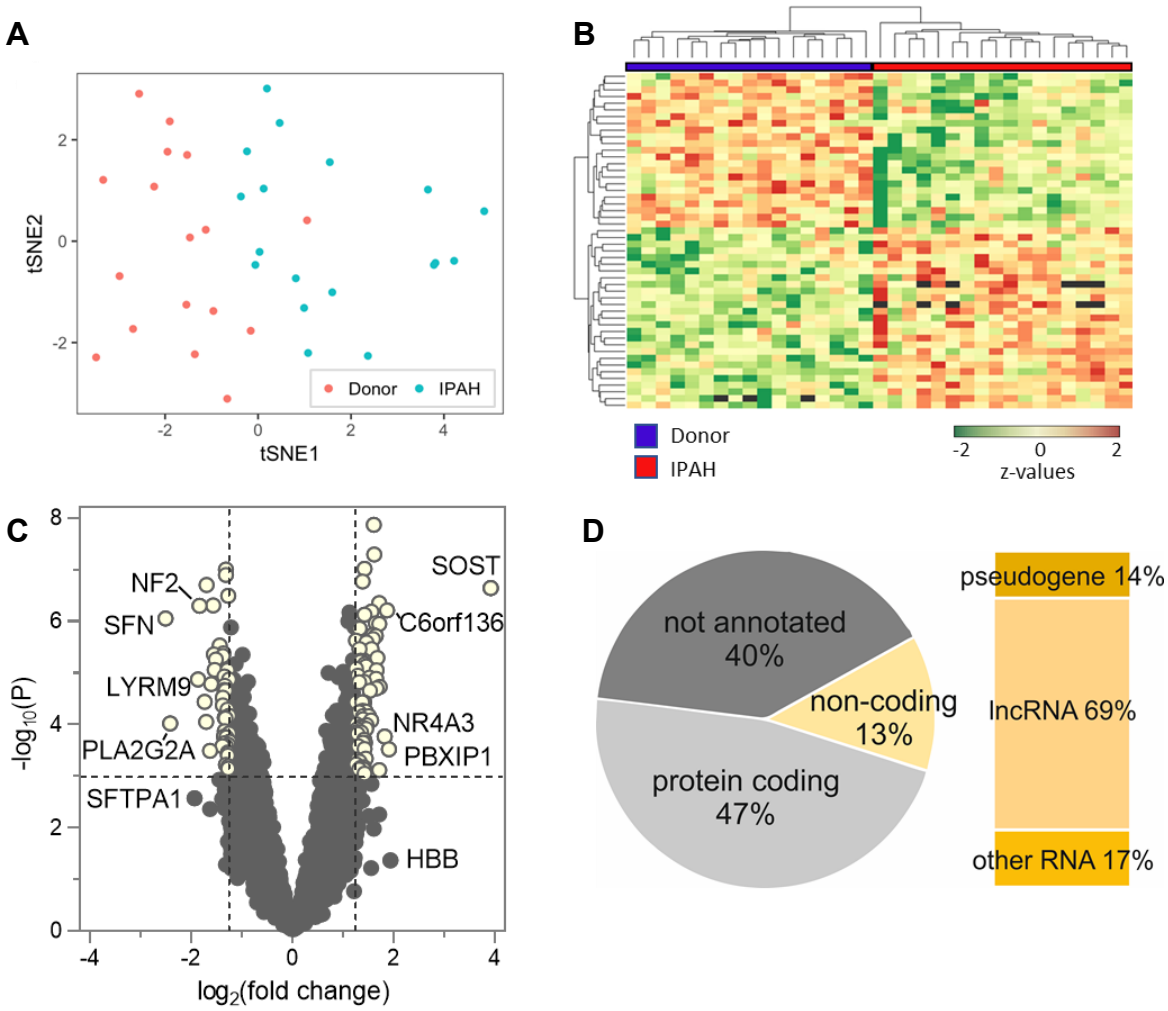

Figure 5. **Transcriptomic analysis of laser capture micro-dissected PA in donor and IPAH.** A) t-distributed stochastic neighbour embedding (t-SNE) analysis showing individual IPAH and donor samples. B) A heatmap with unsupervised hierarchical clustering representing the 50 most significantly regulated genes, demonstrating clear separation between the two groups. C) The volcano plot comprises the fold changes (log_2(fold change), LFC) and significances ($-log_{10}$(P)) calculated for each detected gene in our analysis. The genes with the strongest regulation (LFC) are labelled. D) Contribution of different RNA subtypes to IPAH transcriptome. Figures A and B were created with the help of Dr. Jochen Wilhelm, Justus-Liebig-University Giessen. Adapted from (141) in accordance with J Pathol. and the CC BY 4.0 license.

Table 9. **The strongest differential expressions among the protein coding genes.**

Gene ID	Gene Name	LFC	$-\log_{10}(P)$
SOST	Sclerostin	3,91	6,64
TMEM198	Transmembrane protein 198	1,71	6,35
NF2	Neurofibromin 2 (merlin)	-1,84	6,30
C6orf136	Chromosome 6 open reading frame 136	1,86	6,21
SFN	Stratifin	-2,51	6,05
ZWINT	ZW10 interacting kinetochore protein	1,71	5,95
LYRM9	LYR motif containing 9	-1,87	4,87
THSD4	Thrombospondin, type I, domain containing 4	1,72	4,73
SPON2	Spondin 2, extracellular matrix protein	-1,74	4,44
SPI1	Spi-1 proto-oncogene	-1,71	4,05
PLA2G2A	Phospholipase A2, group IIA (platelets, synovial fluid)	-2,42	4,02
NR4A3	Nuclear receptor subfamily 4, group A, member 3	1,82	3,77
PBXIP1	Pre-B-cell leukemia homeobox interacting protein 1	1,90	3,52
RFX2	Regulatory factor X, 2 (influences HLA class II expression)	1,71	3,12
SFTPA1	Surfactant protein A1	-1,94	2,57

Adapted from (99) in accordance with J Pathol. and the CC BY 4.0 license.

Functional enrichment analyses performed on the differentially regulated data set using the KEGG and GO ontology databases revealed perturbation in metabolic, immunological, cytoskeletal and proliferative processes in IPAH (Figure 6). A gene network analysis visualizes the central genes that are involved in the top 10 affected KEGG pathways. This exemplarily included gene members of the alpha-actin binding protein gene family (ACTN1, ACTN2, ACTN4), members of the integrin family (ITGA2, ITGA5, ITGB1, ITGB5) and gene members of the Toll-like receptor family (TLR2, TLR4) (Figure 7).

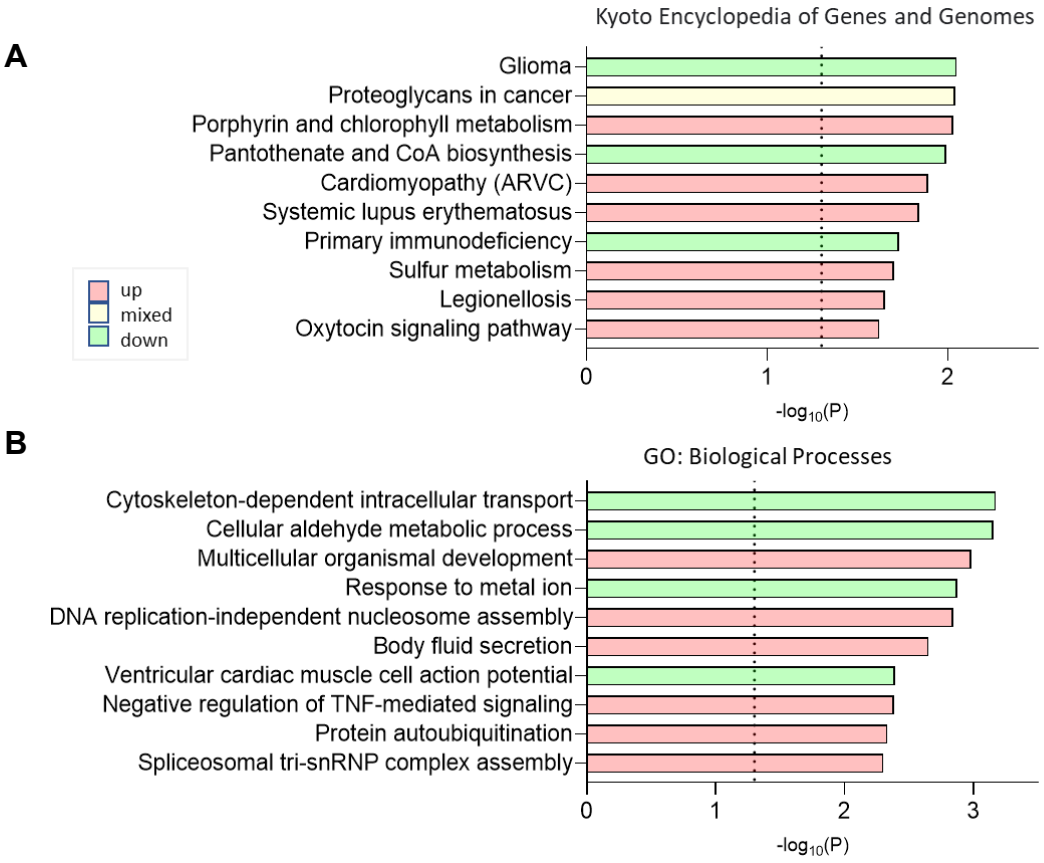

Figure 6. **Gene Set Enrichment Analysis of the differentially expressed coding genes in IPAH.** Top ten KEGG pathways (A) and top ten gene ontology (GO) terms for biological processes resulting from a gene set enrichment analysis using all significantly expressed genes are represented here. The direction of the regulation (annotated as up, down or mixed) is estimated depending in the total number of up or down regulated genes in the respective pathway/term. Adapted from (99) in accordance with J Pathol. and the CC BY 4.0 license.

KEGG and gene ontology analysis of overrepresented genes mainly indicated enrichment in neuronal and metabolic pathways, Relaxin and MAPK signalling, as well as in the biological processes revolving around metabolism, apoptosis and signal transduction (involving tyrosine receptor kinases and Notch signalling) and cartilage development (Figure 8). A comparable pathway analysis using the Reactome database showed most enrichment in PI3K, Notch and thrombin signalling and metabolic events (Figure 9A). Interestingly, our cellular component analysis of differentially regulated genes in IPAH suggested a sole enrichment for the ECM compartment (Figure 9B). Taken together, the different means of functional analysis all reveal

that fundamental biologic pathways are perturbed in IPAH, and they confirmed that ECM plays a central role in IPAH.

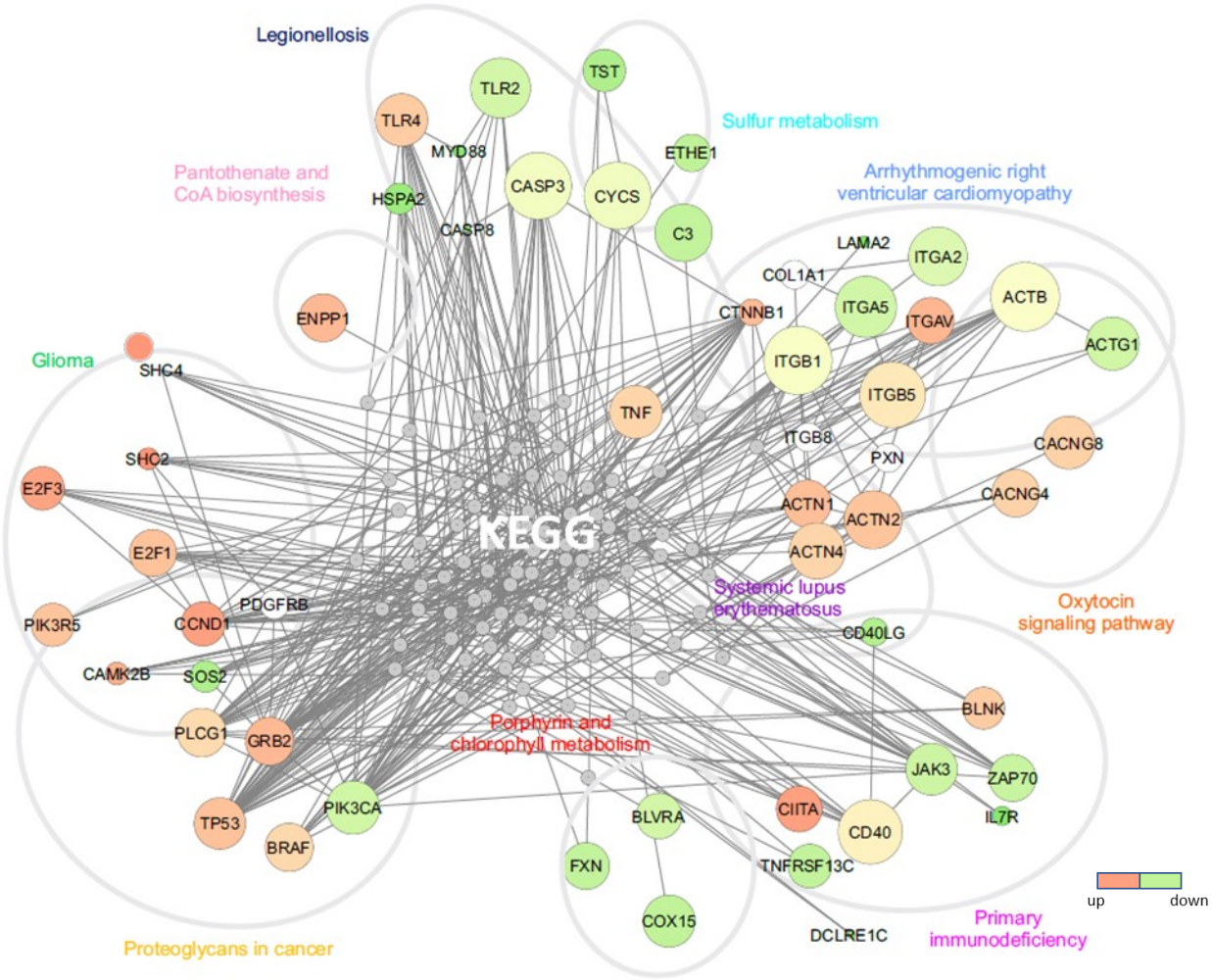

Figure 7. **Network of genes involved in the affected KEGG pathways in IPAH.** A minimum network representation was chosen to show protein-protein interactions and the regulatory tendency of the genes involved in the pathways regulated in IPAH as determined in Figure 6A (analysis performed using NetworkAnalyst (165), based on STRING interactome; confidence score: 900). Adapted from (99) in accordance with J Pathol. and the CC BY 4.0 license.

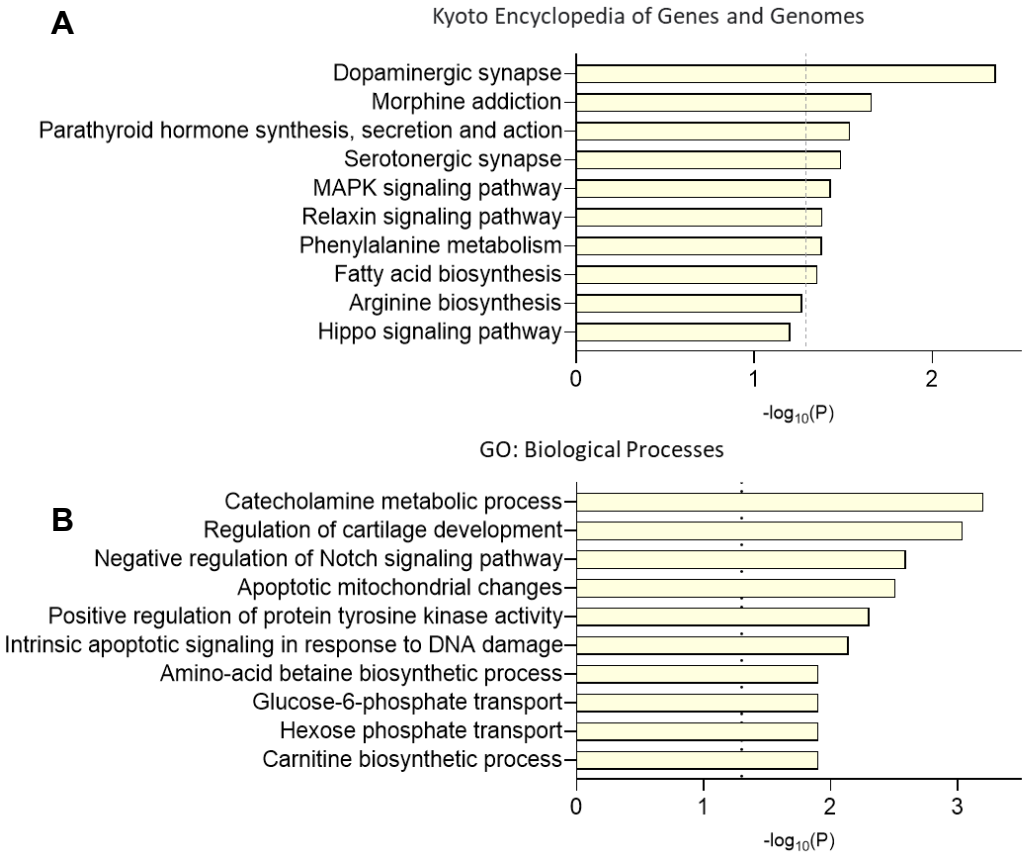

Figure 8. **Overrepresentation Analysis of the differentially expressed coding genes in IPAH - I.** Top ten KEGG pathways (A) and top ten gene ontology (GO) terms for biological processes resulting from an overrepresentation analysis, where the top 50 most significantly regulated coding genes are analyzed.

Knowing about the central role of the extracellular matrix in IPAH progression (31), as a next step, we focused on all ECM related genes that are regulated in IPAH pulmonary arteries by looking at their interactome and IPAH dependent regulation (Figure 10).

We found several collagens, metalloproteinases and other ECM components that are significantly regulated in IPAH PA. Exemplary, proteinases and proteinase inhibitors that showed altered expression in IPAH, reinforcing the reported proteolytic imbalance in IPAH (12, 38), included TIMP1, TIMP3, TIMP4, ADAM10 and MMP23B. ELN (Elastin; elastic fiber), FREM1 (FRAS1 Related Extracellular Matrix 1; a basement membrane protein), COL18A1 (Collagen XVIII; collagen of the multiplexin family) and RELN (Reelin; involved in cell-cell interaction) are examples of upregulated ECM components in IPAH. Exemplary genes that were downregulated in IPAH include SPON2 (Spondin2; a cell adhesion protein), MMRN1

(Multimerin; an adhesive protein) and LAMA2 (Laminin; an essential basement membrane component) (Figure 10). Interestingly, many of the ECM components, such as collagen IV, Collagen XVIII, Fibronectin, Laminin or FRAS1 Related Extracellular Matrix 1, detected in the transcriptomic ECM profiling in IPAH were particularly characteristic of the basement membrane (Figure 10).

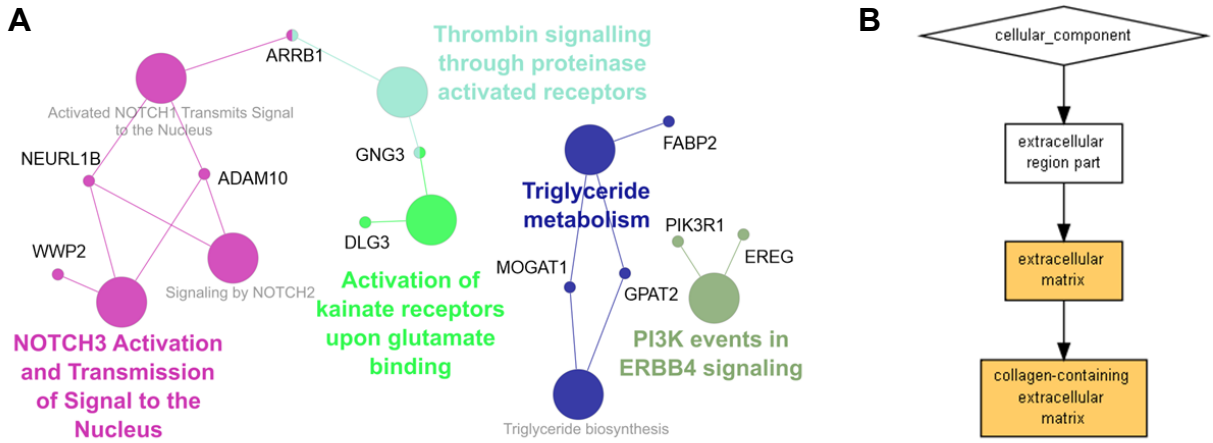

Figure 9. **Overrepresentation analysis of the differentially expressed coding genes in IPAH - II .** A) Reactome pathway analysis applying a cutoff of minimum significance ($-\log_{10}(P)$) of 3 and a minimum absolute $\log_2$(fold change) (LFC) of 1.25 as margined in Figure 5C. B) Gene Ontology analysis (performed by GOrilla analysis (148, 166): Cellular Component Analysis applying a cutoff of LFC I1I; $-\log_{10}(P) > 1.3$ against background) showing sole enrichment for ECM for cellular components.

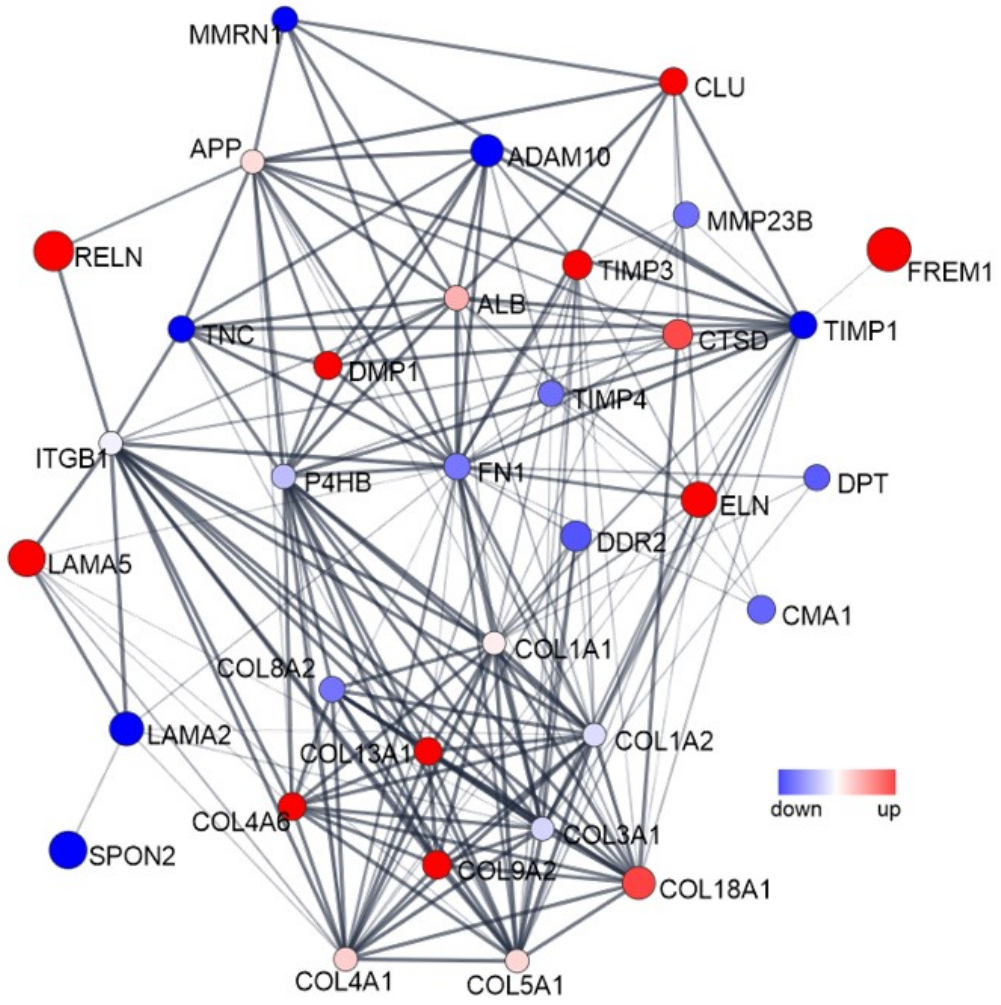

Figure 10. **Transcriptomic ECM profile.** Network analysis (Cytoscape 7.8; String Database) was performed on the ECM related genes significantly regulated in IPAH in comparison to healthy controls. The node size reflects the significance, the color coding the regulation in IPAH, and the edge thickness the weight of the relation between the molecules.

Additional to the microarray, we also explored the expression of several selected ECM components via qRT-PCR using RNA samples from laser-capture microdissected pulmonary arteries (Figure 11). Here we detected a significant upregulation of DCN (Decorin), COL14A1 (Collagen Type XIV Alpha 1 Chain), FBLN1 (Fibulin 1), AGRN (Agrin) and COL4A5 (Collagen Type IV Alpha 5 Chain) in the small PA. Furthermore, due to previous reports that show positive correlation of collagen XVIII (COL18A1) and its cleavage product Endostatin with IPAH disease severity (12, 77), we also had a closer look at COL18A1 in IPAH. Confirming our finding from the microarray experiment, qRT-PCR confirmed the significant upregulation of COL18A1 in the small PA of IPAH (Figure 11).

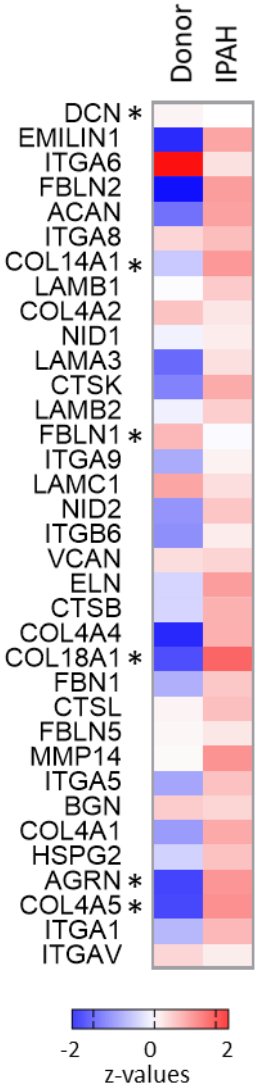

Figure 11. **Differential gene expression of ECM components in IPAH.** Gene expression values (z-scores) for selected ECM related genes in donor (n = 7-12) and IPAH (n=9-12) samples as determined by qRT-PCR. * = $p < 0.05$ as determined by Student's t-test. Adapted from (167) with permission of the American Thoracic Society.

3.2 Expressional changes in IPAH – the non-coding profile

A significant part of the transcriptome that is dysregulated in IPAH consist of non-coding RNAs (ncRNA) (Figure 5D). These include pseudogenes (duplicate, non-translated/defective DNA copies resembling functional genes (168)), long intergenic non-coding RNAs (lincRNA; a subgroup of lncRNA), antisense RNAs (asRNA; transcribed from opposite strand of coding or

non-coding genes; comprises long and short non-coding RNAs (169)) and other long and small ncRNA transcripts (Figure 5D). Therefore, in our next step, we explored the potential role of ncRNAs in IPAH.

The ncRNA profile of IPAH and donor groups showed clear differences in their transcriptional identity, as evident in the hierarchical clustering performed in Figure 12. We found a total of 146 regulated non-coding genes (excluding non-annotated transcripts and pseudogenes) that contribute to the changes resulting in the unique transcriptomic environment of IPAH vessels. A heatmap representation of the top 50 most significantly regulated ncRNAs is given in Figure 12. The global distribution of all detected non-coding genes, as well as the list of the top regulations are given in Figure 13. Taken together, our transcriptomic analysis revealed that the non-coding transcriptome adds an equally significant value as the coding transcriptome to the altered IPAH landscape.

The differential expression of the listed seven most regulated lncRNAs was additionally analyzed by qRT-PCR for verification. We could confirm the upregulation in IPAH PA for the lncRNA TUSC8 and PAXIP1-AS1 (Figure 14). Having validated TUSC8 and PAXIP1-AS1 upregulation, we further explored current literature at the time to gather all information available on these two lncRNAs.

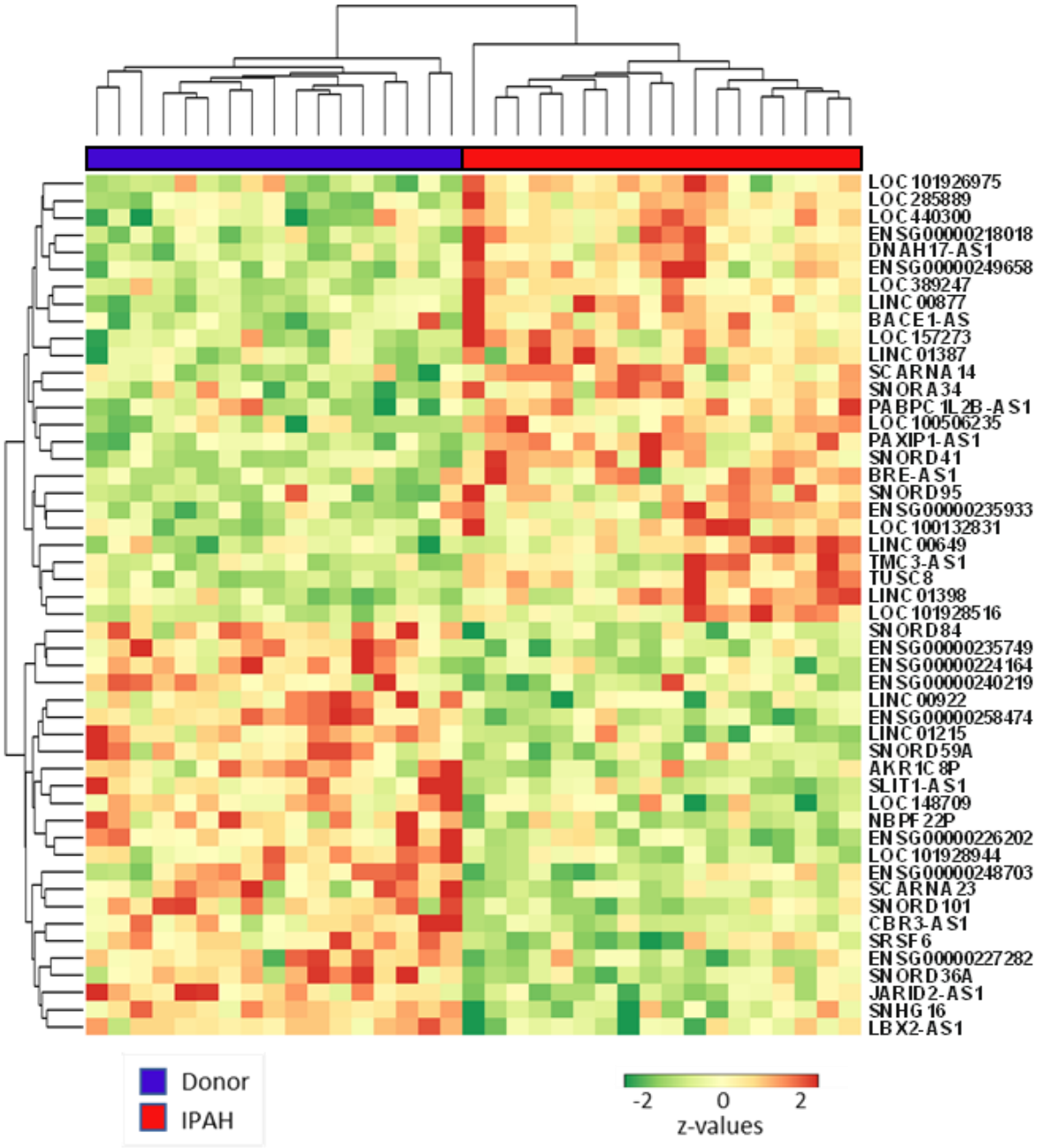

Figure 12. **Non-coding transcriptome in IPAH - I.** A heatmap representation of the 50 most significantly regulated non-protein coding genes in IPAH with unsupervised hierarchical clustering separating the two groups. The heatmap was created with the help of Dr. Jochen Wilhelm, Justus-Liebig-University Giessen. Adapted from (99) in accordance with J Pathol. and the CC BY 4.0 license.

A

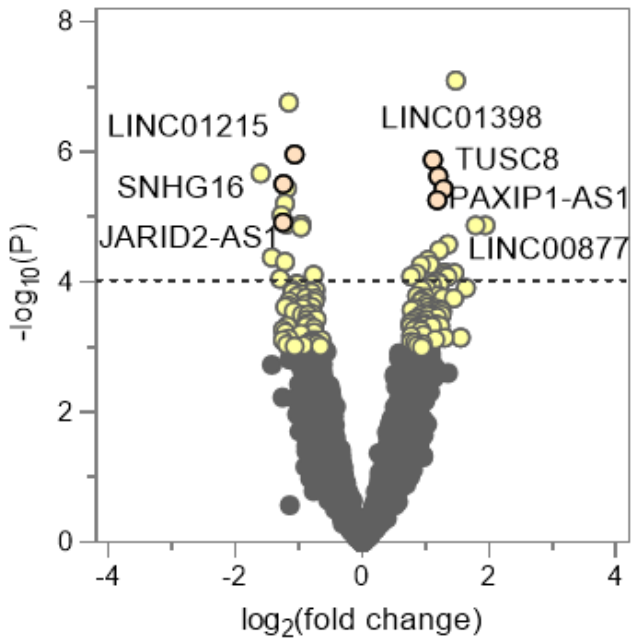

B

Gene	log_2(FC)	$-log_{10}$(P)
LINC01215	-1.07	5.96
LINC01398	1.11	5.88
TUSC8	1.20	5.63
SNHG16	-1.24	5.51
PAXIP1-AS1	1.28	5.43
LINC00877	1.18	5.26
JARID2-AS1	-1.25	4.92

Figure 13. **Non-coding transcriptome in IPAH - II.** A) A Volcano plot shows the global distribution of all expressed non-coding RNAs. B) Top seven lncRNAs and their respective LFC and significances. Adapted from (99) in accordance with J Pathol. and the CC BY 4.0 license.

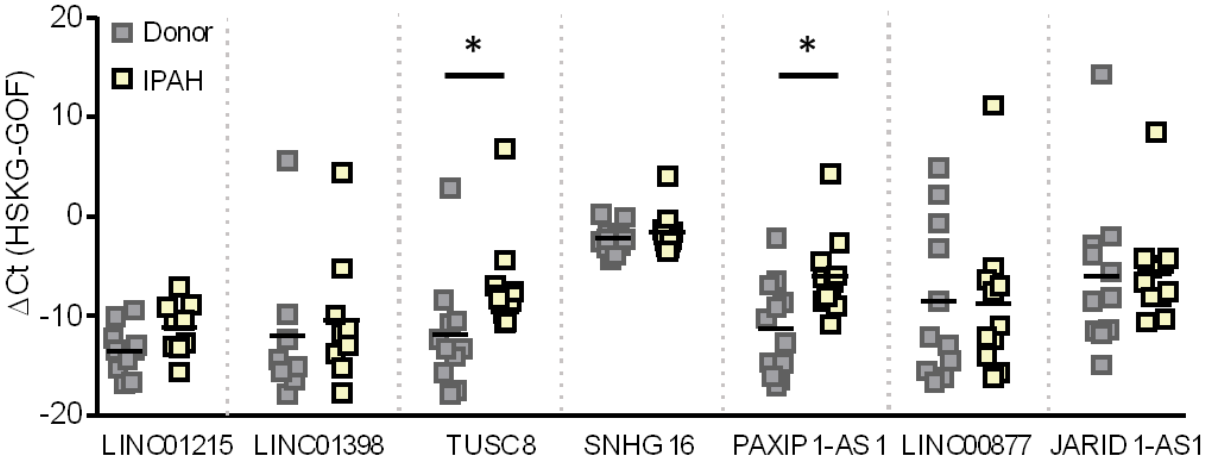

Figure 14. **qRT-PCR verification.** qRT-PCR performed to validate the regulation of the top lncRNA candidates that were detected as differentially expressed in the microarray experiment as listed in Figure 13B. * = $p < 0.05$ as determined by Mann-Whitney-test. Adapted from (99) in accordance with J Pathol. and the CC BY 4.0 license.

TUSC8, or tumor suppressor candidate 8, had been shown to inhibit colorectal cancer by inhibiting proliferation and shown associations with osteosarcoma development (170, 171). In terms of PAXIP1-AS1, the one publication available at the time, suggested the involvement of PAXIP1-AS1 as a regulator of cell death (172).

Both lncRNAs were encouraging to be explored further for involvement in IPAH, as literature suggested a possible entanglement of these lncRNA with proliferative and apoptotic processes; processes that are also central to PAH pathobiology.

3.3 The long non-coding RNA PAXIP1-AS1 in IPAH

Taking a decision to start with PAXIP1-AS1, we moved forward to characterize the lncRNA PAXIP1-AS1 by exploring nucleotide databases and sequence analysis tools. The forward-stranded lncRNA, which meanwhile is re-named to PAXIP1-DT, lies on Chromosome 7 (7q36.2), consists of a single exon and is 2271 bases long (Figure 15).

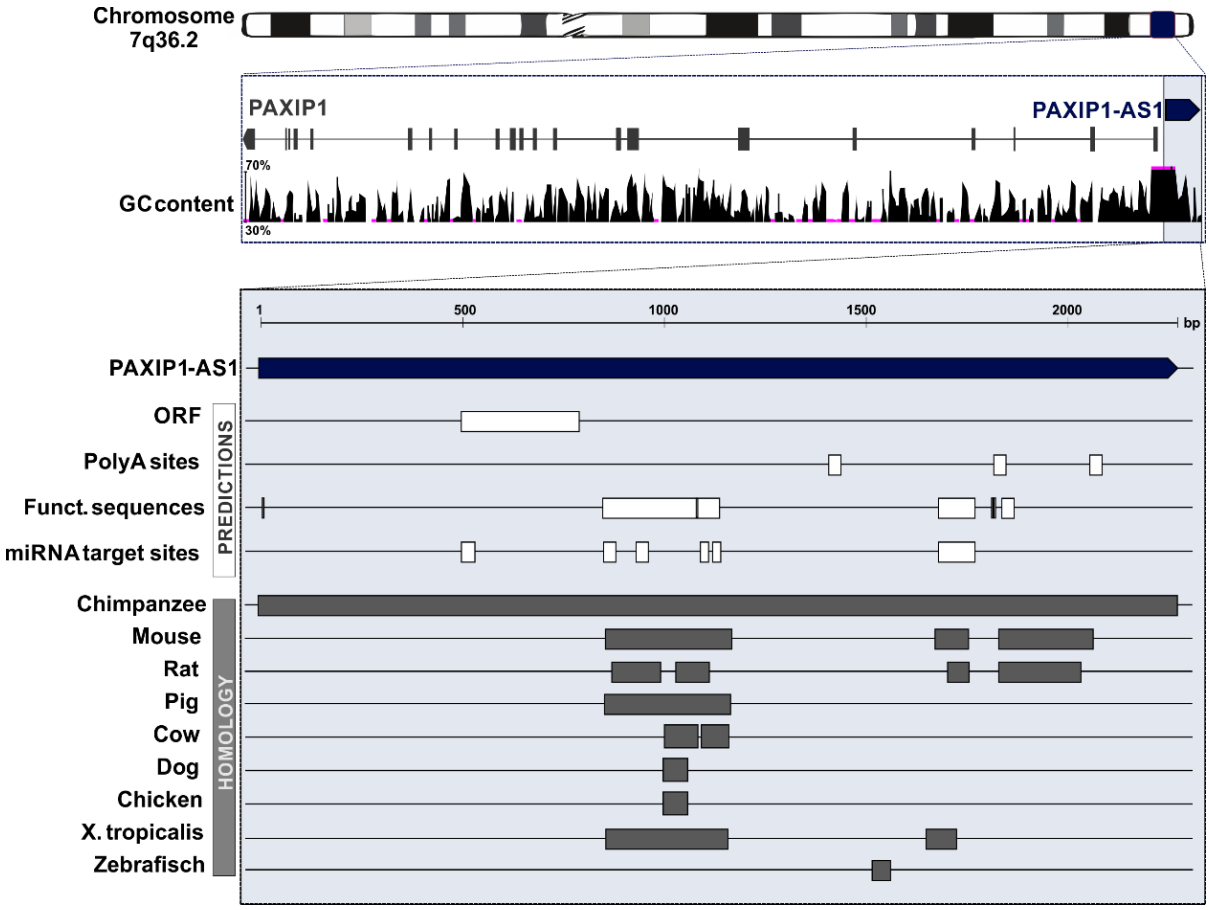

Figure 15. **PAXIP1-AS1**. Characteristics of the lncRNA PAXIP1-AS1 transcript is summarized in this image adapted from the entry in UCSC Genome Browser on Human,

December 2013 (GRCh38/hg38) Assembly; UCSC ID: ENST00000608317.1, and the analysis results won using BLASTN 2.13.0+ (173) and the online tool RegRNA.2.0 (154). Several predicted functional features of this lncRNA as well as homologous regions in the transcript are highlighted. Adapted from (99) in accordance with J Pathol. and the CC BY 4.0 license.

The terming PAXIP1-AS1 leads to the wrong assumption that this lncRNA is an anti-sense RNA (asRNA), with a complementary sequence to its neighbouring coding gene PAXIP1 on the reverse strand. In fact, PAXIP1-AS1 is a divergent transcript that has no overlapping, complementary region with PAXIP1. Around 250 bp separate the two genes; but they share a common promoter region due to their proximity (see the course of GC content in Figure 15; GC-rich regions are characteristic of promoter regions (174)). Further *in silico* analyses revealed that the PAXIP1-AS1 sequence harbours several interesting, functionally important RNA features: several Alu elements, SRP RNA regions (RNA components of the signal recognition particle), A- and C-repeats, and an AU-rich element were identified in the sequence (see Figure 15 and Table 10).

Table 10. **Functional motives in PAXIP1-AS1**

Motif Type	Position
Open reading frame (ORF)	508 ~ 798
Polyadenylation sites	1416 ~ 1447
	1819 ~ 1850
	2056 ~ 2087
AU-rich element	1852 ~ 1864
SRP RNA/7SL RNA sequences and Alu elements	865 ~ 1152
	1667 ~ 1764
Repeats	12 - 20
	1150 - 1158
	1791 - 1799
	1810 - 1819

Adapted from (99) in accordance with J Pathol. and the CC BY 4.0 license.

Moreover, it showed that PAXIP1-AS1 harbours a number of binding sites for miRNA (see Table 11) and transcription factors (Figure 16). The plethora of TF and miRNA bindings sites identified inside the PAXIP1-AS1 transcript likely hints towards its functional importance. This lncRNA transcript may exert its function by binding TFs and miRNAs (111), and either escorting them to certain sites, serving as storages, or by binding and stopping them from fulfilling their

original function . Interestingly, we found that PAXIP1-AS1 also harbors an open reading frame (Figure 15); coding potential calculations as performed by two independent algorithms (CPAT (156) and CPC (155)) nevertheless suggested less protein coding potential for this RNA.

Table 11. **miRNA binding sites in PAXIP1-AS1**

miRNA	Binding position	Length
hsa-miR-1303	1131 ~ 1152	22
hsa-miR-3159	879 ~ 900	22
hsa-miR-3202	523 ~ 544	22
hsa-miR-4430	1105 ~ 1123	19
hsa-miR-5095	875 ~ 895	21
hsa-miR-5096	954 ~ 974	21

Adapted from (99) in accordance with J Pathol. and the CC BY 4.0 license.

Results of a BLAST search, carried out with BLASTN 2.13.0+ suggest that PAXIP1-AS1 lacks conservation across species beyond primates (overall conservation in chimpanzees: 100% coverage, >97% identity; in mice: <19% coverage, ~83% identity; in rats: <5% coverage, and ~76% identity) (Figure 15). This observation is in accordance with a vast majority of lncRNAs, as most of them tend to be poorly conserved with regard to nucleotide sequence similarity, expect short stretches that usually encode functional sequences (111). In the case of PAXIP1-AS1, the little homology observed across species also exactly falls into the regions with predicted functional importance (Figure 15).

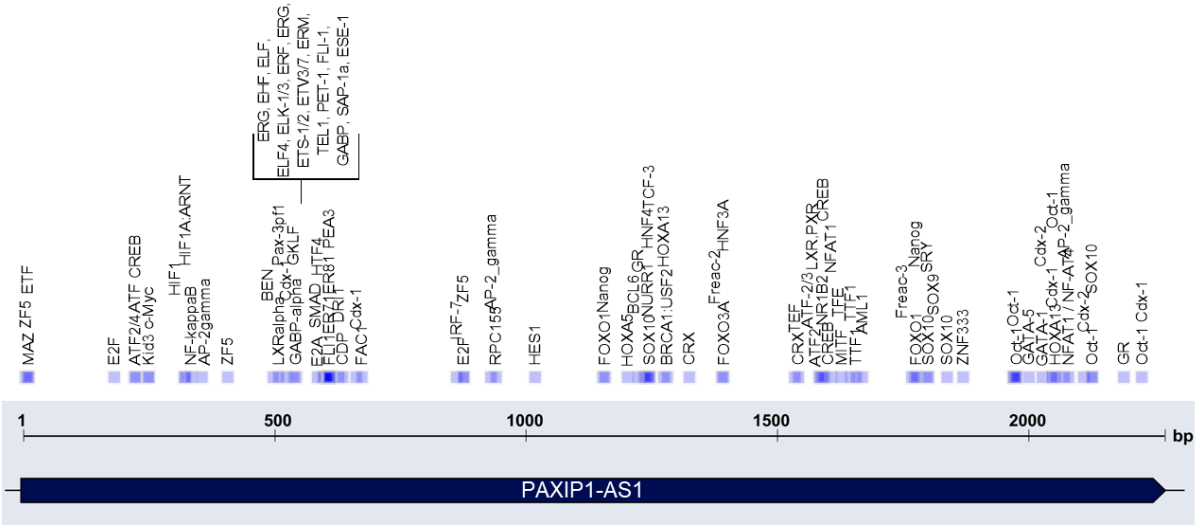

Figure 16 **Transcription factor binding sites.** Visualization of the binding sites for transcription factors in PAXIP1-AS1. Adapted from (99) in accordance with J Pathol. and the CC BY 4.0 license.

Contrary to the poor sequential conservation level, lncRNA are more preserved at structural and functional levels (111). We here used a dynamic programming algorithm developed by Mathews et al. that combines the free energy model with chemical modification constraints, to predict the secondary structure of PAXIP1-AS1 (157, 175). The secondary structure prediction of PAXIP1-AS1 resulted in a complex assembly consisting of several stem and loop structures, including: stems (e.g. at position 1320), bulges (e.g. at position 929), hairpin loops (e.g. at position 965-980), multiway junction loops (e.g. at position 25), internal loops (e.g. at position 840), kissing hairpins (e.g. at position 1120) and pseudoknots (e.g. at position ~1600, 1820) (Figure 17).

The cumulated occurrence of functional elements, binding sites and the structural complexity, all together speak in favour of substantial functional importance of this lncRNA.
Due to their stability, circular variants of lncRNA (circRNA) serve as exceptional tools to be used as biomarkers for diseases (176). Therefore, we explored publicly available circRNA datasets (177) to judge the circRNA potential for PAXIP1-AS1. No circRNA prediction was identified for PAXIP1-AS1 using this database.

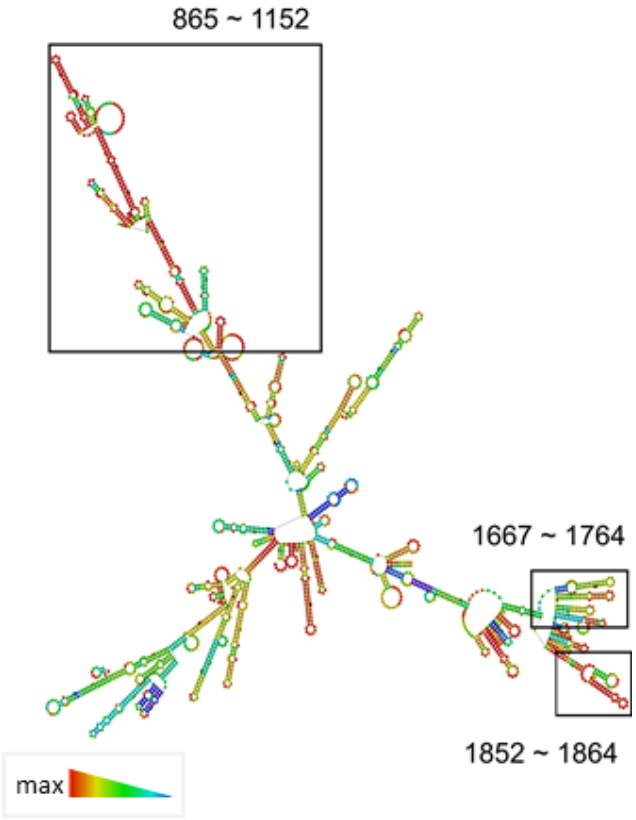

Figure 17. **PAXIP1-AS1 structure.** The secondary RNA structure predicted (using the Vienna RNA Websuite (157)) as per partition function and base-pairing probability matrix in addition to the minimum free energy (MFE) structure reveals the most optimal composition

at ΔG = −776.20 kcal/mol. The annotation of the regions marks the sites of functional importance as shown in Figure 15 and Table 4. The colour coding represents base-pairing probabilities (red = most likely; colour at unpaired regions denotes probability of being unpaired). Reproduced from (99) in accordance with J Pathol. and the CC BY 4.0 license.

Further characterizing the lncRNA, we next explored a public gene expression database, the GTEX portal, to outline the overall expression of PAXIP1-AS1 in different tissues (Figure 18). Here, a low, but ubiquitous expression was observed for this lncRNA across the different tissues, with a notable enrichment in the cerebellum. In our first step, we had already validated that PAXIP1-AS1 is expressed in the arteries of the lungs (Figure 14). To have a closer look at the PAXIP1-AS1 abundance circumjacent to the PA, we performed fluorescence in situ hybridization on lung sections and visualized PAXIP1-AS1 localization (Figure 19). We found PAXIP1-AS1 expression distributed all around in the lung, with more abundance in aSMA (α-smooth muscle actin, ACTA2; a terminal PASMC differentiation marker) co-expressing sections.

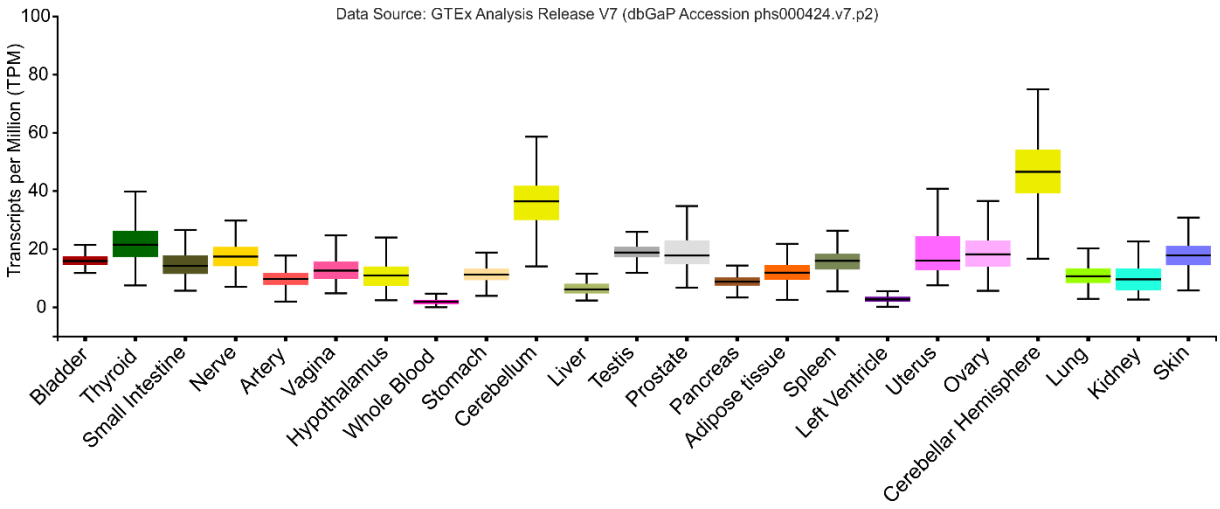

Figure 18. **PAXIP1-AS1 expression in different tissues.** Data illustrated here comes from various RNASeq experiments and is obtained from the GTEx Portal, on 1 August 2018 and has the dbGaP accession number phs000424.v7.p2. Adapted from (99) in accordance with J Pathol. and the CC BY 4.0 license.

Adding more light to the spatial expression of PAXIP1-AS1, the qRT-PCR revealed PAXIP1-AS1 to be most abundant in the pulmonary artery smooth muscle cells (PASMC) within the PA, while the parenchymal fibroblasts (pFB) also showed very good expression of this lncRNA (Figure 20).

Subsequently, we looked at the expression of PAXIP1-AS1 in donor and IPAH PASMC, and found that PASMC significantly contribute to the upregulation of PAXIP1-AS1 we observed in IPAH pulmonary arteries (Figure 21). This upregulation in isolated PASMC was supported by the fluorescence in situ hybridization performed with PAXIP1-AS1 probes (Figure 22). Keeping in mind that compartment-specific expression and the subcellular localization can be determinant of the functional property of lncRNA, it was also noted that PAXIP1-AS1 expression was present in the cytoplasm as well as in the nucleus (Figure 22).

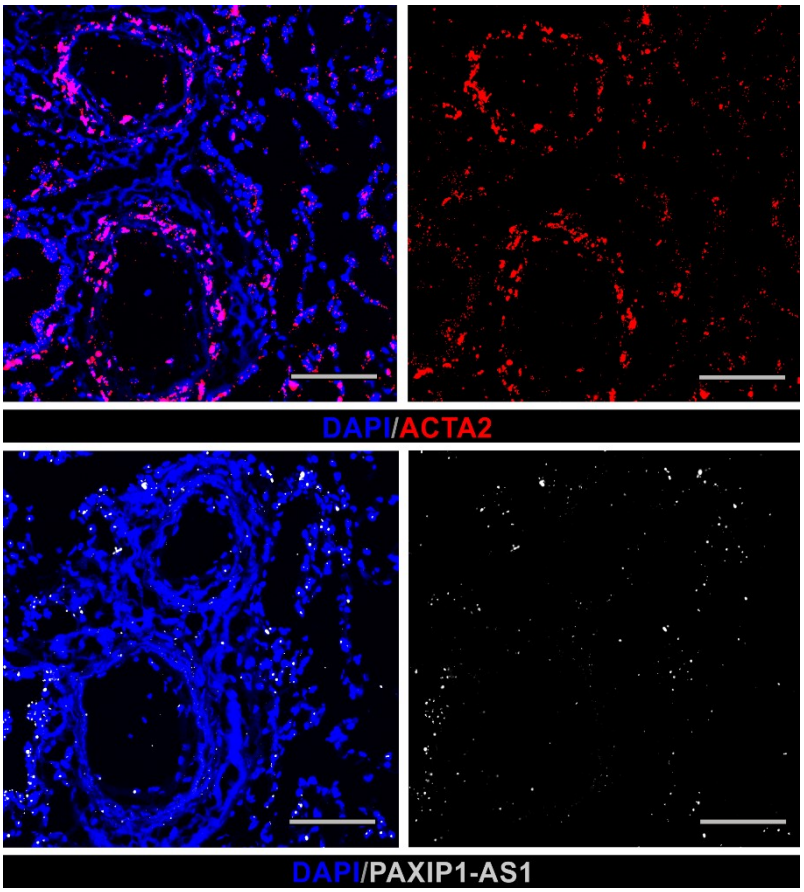

Figure 19. **PAXIP1-AS1 in the lung.** Representative fluorescence in situ hybridisation images of ACTA2 (in red) and PAXIP1-AS1 (in grey) on serial cryo sections (5 µm) of IPAH lungs (n = 2). The scale bar indicate 100 µm. Reproduced from (99) in accordance with J Pathol. and the CC BY 4.0 license.

Because a substantial PAXIP1-AS1 expression was also detected also outside the pulmonary arteries (Figure 19, Figure 20), we compared the expression of PAXIP1-AS1 in donor and IPAH parenchymal fibroblasts, but detected no differences (Figure 23A). On the other hand, PAXIP1-AS1 expression was significantly upregulated in the pulmonary artery adventitial

fibroblasts (PAAdFB) (Figure 23B), underlining the specific upregulation of this lncRNA in the pulmonary arteries in IPAH, not in the parenchyma.

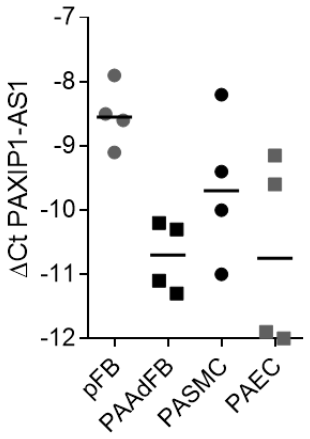

Figure 20. **PAXIP1-AS1 expression in PA compartments.** qRT-PCR was performed to measure PAXIP1-AS1 expression in pulmonary cells (pFB, parenchymal fibroblasts; PAAdFB, pulmonary artery adventitial fibroblasts; PASMC, pulmonary artery smooth muscle cells; PAEC, pulmonary artery endothelial cells). Adapted from (99) in accordance with J Pathol. and the CC BY 4.0 license.

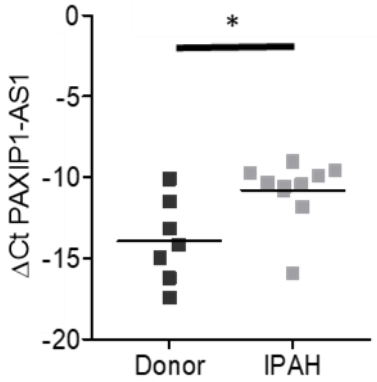

Figure 21. **PAXIP1-AS1 in PASMC - I.** qRT-PCR was applied to measure PAXIP1-AS1 expression in isolated PASMC samples. * = $p < 0.05$ as determined by Mann-Whitney-test. Adapted from (99) in accordance with J Pathol. and the CC BY 4.0 license.

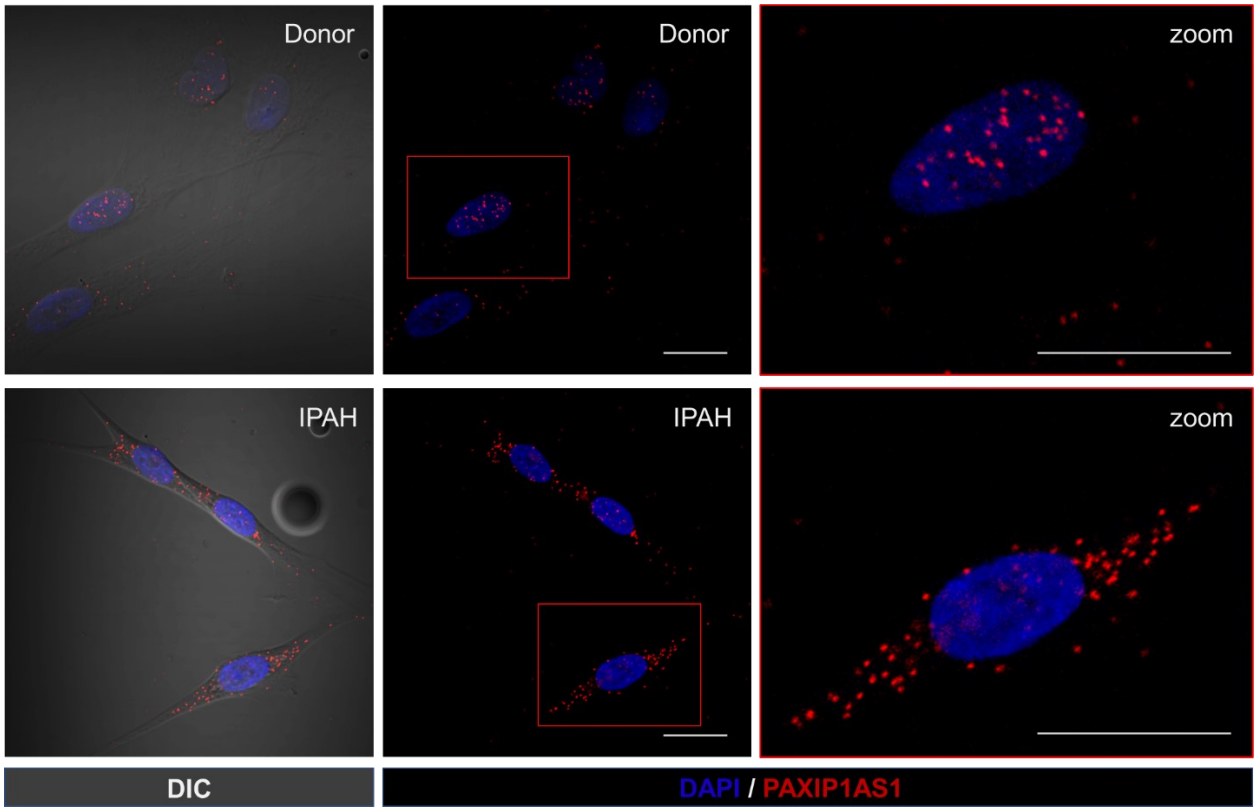

Figure 22. **PAXIP1-AS1 in PASMC - II.** Representative images of fluorescence in situ hybridisation that was performed for PAXIP1-AS1 on isolated donor (n=2) and IPAH (n=2) PASMC. The scale bar indicate 50 µm. DIC, Differential interference contrast/light microscopy image. Data as published in (99).

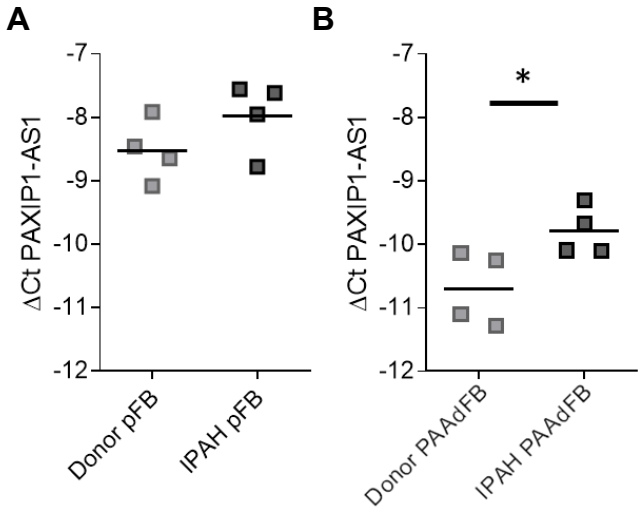

Figure 23. **PAXIP1-AS1 in IPAH fibroblasts.** PAXIP1-AS1 expression as measured via qRT-PCR in donor and IPAH parenchymal fibroblasts (pFB) (A) and pulmonary artery adventitial fibroblasts (PAAdFB) (B). * = $p < 0.05$ as determined by Mann-Whitney-test. Adapted from (99) in accordance with J Pathol. and the CC BY 4.0 license.

PAXIP1-AS1 and its eponym and coding, neighbouring gene PAXIP1 are separated from each other only by a GC-rich region of around 250 bases (Figure 15). Therefore, a coregulation of these genes seemed very likely. Furthermore, there was already one previous report suggesting PAXIP1-AS1 downregulation went hand in hand with PAXIP1 expression in HEK-293 cells (172). PAXIP1, or PAX interacting protein 1, is a coding gene that plays a critical role in maintaining genome stability, in early development and DNA damage response (178). It has three known coding transcripts: two longer and one short isoform (Figure 24A). We designed primers to distinguish the two longer transcripts (primers covering exons 17 to 18) from the short transcript (primers covering exon 2 to 3) and looked at PAXIP1 expression in IPAH PASMC. A significant upregulation was detected for the longer transcripts of PAXIP1, while the expression of the small transcript remained indifferent (Figure 24B). We further verified the upregulation of PAXIP1 in IPAH via immunohistochemical staining (Figure 24C). Here, a higher PAXIP1 expression could be visualized in the remodelled vessels of IPAH, confirming the qRT-PCR data. The first look into PAXIP1 suggest this neighbouring coding protein is a promising player in PAXIP1-AS1 interactome.

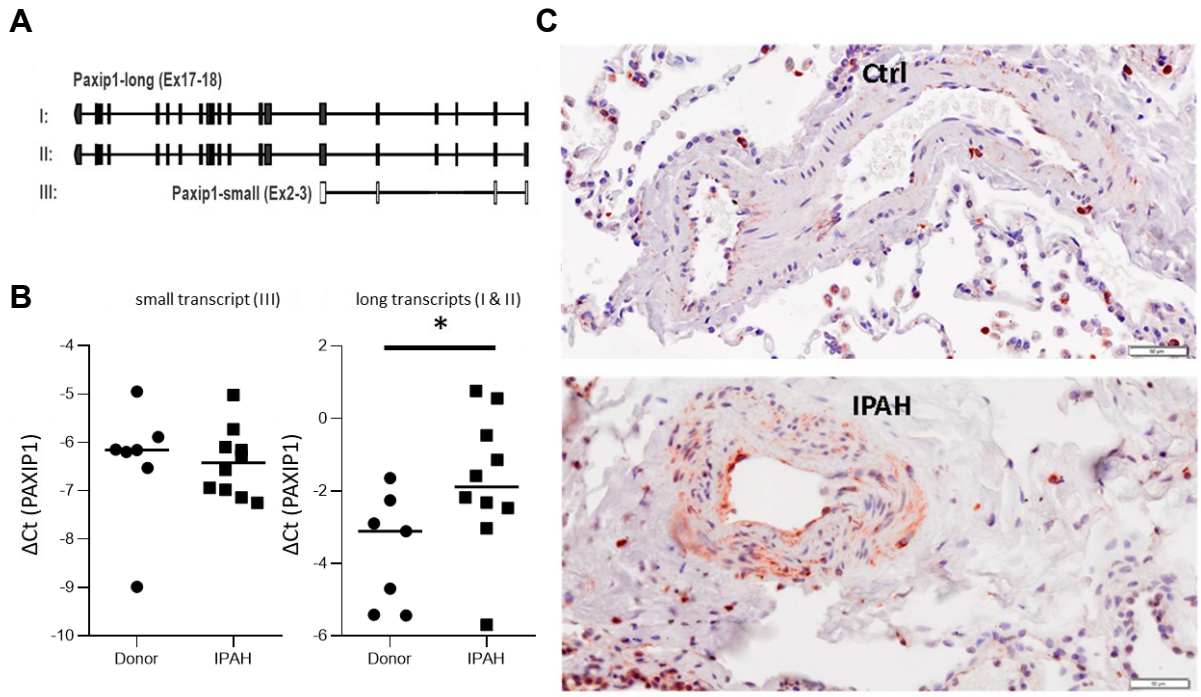

Figure 24. **Neighbouring protein Paxip1 in IPAH.** A) Representation of the three Paxip1 coding transcripts adapted from the entry in UCSC Genome Browser on Human, December 2013 (GRCh38/hg38) Assembly; UCSC ID: ENST00000404141.6; B) qRT-PCR results of Paxip1 transcripts in donor and IPAH PASMC. * = $p < 0.05$ as determined by Student's t test. C) Paxip1 immunohistochemical staining in donor (Ctrl) and IPAH lung sections (paraffin, 2.5 µm) (blue, DAPI; red, Paxip1).

Another aspect that we wanted to investigate was whether PAXIP1-AS1 can be modulated by mediators involved in the pathogenesis of IPAH. Therefore, we analyzed the expression of PAXIP1-AS1 after stimulating the cells with PDGF (platelet-derived growth factor), TNF-α (tumor necrosis factor alpha), ET-1 (endothelin-1), TGF-β (transforming growth factor beta) and IL-1β (interleukin 1 beta). Indeed, treatment with ET-1 lead to an increased PAXIP1-AS1 expression after 24h (Figure 25).

Together with the complex RNA structure, functional sequences, miRNA/TF binding sites, the coregulation with PAXIP1 and the sensitivity to ET-1 treatment, many promising doors opened for investigating and further characterization of the lncRNA PAXIP1-AS1. Next, we decided to systematically explore all affected genes downstream of PAXIP1-AS1 by analyzing the PASMC transcriptome after PAXIP1-AS1 knockdown. Figure 26 shows that PAXIP1-AS1 expression could be efficiently decreased by both GapmeRs and siRNAs.

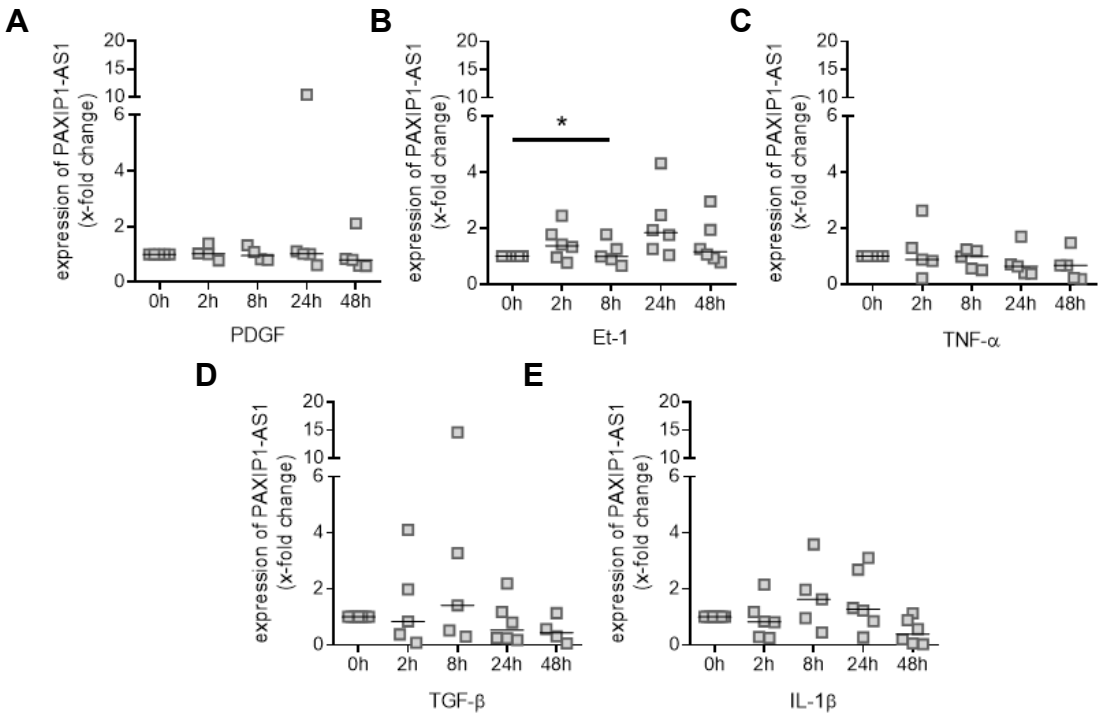

Figure 25. **PAXIP1-AS1 expression in response to various stimuli.** Analysis of PAXIP1-AS1 expression in PASMCs stimulated with (A) PDGF (10 ng/ml), (B) ET-1 (500 nM), (C) TNF-α (10 ng/ml), (D) TGF-β (10 ng/ml) and (E) IL-1β (10 ng/ml). * = $p<0.05$ as performed by one-way ANOVA with Dunnett's post hoc test. PDGF, platelet-derived growth factor; TNF-α, tumor necrosis factor alpha; Et-1, Endothelin-1; TGF-β, Transforming growth factor beta; IL-1β, Interleukin. Adapted from (99) in accordance with J Pathol. and the CC BY 4.0 license.

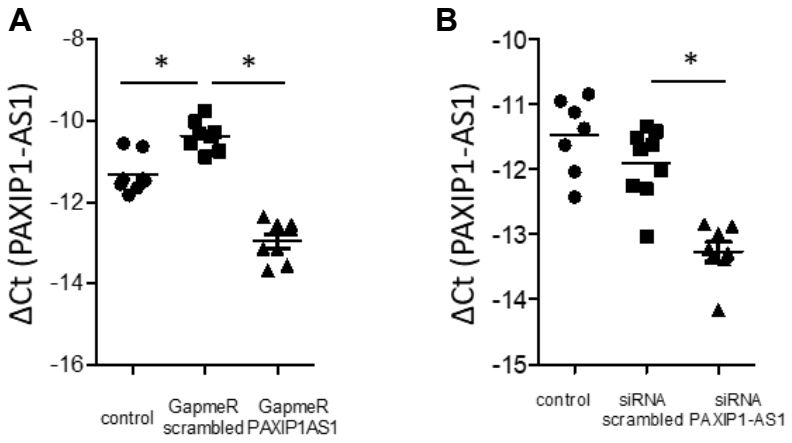

Figure 26. **PAXIP1-AS1 knock down.** PAXIP1-AS1 expression as determined via qRT-PCR after GapmeR (A) or siRNA (B) mediated knock down in PASMC. Adapted from (99) in accordance with J Pathol. and the CC BY 4.0 license.

Followingly, we performed a gene expression analysis on PASMC using microarrays after GapmeR mediated knockdown of PAXIP1-AS1. This microarray experiment was performed in collaboration with Dr. Matthias Brock, University of Zürich and Dr. Jochen Wilhelm from the Justus-Liebig-University Giessen.

To rule out any corruption of the results owing to transcriptional differences caused by the application of GapmeRs themselves, we also included non-transfected negative PASMC controls in the comparative analysis, together with PASMC samples treated with non-targeting scrambled GapmeRs and PAXIP1-AS1 targeting GapmeRs. First, we visualized the global distribution of the detected genes, and saw that a vast number of genes were captured as significantly expressed, with strong changes in expression (LFC) after PAXIP1-AS1 knockdown (Figure 27A). The heatmap representation of the top 100 most significantly regulated genes demonstrates that the untreated control samples give similar expressional values as the scrambled GapmeR samples, while the PAXIP1-AS1 GapmeR silenced samples clearly cluster from the control groups (Figure 27B).

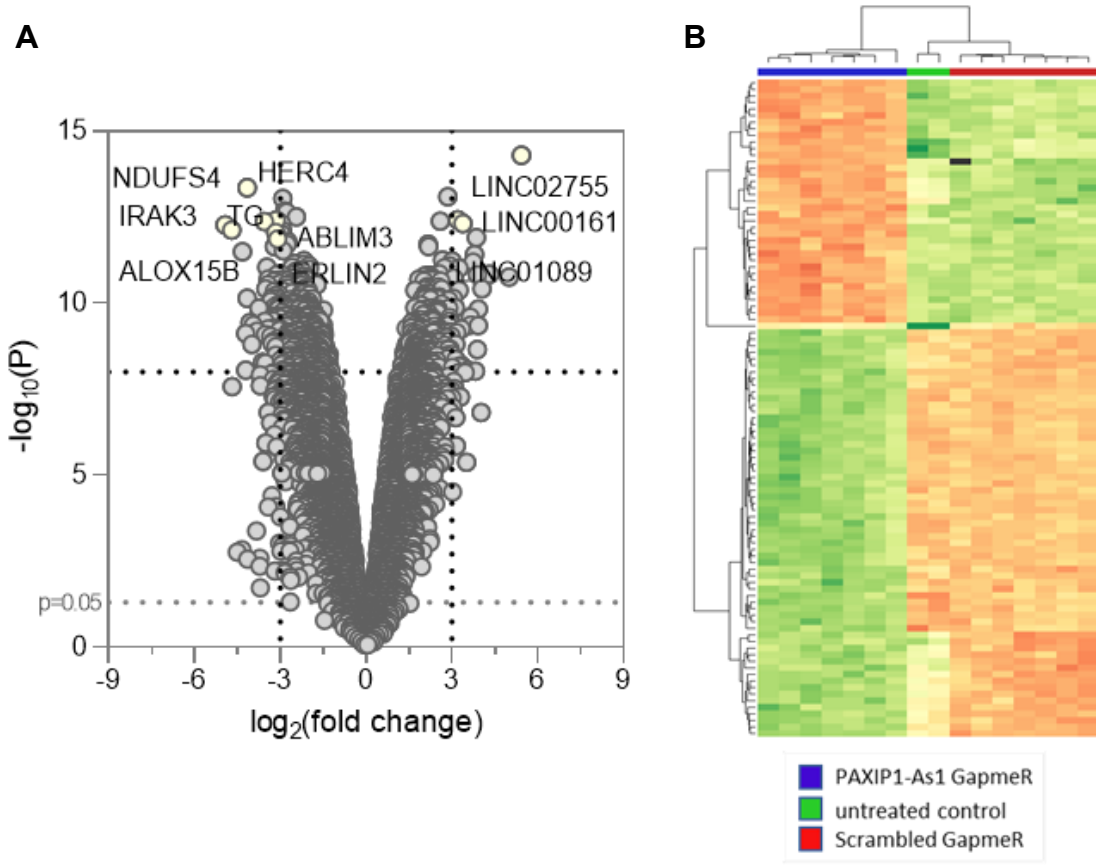

Figure 27. **Downstream genes of PAXIP1-AS 1.** A) Global distribution of all detected genes in the transcriptomic analysis of PASMC after knockdown of PAXIP1-AS1 via GapmeRs. B) Heatmap representing the top 100 most significantly differentially regulated genes. The heatmap was created with the help of Dr. Jochen Wilhelm, Justus-Liebig-University Giessen. Adapted from (99) in accordance with J Pathol. and the CC BY 4.0 license.

A global gene set enrichment analysis using the KEGG database delivered an overview of pathways perturbed after PAXIP1-AS1 knock down (Figure 28A). Interestingly, the pathways affected by PAXIP1-AS1 knock down included protein processing, cytoskeletal interaction at focal adhesions, extracellular matrix, and pathways implicated in metabolic and proliferative processes; all processes that have been previously associated with PAH pathophysiology (50, 60, 179). While having a closer look at the single genes contributing to the regulated KEGG pathways in IPAH (Figure 28B), we noticed that Paxillin (PXN), a focal adhesion adaptor protein, was involved in the downstream signalling of PAXIP1-AS1 perturbing focal adhesion and cancer related pathways. Due to a former study proving involvement of Paxillin in IPAH (59), we added Paxillin to the list of potential candidates that may be under control of the PAXIP1-AS1 axis.

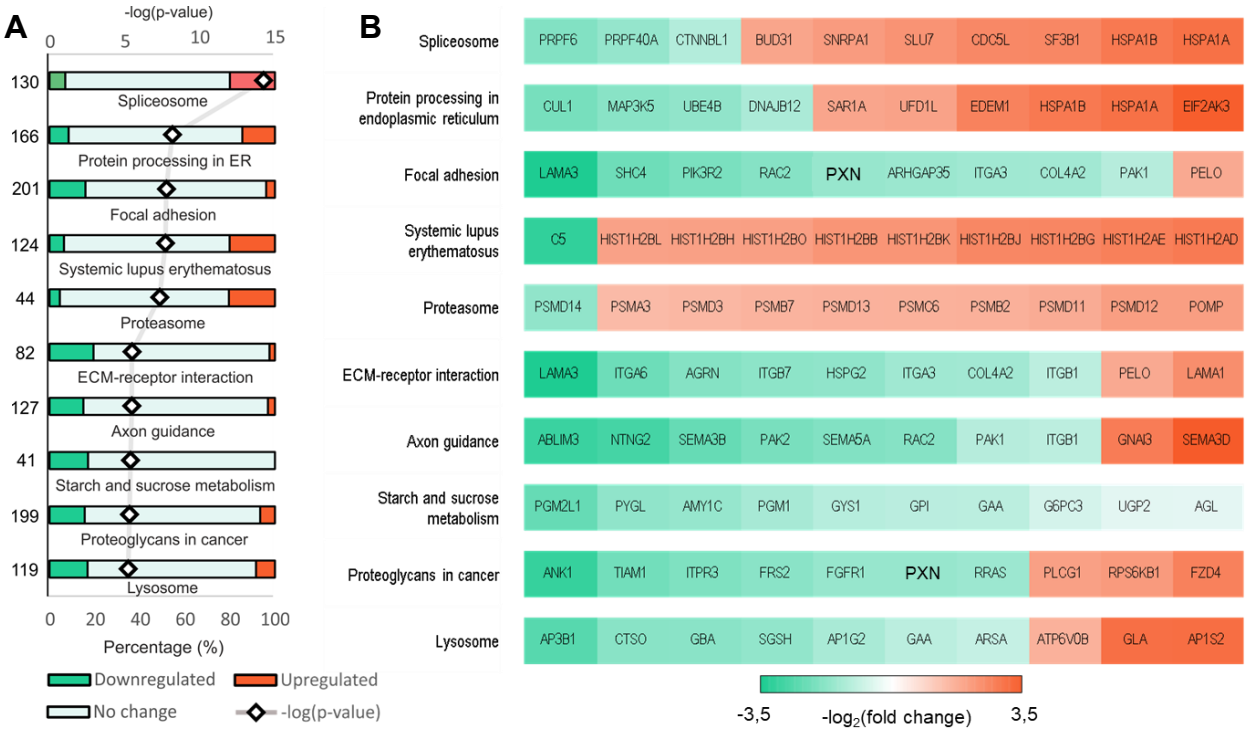

Figure 28. **KEGG analysis of PAXIP1-AS1 downstream genes.** A) A gene set enrichment analysis of all genes detected in PASMC after GapmeR mediated silencing of PAXIP1-AS1. Significance values for the analysis, the total number of genes annotated to the respective pathways (y-axis) and the percentages of genes that are down- and up-regulated are depicted. B) Top ten genes (and their respective LFC values) involved in the respective KEGG pathways as shown in A). Adapted from (99) in accordance with J Pathol. and the CC BY 4.0 license.

Delving further into the mechanisms perturbed by PAXIP1-AS1 knockdown, we next performed an overrepresented gene ontology analysis. While the previous analysis shed light on pathways impacted by the whole PAXIP1-AS1 influenced gene set orchestration, here we look at pathways that are influenced by the most drastic gene expressional changes after PAXIP1-AS1 knockdown (threshold margins applied are outlined in black in Figure 27A). Cell differentiation and proliferation processes came out as the most affected biological process in this analysis, while the basement membrane was the most affected cellular component (Figure 29).

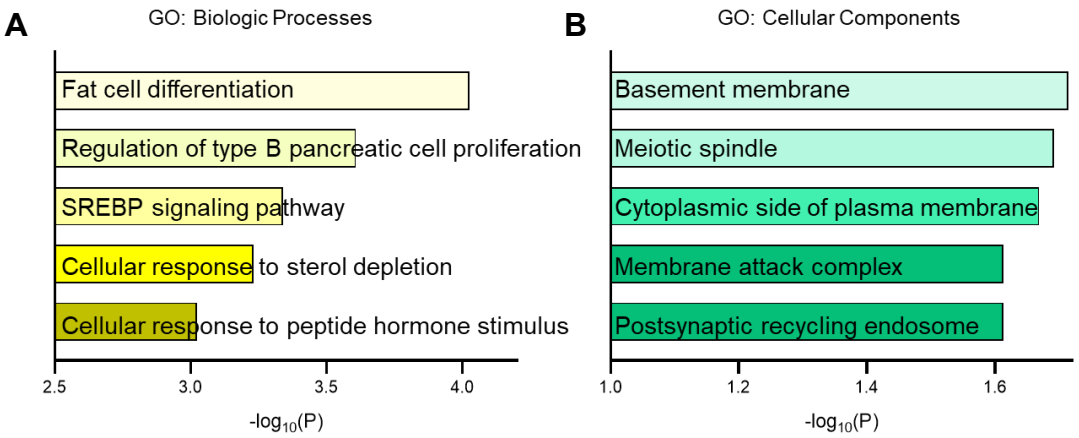

Figure 29. **GO analysis of overrepresented PAXIP1-AS1 downstream genes.** A) A gene ontology analysis of biological processes (A) and cellular components (B) of differentially regulated genes applying a cutoff of $-\log_{10}(P)>8$ and $-\log_2(\text{fold change})>|3|$ performed with thresholds as margined in black in the volcano plot in Figure 28A.

Angling from a different perspective, we next went along with the reasoning that genes downregulated after PAXIP1-AS1 knock down, but upregulated in IPAH, are the genes involved in PAH pathogenesis and under PAXIP1-AS1 regulation. Following this idea, we identified genes that were commonly regulated in both transcriptional analyses (Figure 30A), and then focused on genes where the direction of the regulation was inverse to that in IPAH (Figure 30B). The analysis presented us with several genes implicated in proliferation and apoptosis (e.g. G.associated kinase and cullin 1) (Figure 30B).

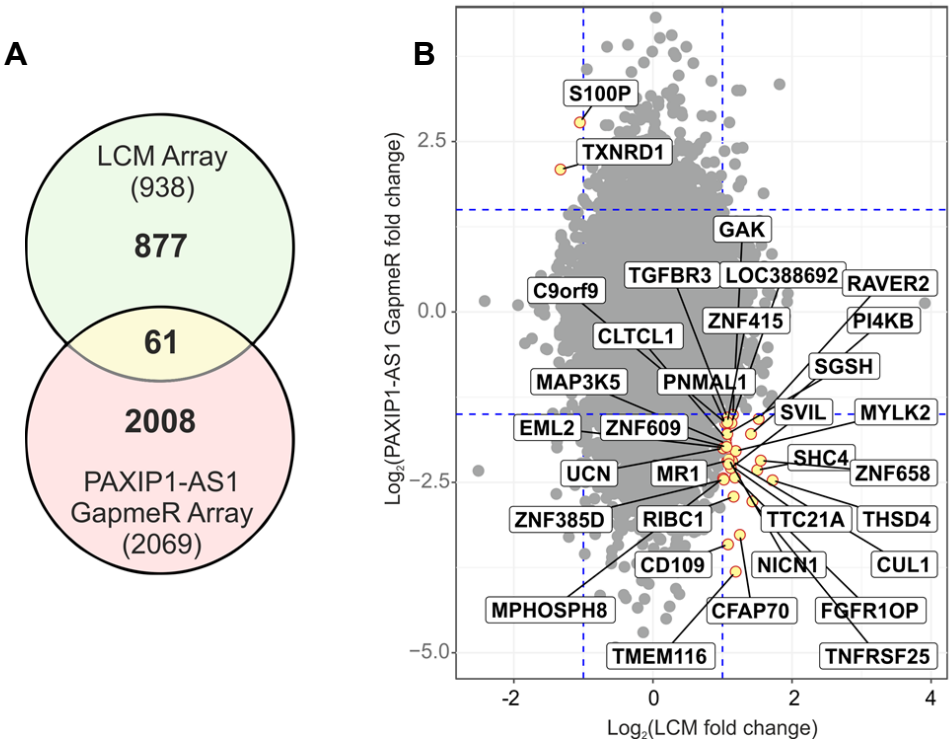

Figure 30. **Genes commonly and divergently regulated in IPAH and PAXIP1-AS1 knock down.** A) A Venn diagram depicting genes that are significantly regulated in both transcriptomic analysis (LCM Array: transcriptomic comparison between IPAH and donor PA; PAXIP1-AS1 GapmeR Array: transcriptomic analysis after PAXIP1-AS1 knock down in PASMC). B) The log_2(fold change) values of both transcriptomics analyses plotted against each other. Inversely regulated genes are highlighted. Adapted from (99) in accordance with J Pathol. and the CC BY 4.0 license.

Taking a hint from the pathway analyses (Figure 28 and Figure 29), we next set out to investigate how PAXIP1-AS1 interferes with the proliferative and apoptotic properties and cytoskeletal coordination of PASMC. To this end, we examined PASMC proliferation post siRNA mediated knockdown of PAXIP1-AS1. We found that PASMC proliferation was significantly downregulated after PAXIP1-AS1 knockdown in PASMC (Figure 31A).

Subsequently, we investigated into the migratory capacity of the PASMC after siRNA mediated knock down. Significant reduction in cell motility was observed after 7 hours of wound healing assay when the lncRNA was knocked down (Figure 32). Apoptosis after PAXIP1-AS1 knockdown was measured by staining of Annexin V in PASMC. Decreased PAXIP1-AS1 expression led to an increase in apoptosis in PASMC (Figure 33).

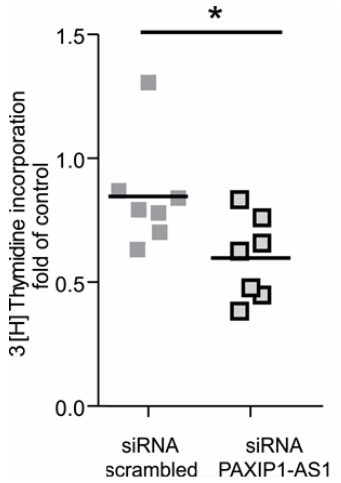

Figure 31. **Proliferation after PAXIP1-AS1 knockdown.** Proliferation of PASMC 48 hours post knockdown as determined by H3-Thymidin incorporation assay. * = $p < 0.05$ as determined by Student's t test. Adapted from (99) in accordance with J Pathol. and the CC BY 4.0 license.

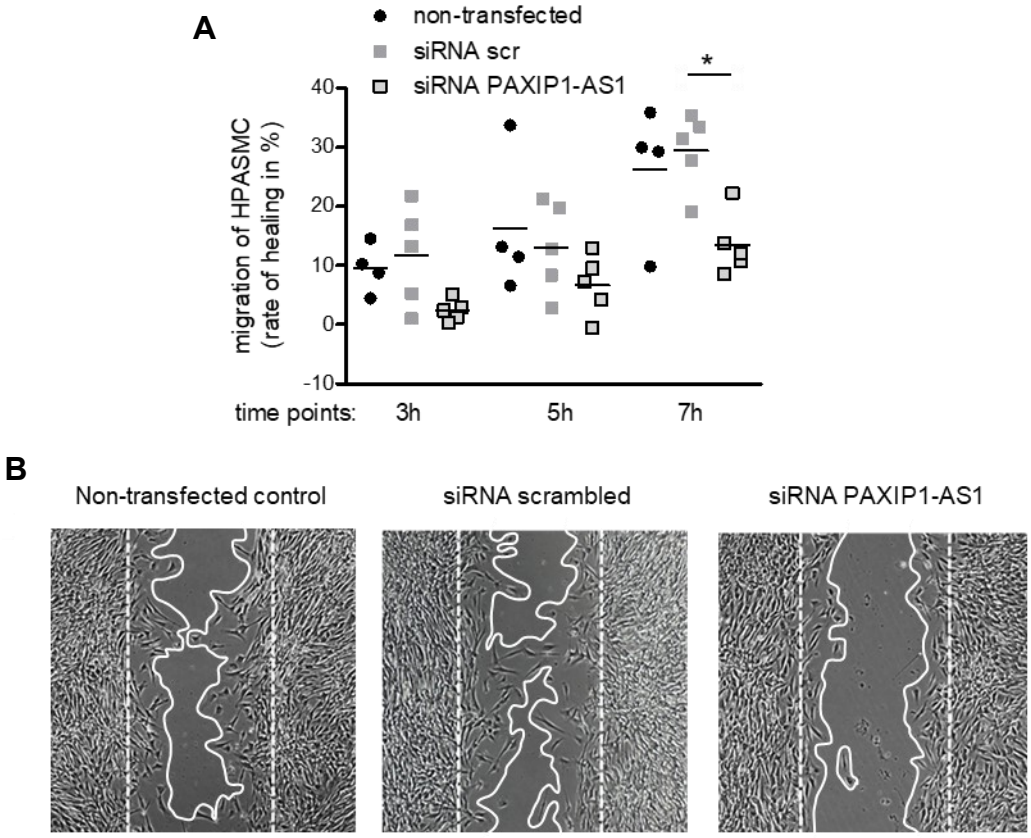

Figure 32. **Migration after PAXIP1-AS1 knockdown.** A) Migration of PASMC measured by a wound healing assay 48 hours post siRNA mediated silencing evaluated at the indicated times. B) Representative images are shown for the 7 hours' time point. * = $p < 0.05$ as

determined by Student's t test. Adapted from (99) in accordance with J Pathol. and the CC BY 4.0 license.

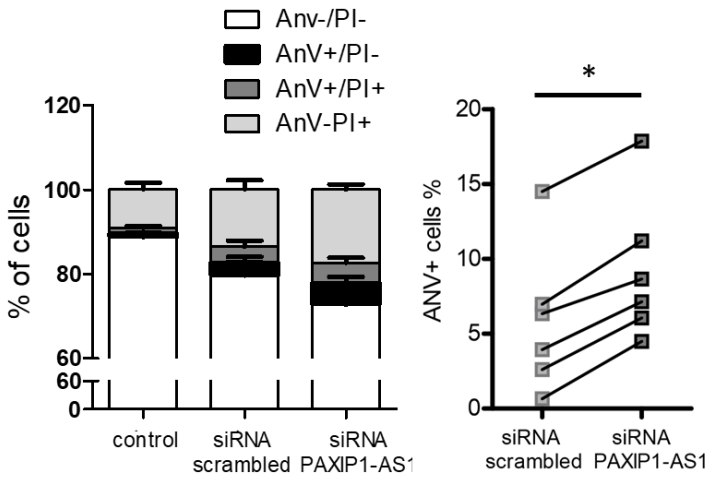

Figure 33. **Apoptosis after PAXIP1-AS1 knockdown PASMC.** Apoptotic behaviour of PASMC after siRNA mediated knock down of PAXIP1-AS1 as measured by flow cytometric AnV/PI staining. * = $p < 0.05$ as determined by Student's t test. Adapted from (99) in accordance with J Pathol. and the CC BY 4.0 license.

Identifying focal adhesion as a main pathway dysregulated downstream of the IPAH-PAXIP1-AS1-axis (Figure 28), we decided to further examine the gene regulation of different focal adhesion related proteins (Figure 34). No expressional changes were to be found here for Paxillin (PXN), Src Tyrosine Kinase (SRC), Tensin1 (TNS1), Vinculin (VCL), Talin1 (TLN1) or Protein Tyrosine Kinase 2/FAK1 (PTK2) after PAXIP1-AS1 knockdown at mRNA level (Figure 34).

Next, we set out to verify the increased paxillin (PXN) expression levels in IPAH, as has been previously reported in (59). We detected a significant downregulation of total paxillin as well as phospho-paxillin at translational level (Figure 35). Complementing this finding, immunofluorescence imaging of PAXIP1-AS1 silenced PASMC also demonstrated a decrease in phosphorylated paxillin. At the same time F-actin (polymeric structural component of the cytoskeleton; microfilament) levels were increased (Figure 36). The western blotting experiment in this section was performed with the help of Eva Grasmann from the Ludwig Boltzmann Institute for Lung Vascular Research, Graz. The immunofluorescent imaging was performed with the help of Dr. Katharina Jandl from the Ludwig Boltzmann Institute for Lung Vascular Research, Graz.

Paxillin is a central component of the focal adhesion that is also important for the communication with the ECM. Cell attachment, spreading and migration via reorganization of the actin cytoskeleton are processes that are controlled by the paxillin activation through phosphorylation (180). We were able to confirm the increased the paxillin protein levels in donor and IPAH PASMC via western blotting (Figure 37).

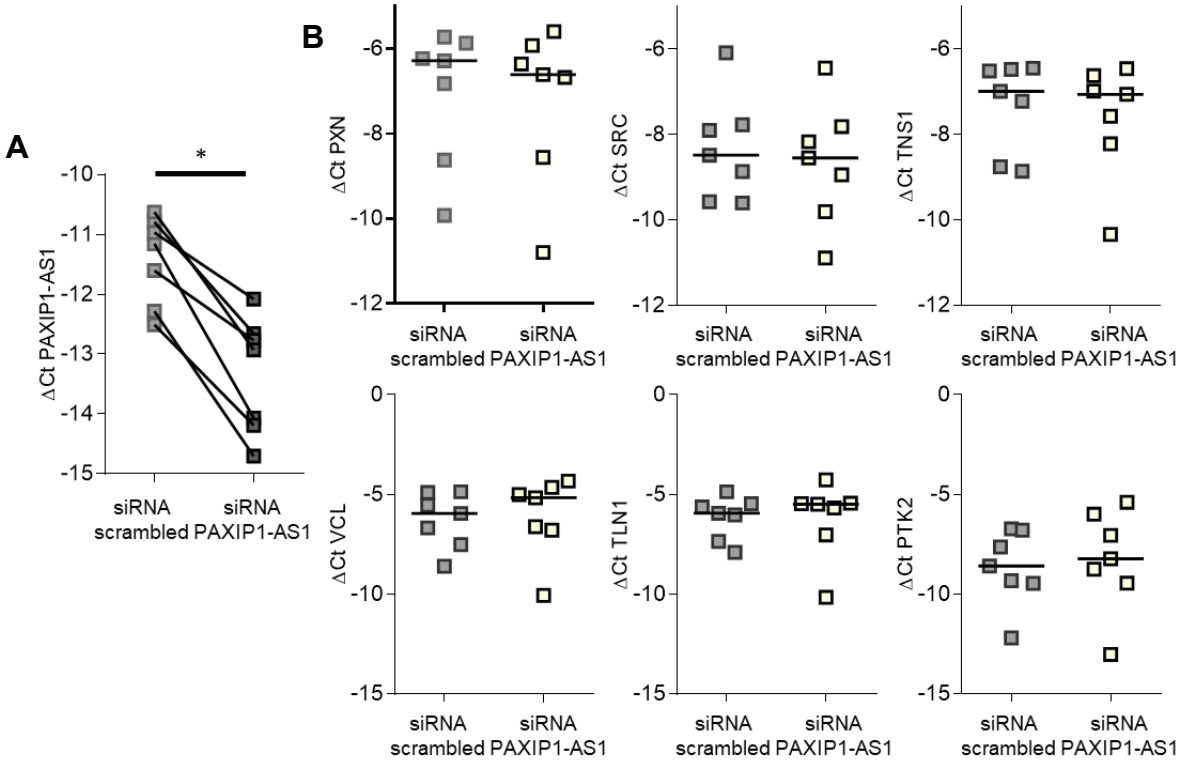

Figure 34. **Regulation of gene members of the focal adhesion pathway after PAXIP1-AS1 knockdown.** A) qRT-PCR validating successful downregulation of PAXIP1-AS1 after siRNA application. B) Expression levels of Paxillin (PXN), Src Tyrosine Kinase (SRC), Tensin1 (TNS1), Vinculin (VCL), Talin1 (TLN1) and Protein Tyrosine Kinase 2/FAK1 (PTK2) after PAXIP1-AS1 knock down as determined via qRT-PCR. * = $p < 0.05$ as determined by Student's t test. Adapted from (99) in accordance with J Pathol. and the CC BY 4.0 license.

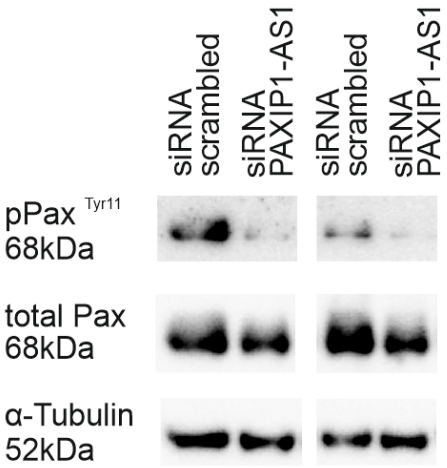

Figure 35. **PAXILLIN protein expression after PAXIP1-AS1 knockdown - I.** Paxillin and p-Paxillin (Tyr118) expression levels relative to α-tubulin 48 hours after siRNA-mediated knockdown as determined via western blotting. Adapted from (99) in accordance with J Pathol. and the CC BY 4.0 license.

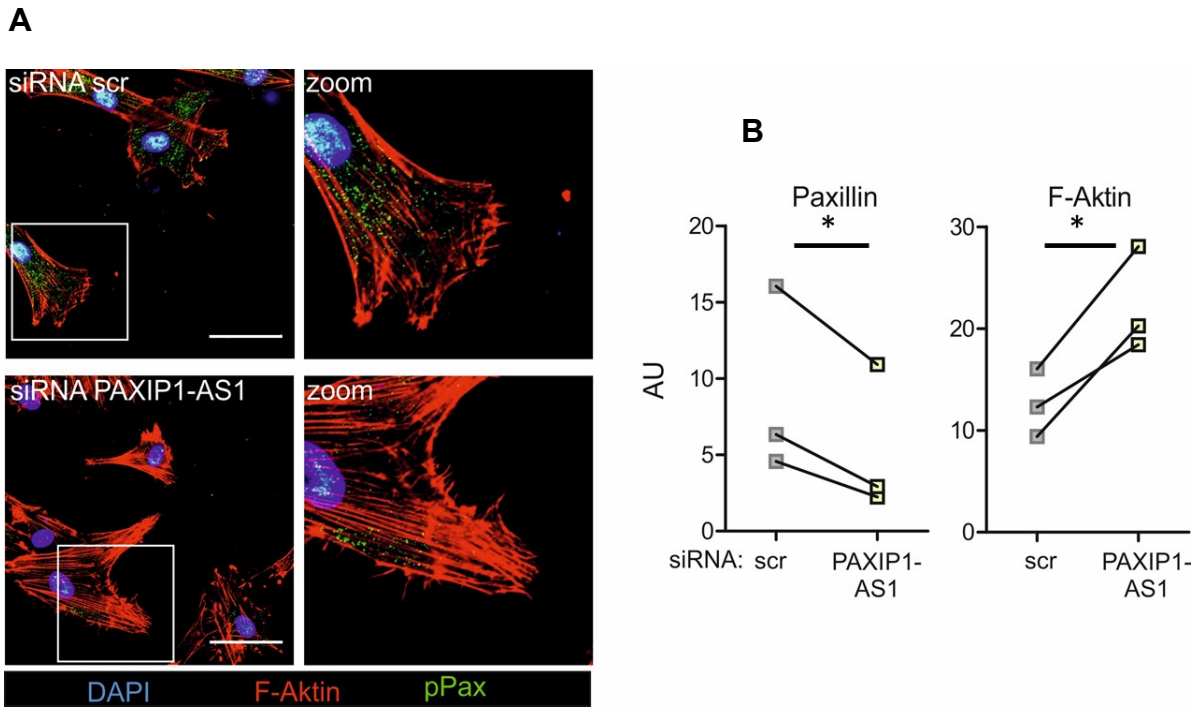

Figure 36. **PAXILLIN protein expression after PAXIP1-AS1 knockdown - II.** pPaxillin and F-actin expression as visualized via immunofluorescence imaging in siRNA treated PASMC cells (A) and corresponding quantification of fluorescent intensities (B). * = $p < 0.05$ as

determined by Student's t test. AU = arbitrary units. Adapted from (99) in accordance with J Pathol. and the CC BY 4.0 license.

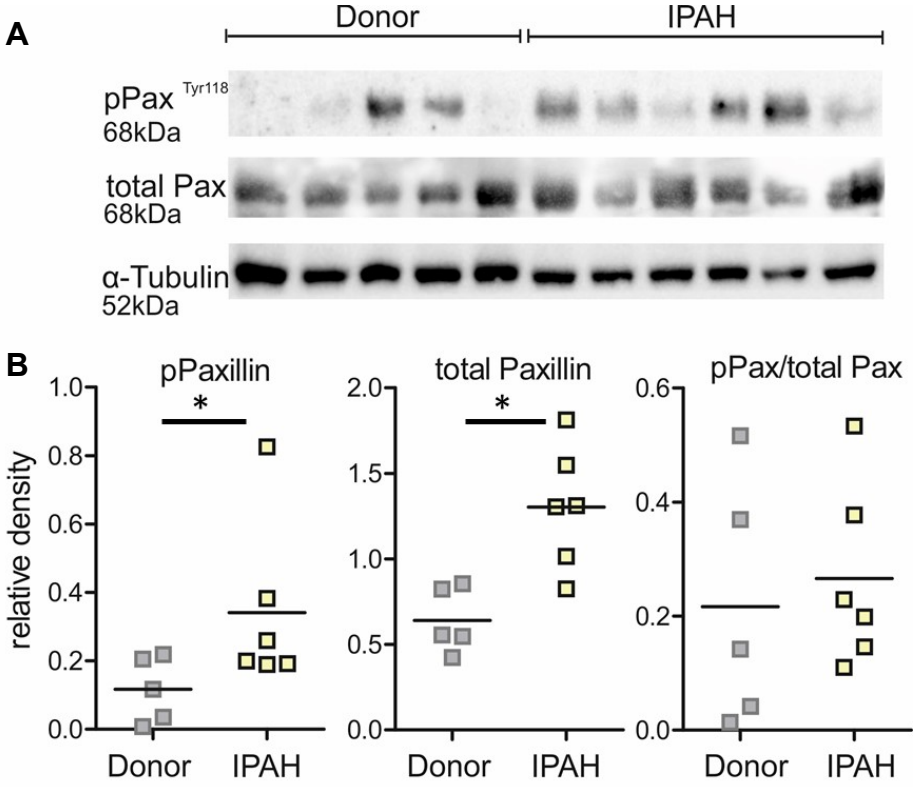

Figure 37. **PAXILLIN protein expression in IPAH.** Paxillin and p-Paxillin (Tyr118) expression levels relative to α-tubulin in donor and IPAH PASMC as determined via western blotting (A). Corresponding densitometry is represented in B). * = $p < 0.05$ as determined by Student's t test. Adapted from (99) in accordance with J Pathol. and the CC BY 4.0 license.

Next, we looked at the effect of PAXIP1-AS1 knockdown in IPAH PASMC. Decrease of PAXIP1-AS1 expression also robustly reduced total paxillin protein levels in IPAH PASMC (Figure 38). Aiming for a rescue-experiment with PAXIP1-AS1 silencing and paxillin overexpression, we next established and validated the co-transfection setting for PAXIP1-AS1 siRNA and paxillin overexpression plasmid, and respective controls (scrambled siRNAs or empty plasmid controls). A previously established paxillin overexpression plasmid with pcDNA3.1 backbone was used for this study (59). Expression results after the co-transfection show that paxillin overexpression strongly upregulated PAXIP1-AS1 expression, completely fading away the effects achieved by the siRNAs (Figure 39). Apoptotic susceptibility was also

increased in IPAH PASMC following knock down of PAXIP1-AS1 but could be rescued by simultaneous overexpression of paxillin (Figure 40).

As we assumed that the reversal of the effects was caused by paxillin inducing PAXIP1-AS1, we also wanted to investigate the effect of direct overexpression of PAXIP1-AS1 in donor and IPAH PASMC. Therefore, we first amplified the full length PAXIP1-AS1 fragment via PCR using forward and reverse primers with NheI and HindIII extensions, respectively, to later insert the amplified full size PAXIP1-AS1 fragment into the plasmid backbone of pcDNA3.1(+) (see section 2.15 for details). The successful cloning, resulting in a PAXIP1-AS1 overexpression plasmid as represented in Figure 41A, was checked through SalI digestion of the plasmid and comparison of the resulting band sizes on an agarose gel (Figure 41B). The dual cutting restriction enzyme SalI gives characteristic band sizes (2185bp and 5504 bp as shown in (Figure 41B)) if the insertion of the PAXIP1-AS1 sequence was successful. The correct placement of the PAXIP1-AS1 sequence in pcDNA3.1 was also additionally confirmed via Sanger sequencing. Successful overexpression of PAXIP1-AS1 using this construct was further confirmed via qRT-PCR (Figure 42A). In balance with the previous findings, overexpression of PAXIP1-AS1 lead to significantly decreased apoptotic susceptibility in both donor and IPAH cell types (Figure 42B).

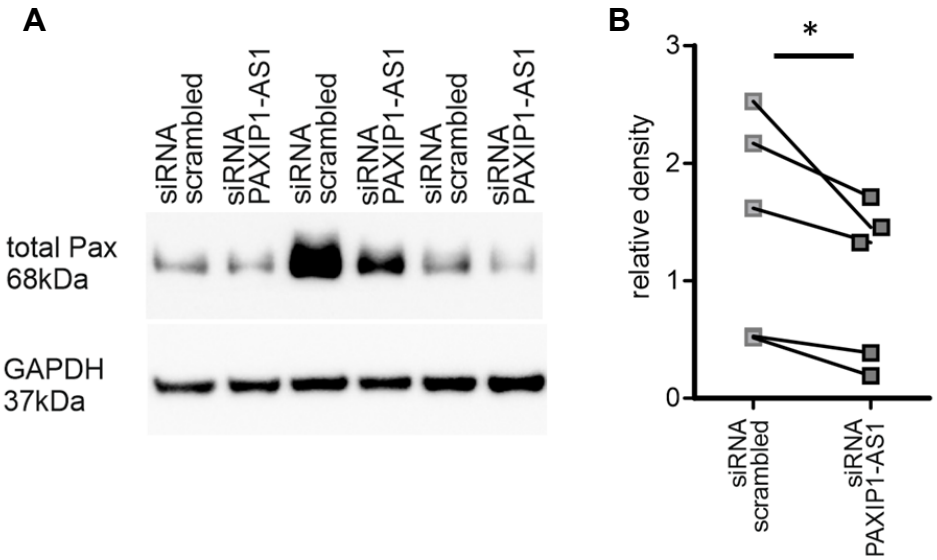

Figure 38. **Paxillin protein expression after PAXIP1-AS1 knockdown in IPAH PASMC.** Representative western blot analysis showing paxillin expression levels relative to GAPDH 48 hours after knockdown in PASMC (A). Densitometry of performed western blot analyses (B). * = $p < 0.05$ as determined by paired samples t-test. Adapted from (99) in accordance with J Pathol. and the CC BY 4.0 license.

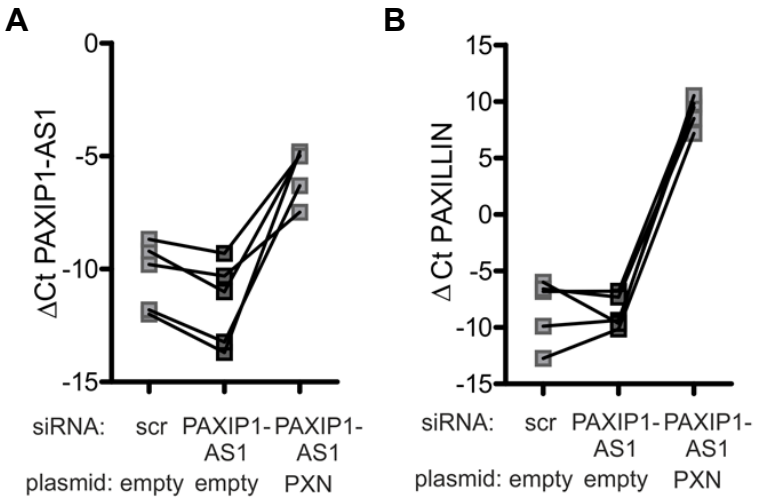

Figure 39. **Paxillin overexpression combined with PAXIP1-AS1 knockdown.** PAXIP1-AS1 (A) and paxillin (B) expression determined via qRT-PCR after siRNA mediated PAXIP1-AS1 knockdown (or scrambled control, scr) and Paxillin co-expression via overexpression plasmid (PXN) or empty plasmid control (empty). Adapted from (99) in accordance with J Pathol. and the CC BY 4.0 license.

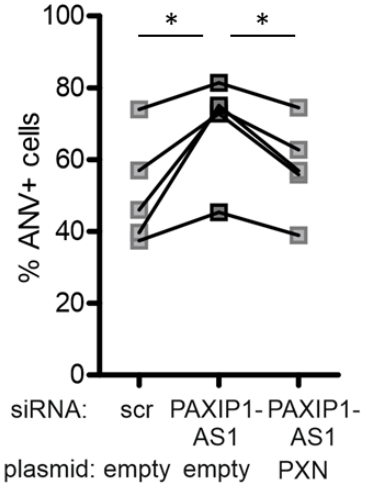

Figure 40. **Apoptosis after PAXIP1-AS1 knockdown and Paxillin (PXN) co-expression.** Apoptosis as measured by flow cytometric AnV/PI staining after 48 hours of PAXIP1-AS1 knockdown (or scrambled control, scr) accompanied by Paxillin overexpression (PXN) or transfection with empty control plasmid (empty). * = $p < 0.05$ as determined by Student's t test. Adapted from (99) in accordance with J Pathol. and the CC BY 4.0 license.

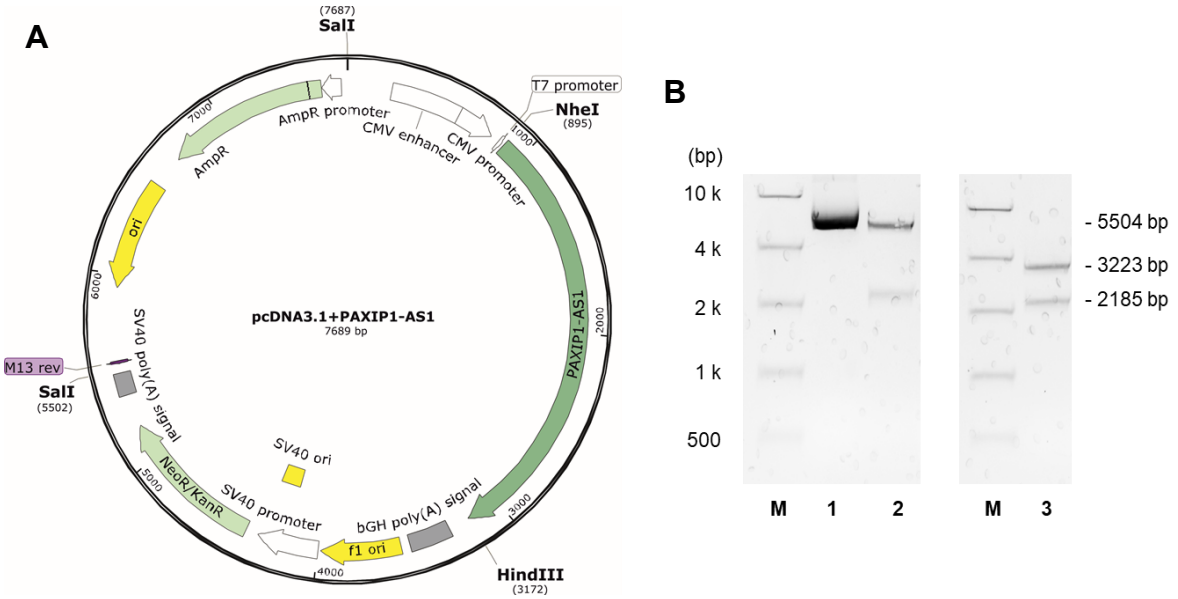

Figure 41. **PAXIP1-AS1 overexpression plasmid.** A) Structure of the PAXIP1-AS1 overexpression plasmid. CMV, human cytomegalovirus immediate early promoter/enhancer; bGH poly(A) signal, bovine growth hormone polyadenylation signal; ori, origin of replication; AmpR, Ampicillin resistance gene; NeoR/KanR, Neomycin/Kanamycin resistance gene. B) Agarose gel run with pcDNA3.1 uncut plasmid (1), SalI digested pcDNA3.1 with insert (2) and SalI digested plasmid without insert (3). M marks the used ladder.

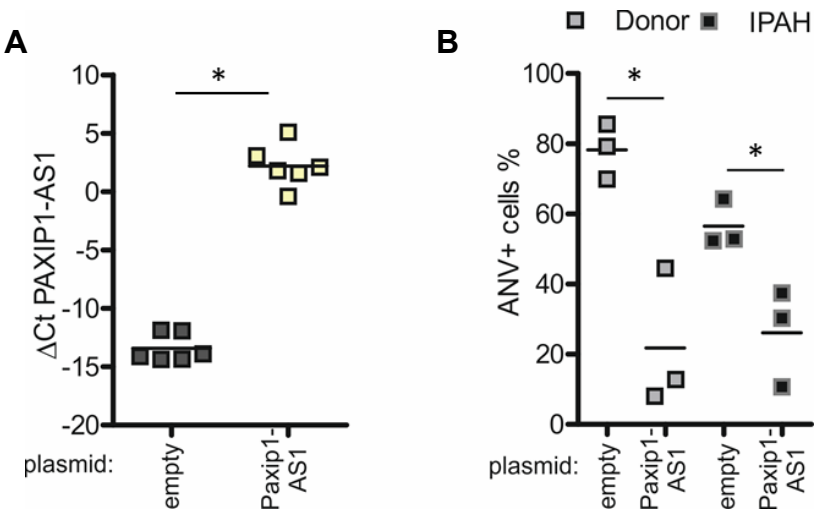

Figure 42. **Apoptosis after PAXIP1-AS1 OE.** A) PAXIP1-AS1 expression as determined by qRT-PCR after transfection with PAXIP1-AS1 overexpression plasmid or empty control plasmid. B) Apoptosis as measured by flow cytometric AnV/PI staining 48 hours after

PAXIP1-AS1 overexpression in donor and IPAH PASMC. * = $p < 0.05$ as determined by Student's t test. Adapted from (99) in accordance with J Pathol. and the CC BY 4.0 license.

3.4 The proteome of the pulmonary arteries

Our next goal was to shed more light on the ECM composition of diseased pulmonary arteries and to screen for global changes in its proteome. Exploring ECM remodelling in IPAH, with the goal to identify potential matrikine origination sites in the diseased ECM, we set out to perform mass spectrometric/proteomic analysis of ECM enriched protein lysates from isolated pulmonary arteries (PA) (Ø 0.5 - 2 mm) of healthy donor lungs and IPAH lungs. The relative insolubility and complexity of ECM proteins complicates the sample processing prior to mass spectrometric analysis. Therefore, a step-by-step adaptation of salt and detergent concentrations in the buffers was performed during the extraction procedure, to enrich the protein lysates from the pulmonary arteries for the poorly soluble ECM proteins.

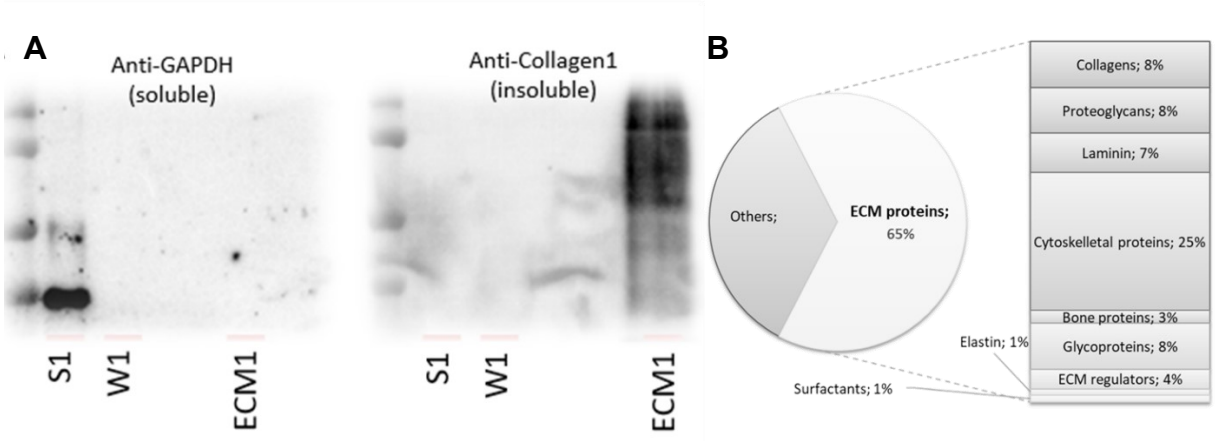

Figure 43. **ECM enrichment.** A) Western blot analysis of the fractions won during protein processing for proteomic analysis. Enrichment for ECM proteins was examined by confirming the presence of the cytosolic protein GAPDH in the soluble fraction (S1) and absence of the same in the wash fraction (W1) and in the ECM enriched fraction (ECM1), as well as by the presence of the ECM protein Collagen1 solely in the ECM enriched fraction (ECM1), and not in the soluble or wash fractions. B) Distribution of the detected protein subtypes in the mass spectrometric analysis of ECM enriched PA protein lysate.

We performed a test run with one enriched PA protein lysate sample and took intermediate samples after each step of protein processing to check for ECM protein enrichment via western blotting. Detecting the presence of only soluble proteins (represented by GAPDH) and no ECM proteins (represented by collagen 1) in the first fractions with low detergent concentration (S1,

W1), and the higher presence of ECM proteins and the absence of soluble cytosolic proteins in later fractions (ECM1) (Figure 43A) verified successful enrichment for ECM proteins with the usage of increasing buffer intensity. The mass spectrometric analysis performed with this test sample, where the separately enriched soluble and insoluble fractions were pooled, detected a high percentage of ECM related proteins (Figure 43B), demonstrating the capacity to capture also sparingly soluble ECM proteins in our analysis. The mass spectrometry was performed in collaboration with Assoc.Prof. Ruth Birner-Gruenberger from the Diagnostic and Research Institute of Pathology, Medical University of Graz.

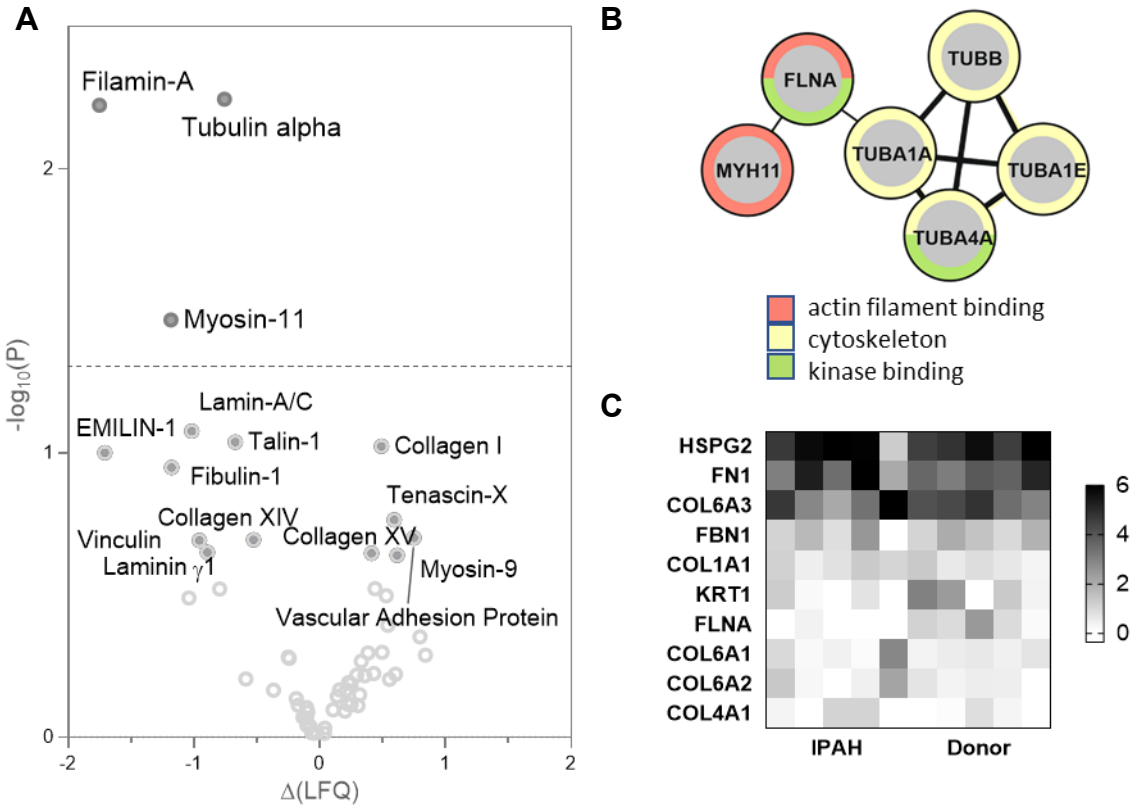

Figure 44. **Proteome analysis of the pulmonary arteries.** A) A volcano plot depicting the distribution of all detected proteins in the ECM fraction. The difference of the mean LFQ values (label free quantitation; Donor - IPAH) is plotted against the difference of the significance ($-\log_{10}(P)$). B) String interaction and GO analysis of the top altered components. C) Heatmap showing single LFQ (label free quantification) intensity values in z-scores for the proteins with the ten highest intensities.

After confirming successful ECM enrichment during protein processing, we proceeded with a comparative proteomic analysis of the ECM enriched protein lysates of pulmonary arteries isolated from donor (n=5) and IPAH (n=5) lungs. Our analysis showed significant ($p<0.05$)

disease dependent regulation of the proteins Filamin-A and Myosin-11 (Figure 44A); both proteins that have been shown to be upregulated in PAH previously (181, 182). A network and gene ontology analysis visualize the interactions of these proteins with each other, and showed functional involvement in actin filament binding, kinase binding and cytoskeletal processes (Figure 44B). Basement membrane components such as perlecan (HSPG2) and non-fibrillar collagens (e.g. Collagen VI and Collagen IV) were substantial in this assembly. The single LFQ (label free quantitation) intensities of the top 10 detected proteins from donor and IPAH samples is depicted in Figure 44C.

Based on the ECM proteins that were detected in both donor and IPAH pulmonary arteries and exploring current literature, we further compiled a list of potential matrikines that can arise from the pulmonary vascular ECM and can be relevant for IPAH (Table 12).

Table 12. **Matrikines derived from the ECM profile of IPAH and Donor PA**

Parent molecule	**Matrikine**	**Known Function (10, 38, 64, 135, 136)**
Fibulin-1	Neostatin (183)	Anti-proliferative
Fibrillin-1	Fibrillin fragment (184)	Pro-inflammatory (chemotactic)
Nidogen-1	G3 Domain (185)	Anti-angiogenic
Collagen XV a1 chain	Restin (186)	Anti-angiogenic
Collagen IV a5 chain	Pentastatin (187)	Anti-angiogenic, anti-migratory, anti-proliferatory
Fibronectin	Anastellin, Fibstatin (188, 189) (190)	Anti-angiogenic, pro-inflammatory (chemotactic)
Collagen IV a2 chain	Canstatin (191)	Anti-angiogenic, anti-migratory, anti-proliferatory, pro-apoptotic
Collagen XVIII a1 chain	Endostatin (96)	Anti-angiogenic, anti-fibrotic, induces autophagy
Collagen IV a1 chain	Arresten (192)	Anti-angiogenic, anti-migratory, anti-proliferatory, pro-apoptotic

Aggrecan core protein	Metastatin (193)	Anti-angiogenic, pro-apoptotic
Laminin α5	Laminin peptide (194)	Pro-inflammatory (chemotactic)
Laminin γ2	Laminin peptide (195)	Pro-migratory

3.5 Endostatin: matrikine of the basement membrane under PAXIP1-AS1?

Seeking to find a link between matrikines of the ECM and the lncRNA PAXIP1-AS1, we closely examined all ECM related genes that were detected in the transcriptomic analysis post PAXIP1-AS1 knockdown. Many ECM related genes, especially components of the basement membrane were downregulated after PAXIP1-AS1 knockdown, including COL18A1 (Figure 45). From the list of identified potential matrikines (Table 12) that may play a role in IPAH, we concentrated on basement membrane derived matrikines, as it had turned out to be the most affected cellular component after PAXIP1-AS1 knockdown (Figure 29B, Figure 45).

The proteomic as well as the transcriptomic analysis (Figure 10, Figure 44) of the pulmonary arteries had identified COL4A5 and COL18A1 as prominent basement membrane collagens in the PA, for which we could also confirm significant upregulations in IPAH (Figure 10, Figure 11). Consequently, we chose to explore the role of the proteolytic product of COL18A1, endostatin (ES) in more detail.

First, we set out to investigate the impact of recombinant native human endostatin treatment in PAEC. To foster PAEC reactivity to ES, the cells were first starved in basal medium (containing 0.5% FBS; without additives), before exposing to 1 µg/ml of ES for 24 hours in the respective conditions and conducting the readout. In cell culture, PAEC are more susceptible to starvation stress than PASMC, which is why instead of using serum-free basal medium, 0.5% FBS was added, and starvation was limited to 2.5 hours.

In starvation conditions, ES treatment did not affect cell proliferation, as measured by EdU staining. However, when PAECs were maintained in full media, thus in a proliferative state, ES treatment showed a strong tendency towards decreased proliferation. This was also

showcased by the significant increase of PAEC proliferation in presence of FM in comparison to basal conditions, that diminished when in combination with ES (FM+ES) (Figure 46).

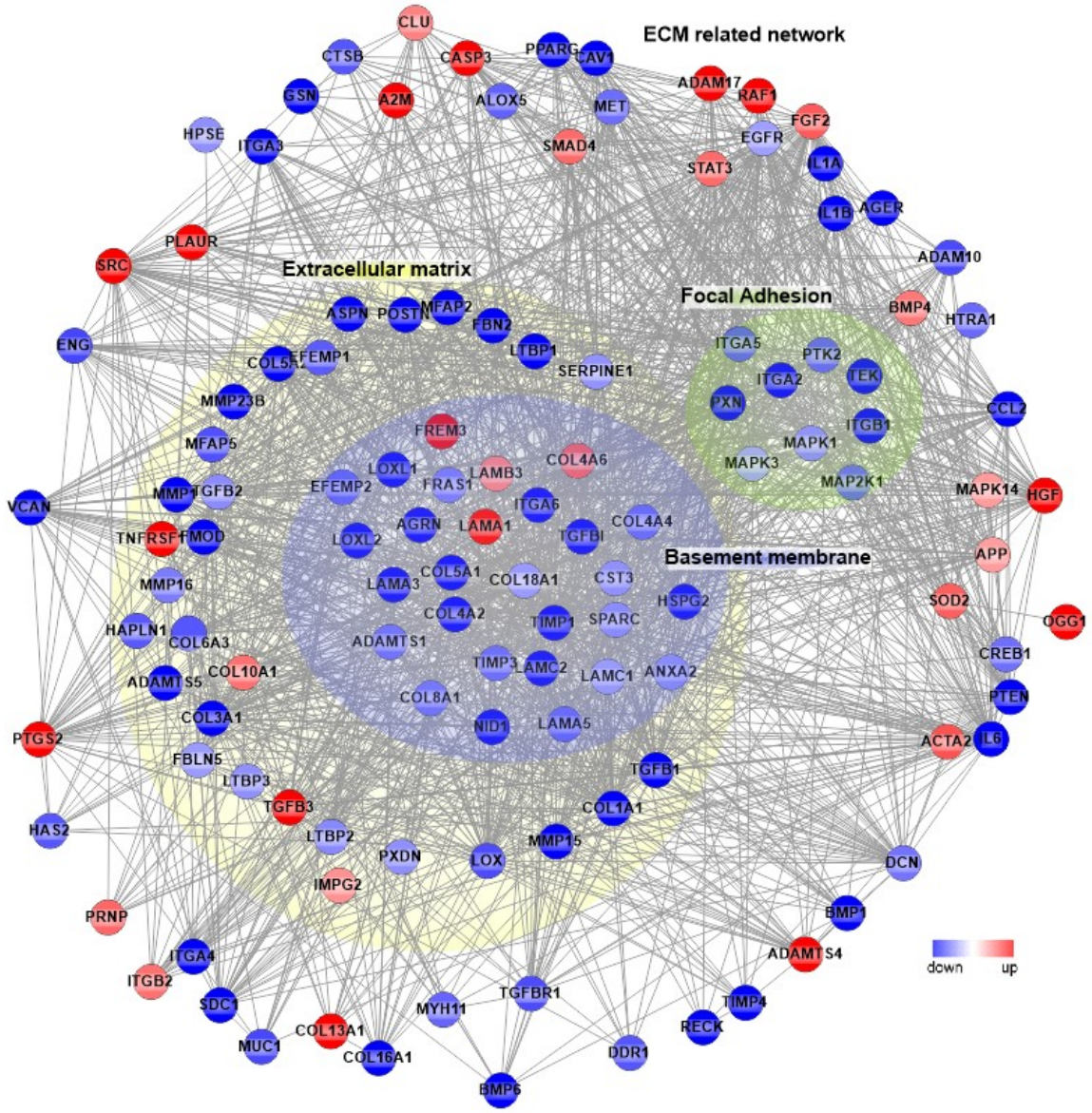

Figure 45. **Transcriptomic ECM profile downstream of PAXIP1-AS1.** String Network analysis performed on all ECM related genes significantly regulated after Gapmer mediated knock down of PAXIP1-AS1. The direction of the gene regulation after PAXIP1-AS1 knockdown is colour-coded. Direct components of the ECM, Basement membrane and Focal Adhesion are grouped for better overview.

To complement this experiment, the colorimetric CCK-assay was applied (a method that measures the metabolic activity, as opposed to the EdU assay that monitors cells that are proliferating and incorporates EdU into replicating DNA). Interestingly, proliferations did not

affect the metabolic activity as determined by the CCK assay, while full media/VEGF treatment also resulted in significantly increased metabolic activity (Figure 47).

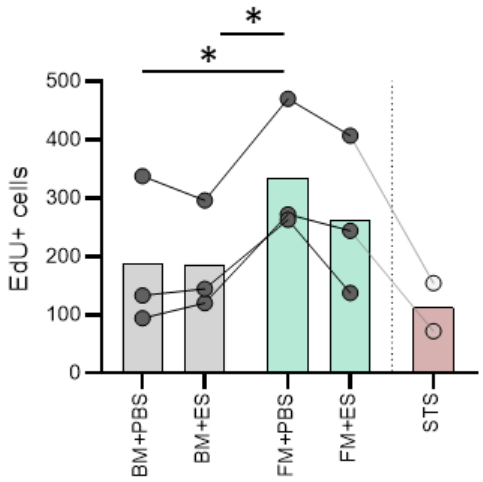

Figure 46. **PAEC proliferation after recombinant native endostatin treatment - I.** PAEC proliferation was measured after 24 hours of recombinant native endostatin (1 µg/ml) or vehicle (PBS) treatment via EdU incorporation assay using either basal or full medium. Staurosporin (STS) served as a control. A) Representative images are shown for each condition. Grey = EdU-647 positive cells; blue = nucleic acid stain Hoechst 33342. B) Total EdU+ cell count is given for each condition. BM=Basal medium; FM=Full medium; ES=Endostatin; PBS=Phosphate buffered saline. * = $p < 0.05$ as determined by one-way ANOVA and Tukey's multiple comparisons test.

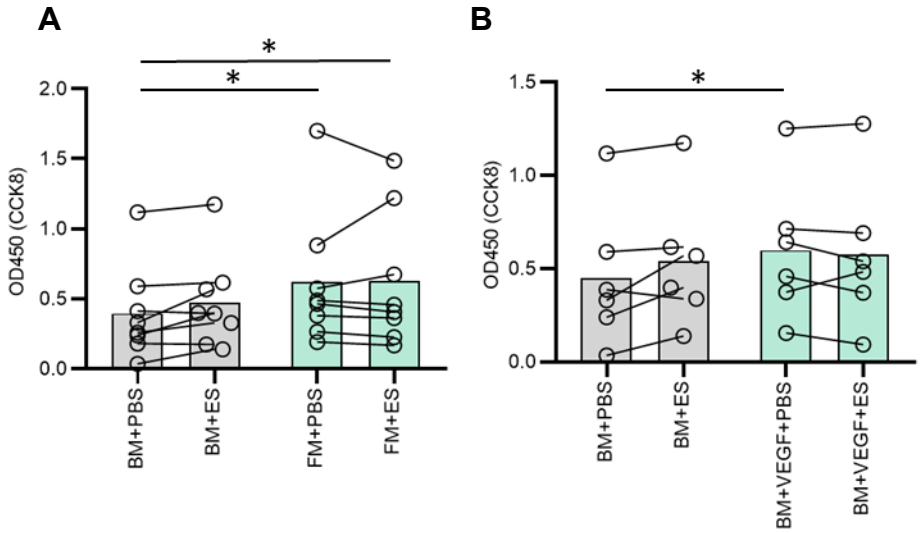

Figure 47. **PAEC proliferation after recombinant native endostatin treatment - II.** The effect of recombinant native endostatin treatment (1 µg/ml; 24 h) on PAEC metabolic activity was assessed using the CCK-8 assay comparing basal conditions to A) full medium and B)

to VEGF stimulation. BM=Basal medium; FM=Full medium; VEGF=Vascular Endothelial Growth Factor; ES=Endostatin; PBS=Phosphate buffered saline. * = $p < 0.05$ as determined by one-way ANOVA and Tukey's multiple comparisons test.

To complement the recombinant endostatin treatment approach, we decided to perform functional studies after overexpressing endostatin using Adeno-Associated Viruses (AAV2). For this purpose, we decided to use endostatin with a point mutation where proline at position 125 is substituted with alanine (ES-P125A). ES-P125A has been shown to exhibit stronger biological activities due to better binding capabilities won through this point mutation (144).

Moreover, our ES expression vector design included a IgK signal peptide that leads to the secretion of the expressed protein, a N-terminal HIS-tag allowing for a potential ES isolation using affinity chromatography at a later stage and a C-terminal reporter gene EGFP. The self-cleaving peptide P2A was placed between ES and EGFP. This leads to cleavage of the fusion protein at the P2A linkage site after expression leaving two separate functional proteins, allowing us to investigate the effect of ES without having the effects of the relatively large EGFP reporter tied to it. Details of the AAV design are given in Figure 48.

Successful overexpression of endostatin via AAV-ES-P125A overexpression was validated via detection of the EGFP marker expression, western blotting and ELISA (Figure 49). A concentration of around 40 pg/ml was measured in the medium of ES overexpressing PAEC.

To this end, we looked at the effects of endostatin (AAV-ES-P125A) overexpression on the proliferative behaviour of PAEC. Proliferation was tendentially decreased in transfected PAEC (Figure 50), but given the low n-number in this experiment, this did not yet reach significance (experiment performed in parallel to CCK8 assay in Figure 47; PAEC cultured in FM showed increased proliferation in comparison to basal treated cells).

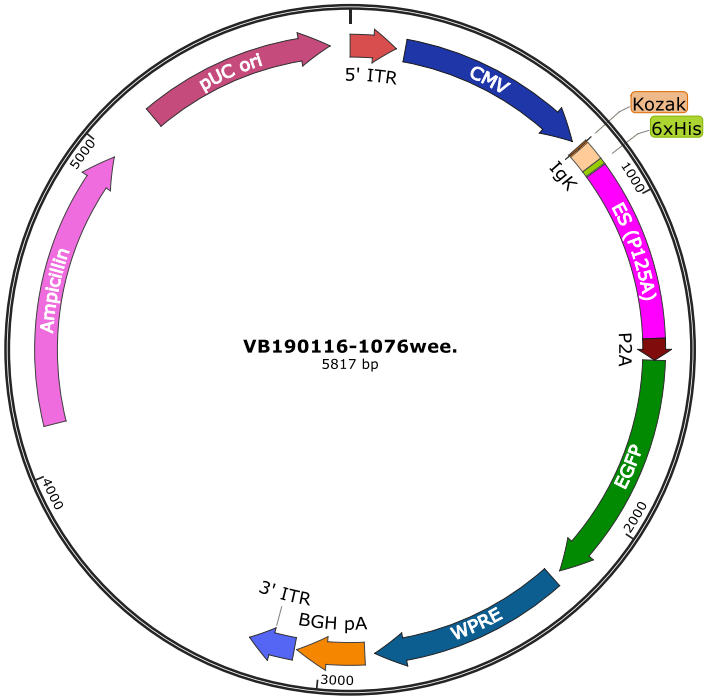

Figure 48. **AAV-2 mediated overexpression of endostatin P125A - I.** The structure of the AAV vector designed for overexpression of endostatin (designed using VectorBuilder's online vector construction tool). pUC ori, origin of replication; ITR, inverted terminal repeats; CMV , cytomegalovirus gene promoter; IgK, secretion sequence; 6xHis, His Tag; ES P125A, endostatin with point mutation at position 125; P2A, self-cleaving peptide; EGFP, eukaryotic green fluorescent protein; WPRE, woodchuck hepatitis virus posttranscriptional regulatory element, BGH pA, bovine growth hormone polyadenylation.

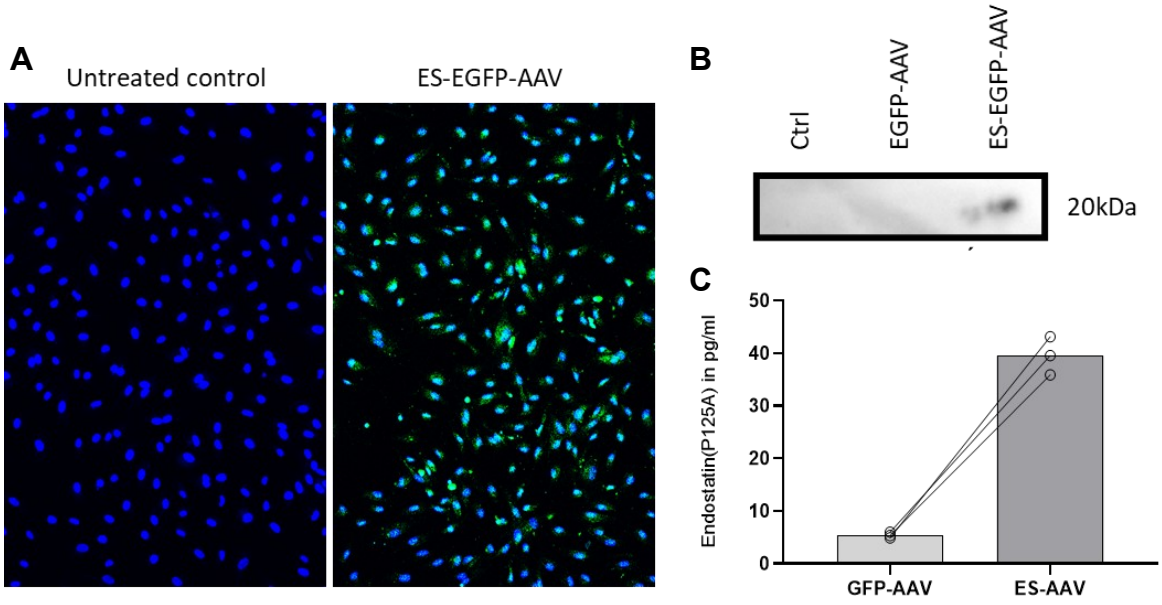

Figure 49. **AAV-2 mediated overexpression of endostatin P125A - II.** A) Fluorescence imaging of PAEC after transfection with endostatin overexpressing AAVs (ES-EGF-AAV) and non-transfected control cells. B) Western blot analysis of protein samples won from untreated control PAEC (ctrl), cells transfected with control plasmid (EGFP-AAV) and cells transfected with endostatin overexpression vectors (ES-EGFP-AAV). C) Endostatin ELISA results suggesting an endostatin concentration between 35 and 45 pg/ml in the medium of ES-EGFP-AAV transfected PAEC.

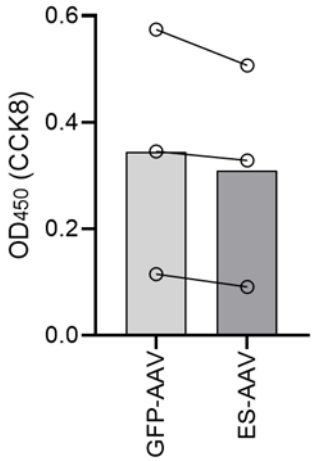

Figure 50. **Proliferation in endostatin overexpressing PAEC.** Effects of endostatin overexpression via AAV-2 assessed via CCK8 assay in PAEC.

Metalloproteases play a crucial role in the generation of endostatin from COL18A1 (136, 196). MMP1, a metalloprotease, that is known to be produced by endothelial cells (197), was also downregulated after PAXIP1-AS1 knockdown in our transcriptomic analysis. Consequently, we hypothesized increased MMP1 levels and activity could be responsible for the increased endostatin levels in IPAH. Aiming at establishing the functional relationship between PAXIP1-AS1, MMP1 and endostatin, we first looked at the expression of MMP1 after overexpression of PAXIP1-AS1 in PAEC. Contrary to our expectation, we found MMP1 to be tendentially downregulated after PAXIP1-AS1 and Paxillin overexpression (Figure 51A, B).

Nevertheless, this downregulation of MMP1 after PAXIP1-AS1 knockdown goes in conformity with the observed MMP1 downregulation that we observed in IPAH (Figure 51C, D). While MMP1 may play a limited role downstream of PAXIP1-AS1 with regards to endostatin generation, our results suggested a definite importance for this metalloprotease in IPAH (Figure 51C, D).

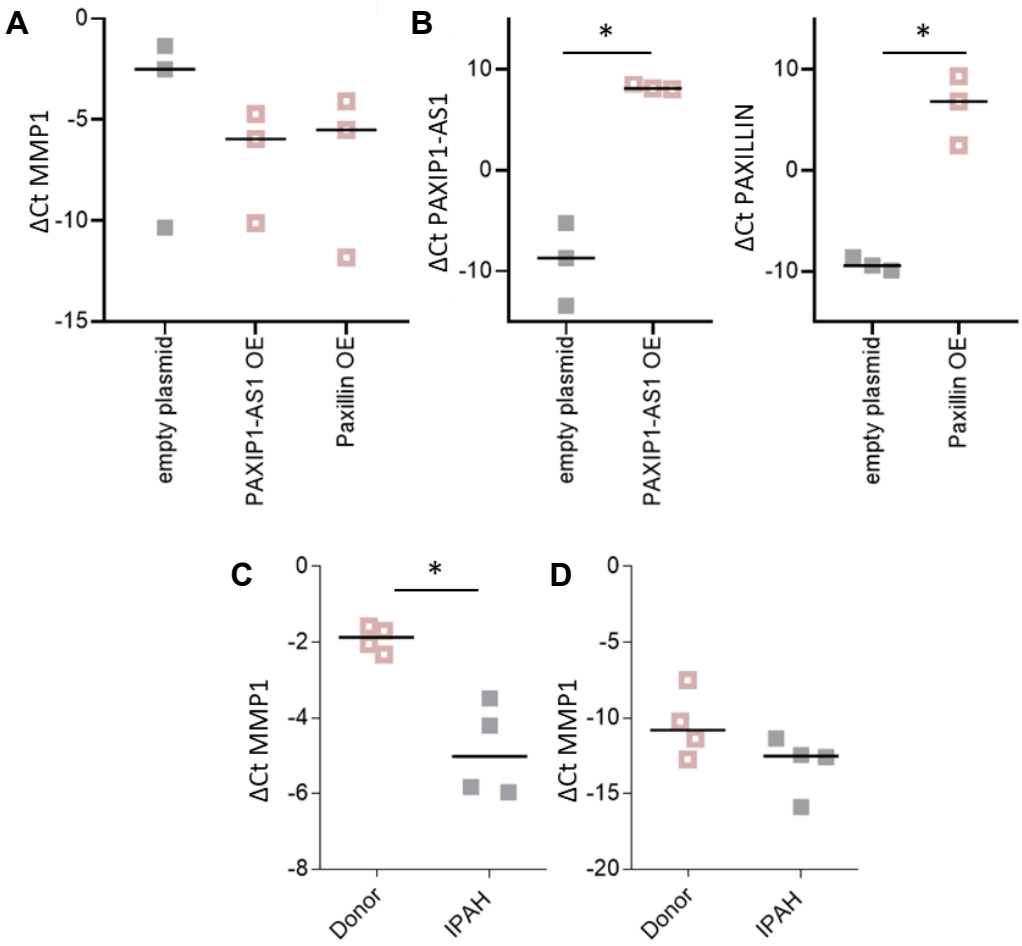

Figure 51. **MMP1 after PAXIP1-AS1 overexpression and in IPAH.** A) MMP1 expression measured via qRT-PCR after PAXIP1-AS1 and Paxillin overexpression in PAEC. B) Successful overexpression of PAXIP1-AS1 and Paxillin shown by qRT-PCR analysis. MMP1 expression in IPAH PASMC (C) and PAAdFB (D) as analysed by qRT-PCR. * = $p<0.05$ as determined by Student's t-test.

Next, we wanted to investigate the effect of PAXIP1-AS1 and paxillin on endostatin expression. Therefore, we first transfected PAEC, PASMC and PAAdFB with the respective overexpression plasmids and collected the supernatants after 48 hours. We quantified ES release amount in the supernatant after PAXIP1-AS1 and paxillin overexpression by measuring the ES levels using a quantitative ELISA. Disproving our hypothesis though, the quantification of secreted endostatin showed no PAXIP1-AS1 or paxillin overexpression related increase (Figure 52).

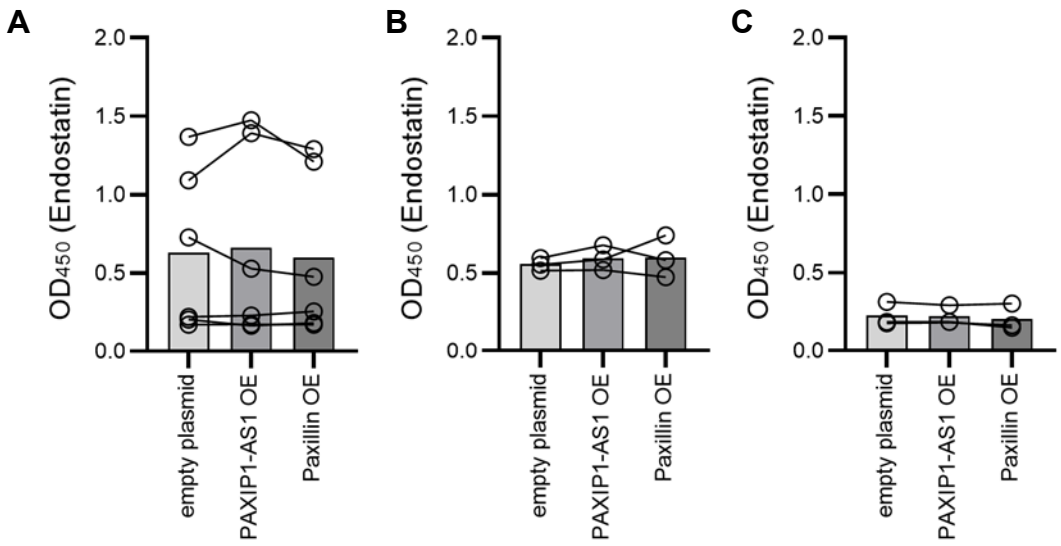

Figure 52. **Endostatin release after PAXIP1-AS1 and Paxillin overexpression.** The release of endostatin quantified in the medium of PAXIP1-AS1 and Paxillin overexpressing A) PAEC, B) PASMC and C) PAAdFB using a quantitative ELISA.

4. Discussion

IPAH is a devastating, fatal disease where the underlying disease mechanism has not been thoroughly understood yet to be able to develop much-needed targeted therapies. Major advancement has been achieved in the past 30 years in the treatment of IPAH, considerably improving quality of life of affected patients. However, the current medical therapy does not address the underlying cause of the problem, as IPAH remains a progressively deteriorating disease with no cure (198). Drug classes currently in use for IPAH are exclusively directed at interfering with just three signalling pathways in IPAH (1), while the disease complexity has become increasingly evident thanks to ongoing research (13, 25, 50). There still is a considerable knowledge gap that needs to be addressed to be able to utilize other molecular signalling mechanisms to effectively treat and cure IPAH. Largescale -omics approaches serve as powerful tools that allow us to expand our knowledge about differential gene expression and preserved pathways in diseased context. In the case of IPAH though comprehensive expressional studies applying -omics are compounded, simply by the fact that IPAH samples are scarce, as the access to human lung explants of diseased IPAH patients and of referenceable healthy donors is rather limited (164). Furthermore, comprehensive studies of the biological system require not only the understanding of the transcriptome, or the proteome, but requires a transboundary understanding of different -omics interplay in the organism. By identifying the significantly altered expression of several key genes and central biologic pathways perturbed in IPAH, thereby not only covering the coding, but also the non-coding transcriptome, we add another puzzle piece to the complex picture of PAH biology. We demonstrate the disease specific role of the lncRNA PAXIP1-AS1, explore its biological importance in relation to ECM remodelling in IPAH and reveal aspects of its multifaceted interactome that includes its downstream mediator paxillin (see major conclusions of the study in Figure 53).

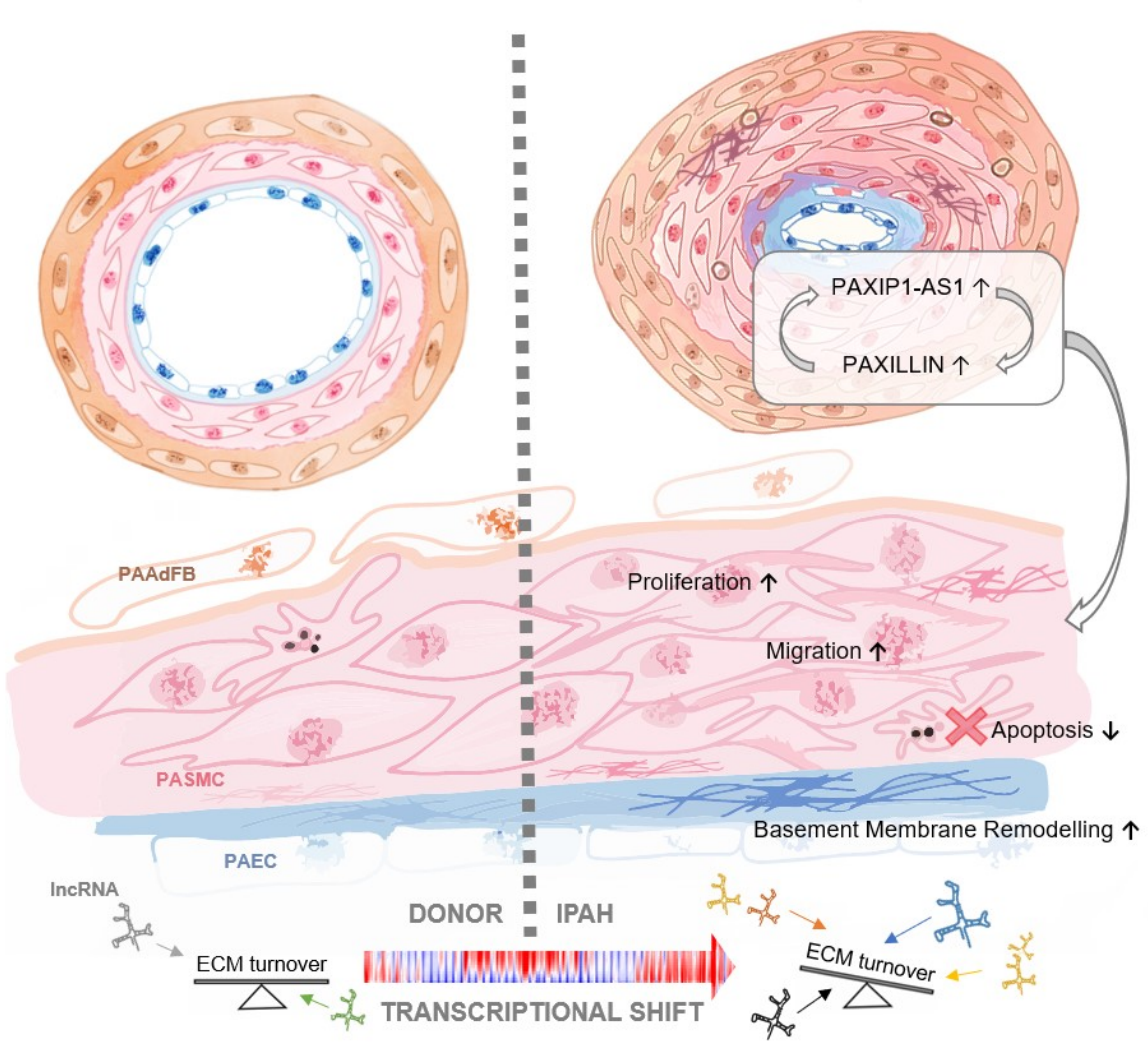

Figure 53. **LncRNAs in IPAH pulmonary arteries – the role of PAXIP1-AS1.** The lncRNA PAXIP1-AS1 is overexpressed in IPAH pulmonary arteries and acts via its downstream target paxillin. PAXIP1-AS1 is significantly involved in orchestrating PASMC function, leading to increased proliferation and migration, and decreased apoptosis in IPAH. Demonstrating that differentially expressed lncRNAs influence ECM turnover in IPAH, transcriptional analysis revealed the basement membrane as the core cellular component affected by IPAH and by PAXIP1-AS1 knockdown.

The transcriptome of the pulmonary arteries in IPAH

Several studies have attempted to analyze the global expressional changes in IPAH. A study published by Geraci et al. uses six lung homogenate samples of PAH and six donor lungs to successfully characterize expressional profiles in idiopathic and familial PAH, leading to the identification of dysregulated kinases, phosphatases, ion channel proteins and oncogenes (199). Underlining the usefulness of this high-throughput screening, a follow up study

performed by Rajkumar et al. almost ten years later uses a similar approach to identify even more differentially regulated genes using a more robust sample set: 18 PAH and 13 control lung homogenate samples. This study reports about expressional changes in proteases, cell adhesion molecules, and about changes in pathways involved in cell signalling, vascular function, cellular development and proliferation (200). IPAH is mainly known as the disease of the small pulmonary arteries. The mentioned studies using lung homogenate samples fight with the disadvantage that they only capture a fraction of the expressional differences in IPAH, as only a fraction of the samples won from the lung tissue is made of the pulmonary arteries (164). Other expressional studies performed on isolated cells of the pulmonary arteries, most frequently performed on PASMC, show cell type specific contribution to molecular mechanisms altered in IPAH (201-204). One aspect to keep in mind here is that the procedure of isolation and culturing also significantly influences gene expression (164). In this regard, the use of laser capture micro dissected small pulmonary arteries in our study brings huge advantage over studies using lung homogenate and cell samples, as the very compartment affected by IPAH is being directly analyzed here. A similar fashioned study by Laumanns et al. using six donor and six IPAH subjects had already pioneered here, identifying central mediators of the non-canonical Wnt signalling (planar cell polarity pathway) to be significantly upregulated in IPAH (205).

Overcoming the sample size limitation of the previous study, we here analyze a comparably large cohort of patients by analyzing 17 donor and 18 IPAH pulmonary arteries. In agreement with Laumanns et al. (205) we identified ECM interaction, immune reaction and cell signalling (WNT, MAPK, Ca^{2+}) as highly affected pathways in IPAH. In addition, our analysis revealed shifts in neuronal and metabolic pathways, as well as in processes of apoptosis, proliferation, cartilage development and several signalling pathways (TNF, MAPK, Notch, Relaxin, Hippo). As a disease driven by excessive vascular cell growth, the counteracting processes apoptosis and proliferation play a very important role in the pathogenesis of PAH (11, 37). The metabolic changes in IPAH may be owing to the increased energy expenditure resulting from the increased proliferation of the PASMC, or perhaps it is the hyperproliferative state that induces metabolic shifts (141, 206). The pathways MAPK signalling (32, 207), Notch signalling (208), Hippo-YAP/TAZ signalling (41, 209) and Relaxin signalling (210, 211) are strongly inter-connected pathways with involvement in angiogenic and anti-apoptotic mechanisms. Follow up studies delineating the IPAH transcriptome, such as the microarray study of lung homogenates by Stearman et al. (212) or profiling of individual lung cell populations by Saygin et al. (213), confirm several of our findings, including the importance of the ECM, Notch-, TNF-

and osteo-related signalling in IPAH. In fact, our top hit among the differentially expressed coding genes was Sclerostin (SOST), a bone morphogenetic protein (BMP) antagonist, that has been reported to be a biomarker for arterial stiffness in hypertension (214). The recent study by Saygin et al. brings an important advantage over microarrays as it applies single cell RNA sequencing (RNASeq), however it is limited by low sample sizes. RNASeq allows for a detailed simultaneous description of the transcriptomic phenotype of each cell type in the tissue, allowing an analysis of the cell type specific contribution (213).

In comparison to RNASeq, the unbiasedness of the microarray is only true up to the level the technique allows for. Microarrays only include the genes that have been annotated in the genome, meaning that a fraction of genes that are not yet known but of relevance for the study may be missed/miss-interpreted by the design, if not aware of this fact. In our case, by choosing a microarray platform that is not specifically optimized to capture small RNA species such as the miRNAs, we for example completely neglect the prevailing relevance of miRNA in IPAH (215). Nevertheless, microarrays provided a comparably economical solution (at the time) that allowed for a comprehensive study of the whole genome, that still achieves a high concordance (>75%) with RNASeq results (216). Meanwhile, RNASeq already overtook the microarrays and is widely used to analyze the complex transcriptomics. However, by robustly establishing the importance of several interconnected pathways and identifying novel players in IPAH, our study underlines the complexity of pathway dysregulation in IPAH that need to be untangled to be able to efficiently treat the disease.

The IPAH shaped extracellular matrix of the pulmonary arteries

In line with previous research (12, 38, 41, 50, 217), the outcome of our transcriptomic analysis of the small pulmonary arteries confirmed ECM's outstanding role in IPAH: the ECM was the cellular compartment that was most intensely affected in IPAH.

A more detailed transcriptomic analysis of the ECM relevant components revealed several dysregulated collagens, metalloproteinases and other matrix components that highlight the disturbed ECM homeostasis in IPAH. Exemplarily, reelin (RELN), a apolipoprotein that is known to contribute to endothelial dysfunction (218) and tissue inhibitor of metalloproteinase 3 (TIMP-3), an inhibitor of the MMPs (38) counted to the proteins that were upregulated in IPAH, along with different collagen types COL4A6, COL9A, COL13A1 and COL18A19. Among the downregulated genes were e.g. a disintegrin and metalloprotease 10 (ADAM10) that is known to cleave BMPR-II (53), multimerin 1 (MMRN1), a member of the multimerin family that is known to affect cell growth, wound healing and angiogenesis (219-221) and has been

associated with TGF-β mediated vascular remodeling in PH (222) and spondin 2 (SPON2), a protein known to be downregulated in animal models of PAH (223). Among the laminins that generally confer basement membrane stability and barrier integrity, LAMA2 was downregulated. LAMA5 on the other hand was upregulated. LAMA2 encodes a protein of which the deficiency is linked with diseases affecting the basement membrane such as muscular dystrophy (224). While the functionally conserved LAMA2 is associated with muscle development, organization and differentiation (224), LAMA5 bear other roles such as the development of peripheral nervous system, or of the retinal or renal BM, and is not functionally conserved among the species (67, 225). The type-specific regulation hints towards a complex involvement of the laminins and the BM in IPAH. In line with clinical evidence from PAH patients (12, 226), in a recent report (167), we also underline the importance of BM homeostasis and describe the thickened BM composition in IPAH vessels. Our findings here are in accordance with the mentioned studies, and show that BM proteins, such as collagen IV, collagen XVIII, fibronectin and laminin have an outstanding role in shaping the characteristic transcriptome of IPAH.

As a one-to-one translation of the transcriptomic findings is not possible when studying proteins due to the limitations given by the mRNA-protein correlation (227), the use of complementary approaches are required to augment the findings. Of note, mRNA expression of differentially expressed genes correlates more significantly with actual translation into protein when compared to non-differentially expressed genes (228). Many have conducted large scale proteomic studies, that can be very useful in defining the altered ECM and identifying novel biomarkers. A variety of clinical specimen, such as different blood samples, lung tissues and isolated cell types from human PAH patients and murine PAH models have been studied to date, resulting in a number of very comprehensive studies. Exemplarily, Abdul-Salam et al. identified complement 4a as potential diagnostic marker for IPAH using SELDI-TOF MS using IPAH plasma samples, while Yu et al. identified alpha-1-antitrypsin and vitronectin as biomarkers using gel-based proteomic analysis of serum samples of IPAH patients (229, 230). While there are studies, e.g. the proteomic study using PAH lung homogenates by Huang et al. (231), that do reveal the importance of the ECM in IPAH, most of the large scale studies (229, 230, 232-234) miss to capture the altered ECM proteomics in IPAH because they were performed in blood samples or isolated cells. Therefore, using isolated arteries from IPAH patients and healthy controls, and an unbiased bottom-up approach, we wanted to explore the proteomic composition of the pulmonary arteries that are the most affected in IPAH.

Owing to its complexity and insolubility, ECM proteins are difficult to analyze biochemically, and therefore mass spectrometric analysis of the ECM can be problematic. Overcoming this hurdle, in our proteomics approach, we adapted the challenging pipeline previously developed by Schiller et al. (143), to enrich for ECM proteins from isolated pulmonary arteries. The big proportion of detected ECM related proteins in our analysis confirmed a successful experiment setup. Moreover, Filamin-A and Myosin were detected to be most differentially expressed in IPAH, as has been previously reported in other studies (181, 182, 231). Nevertheless, we are limited in making quantitative comparisons between IPAH and donor due to the variability and lack of significance in our experiment outcome.

The general ECM profile of the PA that we were able to create with the outcome of our proteomic analysis, lead to the identification of potential matrikines that may be relevant in IPAH. Interestingly, most of the detected potential matrikines also derived from the basement membrane, again highlighting the central role of the BM that is in direct contact with PAEC (38).

Matrikines represent ideal diagnostic and prognostic biomarker candidates in IPAH: they arise from the ECM - from the very cellular compartment that is most affected in IPAH, and are to be detected in easily accessible blood samples of the patient. In this regard, the identification of endostatin as a determinant of disease severity in PAH (12, 77) can be counted as one of the most recognized and promising discoveries recently in the field of pulmonary vascular biology. Our efforts in delineating the effects of endostatin on PAEC confirmed the anti-proliferative effects previously reported for endostatin (100).

Exploring the non-coding transcriptome: PAXIP1-AS1 and its contribution to the PASMC IPAH phenotype

Another equally important aspect adequately acknowledged and analyzed in our study is the role of non-coding RNAs (ncRNA), especially the long ncRNA, in IPAH. The equally significant, large size of the non-coding transcriptome (53009 lncRNA transcripts in comparison to 87151 protein-coding RNA transcripts, GRCh38.p13) underlines the importance of the long non-coding transcriptome, that had been given less importance to until recently.
Exemplary attempts investigating into the ncRNA landscape in IPAH include the study performed by Wu D et al. (235) or Sarrion et al. (236) where several miRNA, such as miR-26b-

5p or miR23a, were identified as upregulated and involved in the vascular remodelling and hemodynamic changes in IPAH using a non-coding platform. Compared to the studies identifying miRNA that belong to the small non-coding RNAs, there is less to report about the involvement of long non-coding RNAs in IPAH. One early effort to screen for non-coding RNA regulation in IPAH had been made here by Han et al. (138) in 2017, where a number of dysregulated lncRNA were identified in lymphocytes of IPAH patients. Notable is also a follow-up RNASeq study using whole blood samples performed by Rhodes et al. (2020), that lead to the identification of several dysregulated non-coding RNAs, including 3 lncRNA that are reduced in PAH and associated with poor outcomes (237).

Despite the increased knowledge about the lncRNA and their regulatory roles in general cell biology (110), the understanding of the involvement of lncRNA in IPAH is only expanding now with ongoing research, contemporaneous with our study. A number of reports exist by now that demonstrate the role of lncRNAs in various cellular activities vital in the pathophysiology of PAH, such as proliferation, migration, apoptosis, angiogenesis, metabolism or inflammatory responses (132, 137, 237-239). In our study, we demonstrate the robust upregulation of the lncRNA PAXIP1-AS1 in small pulmonary arteries, PASMC and PAAdFB of IPAH patients, and portray its key role in the regulation of PASMC proliferation, migration and apoptosis that it exerts via the focal adhesion adaptor protein paxillin.

Examples for other lncRNA with proven roles in human PASMC function include TUG1, TYKRIL and MALAT1 (238, 240). Pro-proliferative, pro-migrative, and anti-apoptotic effects have been described for TUG1 in PASMC. Downstream, these effects were associated with the transcription factor Foxc1, miR-374c and miR-328 (131, 241). Similar pro-proliferative and anti-apoptotic characteristics have also been described for TYKRIL in IPAH pericytes and PASMC, but was described to exert its function via the p53/PDGFRβ signalling axis (129). MALAT1 was shown to influence human endothelial cell function (239), to inhibit proliferation and migration of PASMC and enhance apoptosis rate (242). He et al. proposed that MALAT1 exerts its function by interacting with miR-503 and TLR-4 receptor (242). In fact, MALAT1 can be counted to one of the most highly and abundantly expressed, and widely studied lncRNA, for which numerous modes of actions have been described in cancer, stress and inflammation related cell biology (243).

In contrast to MALAT1 that shows extraordinary conservation among mammalian species (>50%), especially in proximity of its functional cloverleaf structure at the 3’ end (243, 244),

PAXIP1-AS1 generally is a scarcely conserved, low expressed lncRNA, that but is present across different tissues under physiological conditions. The upregulation of the otherwise low profile lncRNA in IPAH pulmonary artery makes its upregulation a crucial, particularly specific response to the spatial onset of the disease (141). The subcellular localization of a lncRNA is a major determinant of its function. A nuclear-restricted expression for example suggests a role in histone modification and epigenetic transcriptional regulation (245). Having detected PAXIP1-AS1 expression in both nuclear and cytoplasmic cell compartments, we concluded a diverse and widespread role for this lncRNA.

PAXIP1-AS1: sequence, structure and functional possibilities

Several elements characteristic of the PAXIP1-AS1 speak in favour of a versatile functional involvement of this lncRNA: 1) the complex, but stable structure, 2) the cumulated occurrence of functional motifs and 3) the specific binding sites.

In its essence, the RNA molecular consists of paired or unpaired bases, but the combination of these interactions results in complex structures, that determine the functional importance of the respective RNA (110, 246). Nuclear magnetic resonance (NMR), X-ray crystallography and cryoelectron microscopy are reliable, but sophisticated and costly methods to gain such structural information on RNA (247). We used a fast and economical alternative for this; an algorithm, that predicts the RNA structure with >67% accuracy (175). The visualized optimal PAXIP1-AS1 structure included several complex structural RNA features and resulted in a relatively stable RNA composition, suggesting functional relevance (141).

The analysis of PAXIP1-AS1 sequence also revealed the presence of several Alu elements in this lncRNA. Known functions Alu elements in lncRNA perform include RNA editing, regulation of mRNA stability, translation and transcription (248-250). Alu elements are abundant mobile elements that are unique to primates (248). This observation goes in accordance with the primates-restricted conservation of PAXIP1-AS1. AU-rich elements, or ARE, are another characteristic element of PAXIP1-AS1. The presence of ARE in PAXIP1-AS1 suggest that this lncRNA may act as a cis-regulatory element that interacts with RNA binding proteins that recruit effector proteins such as protein kinases or the mRNA decay machinery, exerting translational control over certain mRNAs (251). An example for such a case is Lnc_ASNR: It binds to the trans acting RNA binding protein AUF1 with its AU-rich element. The presence of AUF1 in the cytoplasm increases mRNA degradation, as it then recruits factors required for

mRNA decay. By controlling the cytoplasmic-nuclear distribution of the AUF1, this lncRNA controls the mRNA decay process (252).

The role of lncRNA as miRNA-sponge or transcription factor (TF) recruiter is well established (114, 120, 121, 123, 127). We found several miRNA as well as TF binding sites in PAXIP1-AS1, suggesting a similar activity potential for this lncRNA. Interestingly, the TF binding sites found in PAXIP1-AS1 for example also included HIF1α, HIF2α, NFAT, FOXO1 or NFκB, transcription factors that are also implicated in pulmonary hypertension (141, 253).

While we want to underline the lack of sequence homology, striking here was the observation that the small stretch of sequence similarity that did remain homolog between most species, colocalizes with the main functional sites identified in this lncRNA (141). An interesting approach was chosen by Leisegang et al. in a similar scenario to narrow down the functional region in the lncRNA MANTIS (254): he created and separately investigated putative functional fragments of the lncRNA. Interestingly, in the case of MANTIS, it was the part that contained the Alu element that conveyed the key functionality (254).

Taken together, the analysis of the PAXIP1-AS1 sequence alone leaves us with a plethora of potential functional implications for the lncRNA PAXIP1-AS1.

The PAXIP1-AS1 interactome

The first report about the lncRNA PAXIP1-AS1, to our knowledge, was made by Weirick et al., who described its functional involvement in HEK-293 cells as a regulator of cell death (172). Here it was suggested that this lncRNA exerts its effects via its nearby coding gene PAXIP1. We foster this finding by showing that PAXIP1 is also co-upregulated with PAXIP1-AS1 in IPAH (141). PAXIP1 being a stress response gene required for cell survival (255, 256), it may be speculated that PAXIP1-AS1 acts via PAXIP1 and gets activated upon the injury leading to or further accelerating the vascular remodelling process in IPAH. Our screening for PAXIP1-AS1 regulated genes lead us in a different direction: we identified basement membrane as the most affected cellular component after PAXIP1-AS1 knockdown and found a remarkable enrichment of ECM and focal adhesion related pathways. Moreover, we established that PAXIP1-AS1 exerts its pro-proliferative, pro-migrative, and anti-apoptotic effects via the focal adhesion adaptor protein paxillin (141). Cell motility depends on functional interaction of focal adhesions with the surrounding extracellular matrix (59). In this respect, the migratory and proliferative

effects of PAXIP1-AS1 mediated via paxillin seem conclusive. Focal adhesion proteins, including paxillin, have also been previously associated with IPAH (59, 60, 140, 141). The phosphorylation and following activation of paxillin is driven by the focal adhesion kinase (FAK), a tyrosine kinase. Both FAK and paxillin have been previously reported to be activated in IPAH and proven to be involved in the increased proliferation and migration, as well as the decreased apoptosis of PASMC in IPAH (59, 60, 257). Interestingly, also endostatin has been reported to disrupt the cytoskeletal organization via focal adhesion kinase and paxillin (258). Having established a strong link between PAXIP1-AS1, the focal adhesions, the ECM, and especially the basement membrane, it was imperative to investigate the role of PAXIP1-AS1 in endostatin regulation. The unchanged endostatin levels after PAXIP1-AS1 and paxillin overexpression, and the observed (tendential) downregulation of MMP1 dismantled our initial hypothesis that this lncRNA regulated the secretion of endostatin from COL18A1 via upregulation of MMP1 in IPAH. Nevertheless, while we investigated the possibility of endostatin being regulated downstream of PAXIP1-AS1, the potential for PAXIP1-AS1 expression to be regulated by endostatin also remains to be explored.

Taken together, our first results suggest a huge regulatory potential for this multifaceted lncRNA, mediated via complex regulatory interactions. Clearly, more clarification on the PAXIP1-AS1 interactome is needed to thoroughly understand how PAXIP1-AS1 leads or perhaps only reacts to the remodelling process in IPAH.

PAXIP1-AS1 as a biomarker?

Many studies performed on blood samples aim at identifying (linear) lncRNA that can be used as liquid biomarkers (138). In contrast to linear lncRNA, circular lncRNA (circRNA) possess a far better potential to be applied as biomarker in early diagnosis. The majority of linear lncRNA are not detectable or are only sporadically detectable due to their low abundance and structural instability in plasma (259), while circRNA are more stable due to better resistance to RNases (176). Pioneering in the field of circRNA biomarkers in IPAH, Zang et al. reported that the circular lncRNA transcript hsa_circ_0068481 is overexpressed in the serum of IPAH patients and correlated with clinical parameters evaluated in PAH (260). Even though not to be completely excluded from further research as our conclusions rely on data from computational predictions, our initial investigation showed that PAXIP1-AS1 does not have any circular transcripts.

While the chances are higher for circular RNAs to be useful as a good liquid biomarker (176), there are several studies demonstrating that also linear lncRNA can be stably detected in liquid biopsy samples (e.g. plasma, serum, urine or bronchoalveolar lavage fluid) and efficiently applied as circulating biomarker for diseases (261, 262). MALAT1 is an exemplary lncRNA which has been proven to possess diagnostic and prognostic value in osteosarcoma (263).
Overlaps between transcriptomic studies of blood samples (237, 240) and studies performed on tissue samples (141, 202, 212), support the hypothesis that PAXIP1-AS1 could be used as a liquid biomarker. RNASeq results published in the GTEX platform suggest that PAXIP1-AS1 expression is rather low in whole blood samples, but the fact that it has been detected already makes it worthwhile to enquire how PAXIP1-AS1 is expressed in easily accessible liquid biopsy samples or circulating cells of IPAH patients. If successfully detectable in these samples, one important factor remaining to be assessed when assembling the biomarker panel then is the specificity of PAXIP1-AS1 upregulation, as PAXIP1-AS1 is also associated with gliomas (264).

While our findings bring some light to the molecular mechanisms involving PAXIP1-AS1, it clearly signals that there is more to discover on the molecular grounds that is regulating and being regulated by PAXIP1-AS1. A major limitation of our study is that the IPAH samples we use represent end-stage of the disease (141). We need to decipher early PAXIP1-AS1 mediated molecular ongoings leading to the remodelling, to be able to efficiently use this lncRNA as a biomarker or target for disease treatment. In this regard, the use of preclinical models come in very handy, as they could allow a temporal assessment of lncRNA expression and involvement in PAH progression. Furthermore, they bring the advantage of a more controlled experimental setup (which is less the case when lung samples are used drawn from patients that have been influenced by different treatments and environmental factors) and sample availability (265). The lack of sequence conservation in species other than primates complicates the use of animal models in the case of PAXIP1-AS1 (141). In this respect, a clever solution was applied by Xu et al. where xenografts of glioma cells in nude mice were used to characterize the PAXIP1-AS1 – ETS1 – KIF14 interaction *in vivo*. A more comprehensive study of PAXIP1-AS1 *in vivo* would require humanized animal models (266) for pulmonary arterial hypertension that are not available yet.

To sum up, in this study, we characterize the transcriptome of the remodelled IPAH pulmonary arteries, especially focusing on the expression of ECM related components and demonstrate the significance of lncRNAs in IPAH. Furthermore, we characterize the role of PAXIP1-AS1 in orchestrating PASMC function in IPAH and reveal that it acts via regulation of its downstream

target paxillin, a focal adhesion adaptor protein. While we reveal the basement membrane as the core cellular component affected by IPAH and by PAXIP1-AS1 knockdown, further research is needed to clarify the role of PAXIP1-AS1 and its interactome in this setting.

5. Bibliography

1. Vazquez ZGS, Klinger JR. Guidelines for the Treatment of Pulmonary Arterial Hypertension. Lung. 2020;198(4):581-96.
2. Humbert M, Sitbon O, Simonneau G. Treatment of pulmonary arterial hypertension. The New England journal of medicine. 2004;351(14):1425-36.
3. Rubin LJ. Primary pulmonary hypertension. The New England journal of medicine. 1997;336(2):111-7.
4. Humbert M, Sitbon O, Chaouat A, Bertocchi M, Habib G, Gressin V, et al. Survival in patients with idiopathic, familial, and anorexigen-associated pulmonary arterial hypertension in the modern management era. Circulation. 2010;122(2):156-63.
5. Prins KW, Thenappan T. World Health Organization Group I Pulmonary Hypertension: Epidemiology and Pathophysiology. Cardiology clinics. 2016;34(3):363-74.
6. Simonneau G, Montani D, Celermajer DS, Denton CP, Gatzoulis MA, Krowka M, et al. Haemodynamic definitions and updated clinical classification of pulmonary hypertension. European Respiratory Journal. 2019;53(1):1801913.
7. Deborah Jo Levine MF. Pulmonary Arterial Hypertension: Updates in Epidemiology and Evaluation of Patients. Supplements and Featured Publications. 2021;27(3).
8. Coons JC, Pogue K, Kolodziej AR, Hirsch GA, George MP. Pulmonary Arterial Hypertension: a Pharmacotherapeutic Update. Current cardiology reports. 2019;21(11):141.
9. Rabinovitch M. Pathobiology of pulmonary hypertension. Annual review of pathology. 2007;2:369-99.
10. Ricard-Blum S, Salza R. Matricryptins and matrikines: biologically active fragments of the extracellular matrix. Experimental dermatology. 2014;23(7):457-63.
11. Humbert M, Morrell NW, Archer SL, Stenmark KR, MacLean MR, Lang IM, et al. Cellular and molecular pathobiology of pulmonary arterial hypertension. Journal of the American College of Cardiology. 2004;43(12 Suppl S):13s-24s.
12. Hoffmann J, Marsh LM, Pieper M, Stacher E, Ghanim B, Kovacs G, et al. Compartment-specific expression of collagens and their processing enzymes in intrapulmonary arteries of IPAH patients. American journal of physiology Lung cellular and molecular physiology. 2015;308(10):L1002-13.
13. Dodson MW, Brown LM, Elliott CG. Pulmonary Arterial Hypertension. Heart failure clinics. 2018;14(3):255-69.
14. Steffes LC, Froistad AA, Andruska A, Boehm M, McGlynn M, Zhang F, et al. A Notch3-Marked Subpopulation of Vascular Smooth Muscle Cells Is the Cell of Origin for Occlusive Pulmonary Vascular Lesions. Circulation. 2020;142(16):1545-61.
15. Masri FA, Xu W, Comhair SAA, Asosingh K, Koo M, Vasanji A, et al. Hyperproliferative apoptosis-resistant endothelial cells in idiopathic pulmonary arterial hypertension. American Journal of Physiology-Lung Cellular and Molecular Physiology. 2007;293(3):L548-L54.
16. Wright L, Tuder RM, Wang J, Cool CD, Lepley RA, Voelkel NF. 5-Lipoxygenase and 5-lipoxygenase activating protein (FLAP) immunoreactivity in lungs from patients with primary pulmonary hypertension. American journal of respiratory and critical care medicine. 1998;157(1):219-29.
17. Tuder RM, Groves B, Badesch DB, Voelkel NF. Exuberant endothelial cell growth and elements of inflammation are present in plexiform lesions of pulmonary hypertension. The American journal of pathology. 1994;144(2):275-85.
18. Cool CD, Stewart JS, Werahera P, Miller GJ, Williams RL, Voelkel NF, et al. Three-dimensional reconstruction of pulmonary arteries in plexiform pulmonary hypertension using cell-specific markers. Evidence for a dynamic and heterogeneous process of pulmonary endothelial cell growth. The American journal of pathology. 1999;155(2):411-9.

19. Westöö C, Norvik C, Peruzzi N, van der Have O, Lovric G, Jeremiasen I, et al. Distinct types of plexiform lesions identified by synchrotron-based phase-contrast micro-CT. American journal of physiology Lung cellular and molecular physiology. 2021;321(1):L17-l28.
20. Chaouat A, Weitzenblum E, Higenbottam T. The role of thrombosis in severe pulmonary hypertension. The European respiratory journal. 1996;9(2):356-63.
21. Varol E, Uysal BA, Ozaydin M. Platelet indices in patients with pulmonary arterial hypertension. Clinical and applied thrombosis/hemostasis : official journal of the International Academy of Clinical and Applied Thrombosis/Hemostasis. 2011;17(6):E171-4.
22. Kurakula K, Smolders V, Tura-Ceide O, Jukema JW, Quax PHA, Goumans MJ. Endothelial Dysfunction in Pulmonary Hypertension: Cause or Consequence? Biomedicines. 2021;9(1).
23. Beaulieu LM, Freedman JE. Chapter 17 - Inhibition of Platelet Function by the Endothelium. In: Michelson AD, editor. Platelets (Third Edition): Academic Press; 2013. p. 313-42.
24. Morrell NW, Aldred MA, Chung WK, Elliott CG, Nichols WC, Soubrier F, et al. Genetics and genomics of pulmonary arterial hypertension. European Respiratory Journal. 2019;53(1):1801899.
25. Schermuly RT, Ghofrani HA, Wilkins MR, Grimminger F. Mechanisms of disease: pulmonary arterial hypertension. Nature reviews Cardiology. 2011;8(8):443-55.
26. Wang J, Feng W, Li F, Shi W, Zhai C, Li S, et al. SphK1/S1P mediates TGF-β1-induced proliferation of pulmonary artery smooth muscle cells and its potential mechanisms. Pulmonary circulation. 2019;9(1):2045894018816977.
27. Perros F, Montani D, Dorfmüller P, Durand-Gasselin I, Tcherakian C, Le Pavec J, et al. Platelet-derived growth factor expression and function in idiopathic pulmonary arterial hypertension. American journal of respiratory and critical care medicine. 2008;178(1):81-8.
28. Wu K, Tang H, Lin R, Carr SG, Wang Z, Babicheva A, et al. Endothelial platelet-derived growth factor-mediated activation of smooth muscle platelet-derived growth factor receptors in pulmonary arterial hypertension. Pulmonary circulation. 2020;10(3):2045894020948470.
29. Selimovic N, Bergh CH, Andersson B, Sakiniene E, Carlsten H, Rundqvist B. Growth factors and interleukin-6 across the lung circulation in pulmonary hypertension. The European respiratory journal. 2009;34(3):662-8.
30. Gore B, Izikki M, Mercier O, Dewachter L, Fadel E, Humbert M, et al. Key role of the endothelial TGF-β/ALK1/endoglin signaling pathway in humans and rodents pulmonary hypertension. PLoS One. 2014;9(6):e100310.
31. Hemnes AR, Humbert M. Pathobiology of pulmonary arterial hypertension: understanding the roads less travelled. European respiratory review : an official journal of the European Respiratory Society. 2017;26(146).
32. Rieg AD, Suleiman S, Anker C, Verjans E, Rossaint R, Uhlig S, et al. PDGF-BB regulates the pulmonary vascular tone: impact of prostaglandins, calcium, MAPK- and PI3K/AKT/mTOR signalling and actin polymerisation in pulmonary veins of guinea pigs. Respiratory research. 2018;19(1):120.
33. Guo ML, Kook YH, Shannon CE, Buch S. Notch3/VEGF-A axis is involved in TAT-mediated proliferation of pulmonary artery smooth muscle cells: Implications for HIV-associated PAH. Cell death discovery. 2018;4:22.
34. You B, Liu Y, Chen J, Huang X, Peng H, Liu Z, et al. Vascular peroxidase 1 mediates hypoxia-induced pulmonary artery smooth muscle cell proliferation, apoptosis resistance and migration. Cardiovasc Res. 2018;114(1):188-99.
35. Goncharov DA, Kudryashova TV, Ziai H, Ihida-Stansbury K, DeLisser H, Krymskaya VP, et al. Mammalian target of rapamycin complex 2 (mTORC2) coordinates pulmonary artery smooth muscle cell metabolism, proliferation, and survival in pulmonary arterial hypertension. Circulation. 2014;129(8):864-74.
36. Teichert-Kuliszewska K, Kutryk MJ, Kuliszewski MA, Karoubi G, Courtman DW, Zucco L, et al. Bone morphogenetic protein receptor-2 signaling promotes pulmonary arterial

endothelial cell survival: implications for loss-of-function mutations in the pathogenesis of pulmonary hypertension. Circulation research. 2006;98(2):209-17.
37. Zhang S, Fantozzi I, Tigno DD, Yi ES, Platoshyn O, Thistlethwaite PA, et al. Bone morphogenetic proteins induce apoptosis in human pulmonary vascular smooth muscle cells. American journal of physiology Lung cellular and molecular physiology. 2003;285(3):L740-54.
38. Chelladurai P, Seeger W, Pullamsetti SS. Matrix metalloproteinases and their inhibitors in pulmonary hypertension. The European respiratory journal. 2012;40(3):766-82.
39. Estrada KD, Chesler NC. Collagen-related gene and protein expression changes in the lung in response to chronic hypoxia. Biomechanics and modeling in mechanobiology. 2009;8(4):263-72.
40. Gan CT, Lankhaar JW, Westerhof N, Marcus JT, Becker A, Twisk JW, et al. Noninvasively assessed pulmonary artery stiffness predicts mortality in pulmonary arterial hypertension. Chest. 2007;132(6):1906-12.
41. Bertero T, Cottrill KA, Annis S, Bhat B, Gochuico BR, Osorio JC, et al. A YAP/TAZ-miR-130/301 molecular circuit exerts systems-level control of fibrosis in a network of human diseases and physiologic conditions. Scientific reports. 2015;5:18277.
42. Bertero T, Cottrill KA, Lu Y, Haeger CM, Dieffenbach P, Annis S, et al. Matrix Remodeling Promotes Pulmonary Hypertension through Feedback Mechanoactivation of the YAP/TAZ-miR-130/301 Circuit. Cell reports. 2015;13(5):1016-32.
43. Bertero T, Oldham WM, Cottrill KA, Pisano S, Vanderpool RR, Yu Q, et al. Vascular stiffness mechanoactivates YAP/TAZ-dependent glutaminolysis to drive pulmonary hypertension. The Journal of clinical investigation. 2016;126(9):3313-35.
44. Stacher E, Graham BB, Hunt JM, Gandjeva A, Groshong SD, McLaughlin VV, et al. Modern age pathology of pulmonary arterial hypertension. American journal of respiratory and critical care medicine. 2012;186(3):261-72.
45. Botney MD, Liptay MJ, Kaiser LR, Cooper JD, Parks WC, Mecham RP. Active collagen synthesis by pulmonary arteries in human primary pulmonary hypertension. The American journal of pathology. 1993;143(1):121-9.
46. Rosenberg HG, Williams WG, Trusler GA, Higa T, Rabinovitch M. Structural composition of central pulmonary arteries. Growth potential after surgical shunts. The Journal of thoracic and cardiovascular surgery. 1987;94(4):498-503.
47. Poiani GJ, Tozzi CA, Yohn SE, Pierce RA, Belsky SA, Berg RA, et al. Collagen and elastin metabolism in hypertensive pulmonary arteries of rats. Circulation research. 1990;66(4):968-78.
48. Jones PL, Cowan KN, Rabinovitch M. Tenascin-C, proliferation and subendothelial fibronectin in progressive pulmonary vascular disease. The American journal of pathology. 1997;150(4):1349-60.
49. Lorenzen JM, Nickel N, Krämer R, Golpon H, Westerkamp V, Olsson KM, et al. Osteopontin in patients with idiopathic pulmonary hypertension. Chest. 2011;139(5):1010-7.
50. Thenappan T, Chan SY, Weir EK. Role of extracellular matrix in the pathogenesis of pulmonary arterial hypertension. American journal of physiology Heart and circulatory physiology. 2018;315(5):H1322-h31.
51. Ruffenach G, Chabot S, Tanguay VF, Courboulin A, Boucherat O, Potus F, et al. Role for Runt-related Transcription Factor 2 in Proliferative and Calcified Vascular Lesions in Pulmonary Arterial Hypertension. American journal of respiratory and critical care medicine. 2016;194(10):1273-85.
52. Vestweber D. How leukocytes cross the vascular endothelium. Nature Reviews Immunology. 2015;15(11):692-704.
53. Hurst LA, Dunmore BJ, Long L, Crosby A, Al-Lamki R, Deighton J, et al. TNFα drives pulmonary arterial hypertension by suppressing the BMP type-II receptor and altering NOTCH signalling. Nature Communications. 2017;8(1):14079.
54. Hanemaaijer R, Koolwijk P, le Clercq L, de Vree WJA, van Hinsbergh VWM. Regulation of matrix metalloproteinase expression in human vein and microvascular endothelial cells.

Effects of tumour necrosis factor α, interleukin 1 and phorbol ester. Biochemical Journal. 1993;296(3):803-9.
55. Tielemans B, Stoian L, Gijsbers R, Michiels A, Wagenaar A, Farre Marti R, et al. Cytokines trigger disruption of endothelium barrier function and p38 MAP kinase activation in BMPR2-silenced human lung microvascular endothelial cells. Pulmonary circulation. 2019;9(4):2045894019883607.
56. Tannenberg P, Tran-Lundmark K. The extracellular matrix in early and advanced pulmonary arterial hypertension. American journal of physiology Heart and circulatory physiology. 2018;315(6):H1684-h6.
57. Lacolley P, Regnault V, Segers P, Laurent S. Vascular Smooth Muscle Cells and Arterial Stiffening: Relevance in Development, Aging, and Disease. Physiological reviews. 2017;97(4):1555-617.
58. Hynes RO. Integrins: bidirectional, allosteric signaling machines. Cell. 2002;110(6):673-87.
59. Veith C, Marsh LM, Wygrecka M, Rutschmann K, Seeger W, Weissmann N, et al. Paxillin regulates pulmonary arterial smooth muscle cell function in pulmonary hypertension. The American journal of pathology. 2012;181(5):1621-33.
60. Paulin R, Meloche J, Courboulin A, Lambert C, Haromy A, Courchesne A, et al. Targeting cell motility in pulmonary arterial hypertension. The European respiratory journal. 2014;43(2):531-44.
61. Umesh A, Paudel O, Cao YN, Myers AC, Sham JS. Alteration of pulmonary artery integrin levels in chronic hypoxia and monocrotaline-induced pulmonary hypertension. Journal of vascular research. 2011;48(6):525-37.
62. Gatseva A, Sin YY, Brezzo G, Van Agtmael T. Basement membrane collagens and disease mechanisms. Essays in biochemistry. 2019;63(3):297-312.
63. Miner JH, Nguyen NM. Extracellular Matrix: Basement Membranes. In: Janes SM, editor. Encyclopedia of Respiratory Medicine (Second Edition). Oxford: Academic Press; 2022. p. 130-6.
64. Mutgan AC, Jandl K, Kwapiszewska G. Endothelial Basement Membrane Components and Their Products, Matrikines: Active Drivers of Pulmonary Hypertension? Cells. 2020;9(9).
65. Glentis A, Gurchenkov V, Matic Vignjevic D. Assembly, heterogeneity, and breaching of the basement membranes. Cell adhesion & migration. 2014;8(3):236-45.
66. Khoshnoodi J, Pedchenko V, Hudson BG. Mammalian collagen IV. Microscopy research and technique. 2008;71(5):357-70.
67. Domogatskaya A, Rodin S, Tryggvason K. Functional Diversity of Laminins. Annual Review of Cell and Developmental Biology. 2012;28(1):523-53.
68. Monboisse JC, Oudart JB, Ramont L, Brassart-Pasco S, Maquart FX. Matrikines from basement membrane collagens: a new anti-cancer strategy. Biochimica et biophysica acta. 2014;1840(8):2589-98.
69. Huang WC, Ke MW, Cheng CC, Shen MC, Huang WT, Lee TR, et al. P6265Pro-inflammatory macrophages upregulate MMP-1 and MMP-10 gene expression in pulmonary arterial hypertension. European Heart Journal. 2017;38(suppl_1).
70. Mumby S, Perros F, Hui C, Xu BL, Xu W, Elyasigomari V, et al. Extracellular matrix degradation pathways and fatty acid metabolism regulate distinct pulmonary vascular cell types in pulmonary arterial hypertension. Pulmonary circulation. 2021;11(1):2045894021996190.
71. George G, Walker J, Summer R. Pulmonary Matrikines: Origin, Function, and Contribution to Fibrotic and Non-fibrotic Lung Disease. In: Willis MS, Yates CC, Schisler JC, editors. Fibrosis in Disease : An Organ-Based Guide to Disease Pathophysiology and Therapeutic Considerations. Cham: Springer International Publishing; 2019. p. 121-33.
72. Abdul Roda M, Fernstrand AM, Redegeld FA, Blalock JE, Gaggar A, Folkerts G. The matrikine PGP as a potential biomarker in COPD. American Journal of Physiology-Lung Cellular and Molecular Physiology. 2015;308(11):L1095-L101.

73. Gaggar A, Jackson PL, Noerager BD, O'Reilly PJ, McQuaid DB, Rowe SM, et al. A novel proteolytic cascade generates an extracellular matrix-derived chemoattractant in chronic neutrophilic inflammation. Journal of immunology (Baltimore, Md : 1950). 2008;180(8):5662-9.
74. Tojais NF, Cao A, Lai YJ, Wang L, Chen PI, Alcazar MAA, et al. Codependence of Bone Morphogenetic Protein Receptor 2 and Transforming Growth Factor-β in Elastic Fiber Assembly and Its Perturbation in Pulmonary Arterial Hypertension. Arterioscler Thromb Vasc Biol. 2017;37(8):1559-69.
75. Chang YT, Chan CK, Eriksson I, Johnson PY, Cao X, Westöö C, et al. Versican accumulates in vascular lesions in pulmonary arterial hypertension. Pulmonary circulation. 2016;6(3):347-59.
76. O'Reilly MS, Boehm T, Shing Y, Fukai N, Vasios G, Lane WS, et al. Endostatin: an endogenous inhibitor of angiogenesis and tumor growth. Cell. 1997;88(2):277-85.
77. Damico R, Kolb TM, Valera L, Wang L, Housten T, Tedford RJ, et al. Serum endostatin is a genetically determined predictor of survival in pulmonary arterial hypertension. American journal of respiratory and critical care medicine. 2015;191(2):208-18.
78. Simpson CE, Griffiths M, Yang J, Nies MK, Vaidya RD, Brandal S, et al. The angiostatic peptide endostatin enhances mortality risk prediction in pulmonary arterial hypertension. ERJ open research. 2021;7(4).
79. Kawamura M, Yamasawa F, Ishizaka A, Kato R, Kikuchi K, Kobayashi K, et al. Serum concentration of 7S collagen and prognosis in patients with the adult respiratory distress syndrome. Thorax. 1994;49(2):144.
80. Sand JMB, Knox AJ, Lange P, Sun S, Kristensen JH, Leeming DJ, et al. Accelerated extracellular matrix turnover during exacerbations of COPD. Respiratory research. 2015;16(1):69.
81. Schumann DM, Leeming D, Papakonstantinou E, Blasi F, Kostikas K, Boersma W, et al. Collagen Degradation and Formation Are Elevated in Exacerbated COPD Compared With Stable Disease. CHEST. 2018;154(4):798-807.
82. Rønnow SR, Sand JMB, Langholm LL, Manon-Jensen T, Karsdal MA, Tal-Singer R, et al. Type IV collagen turnover is predictive of mortality in COPD: a comparison to fibrinogen in a prospective analysis of the ECLIPSE cohort. Respiratory research. 2019;20(1):63.
83. Sand JM, Larsen L, Hogaboam C, Martinez F, Han M, Røssel Larsen M, et al. MMP Mediated Degradation of Type IV Collagen Alpha 1 and Alpha 3 Chains Reflects Basement Membrane Remodeling in Experimental and Clinical Fibrosis – Validation of Two Novel Biomarker Assays. PLOS ONE. 2013;8(12):e84934.
84. Burgess JK, Boustany S, Moir LM, Weckmann M, Lau JY, Grafton K, et al. Reduction of tumstatin in asthmatic airways contributes to angiogenesis, inflammation, and hyperresponsiveness. American journal of respiratory and critical care medicine. 2010;181(2):106-15.
85. Asai K, Kanazawa H, Otani K, Shiraishi S, Hirata K, Yoshikawa J. Imbalance between vascular endothelial growth factor and endostatin levels in induced sputum from asthmatic subjects. Journal of Allergy and Clinical Immunology. 2002;110(4):571-5.
86. Perkins GD, Nathani N, Richter AG, Park D, Shyamsundar M, Heljasvaara R, et al. Type XVIII collagen degradation products in acute lung injury. Critical Care. 2009;13(2):R52.
87. Richter AG, McKeown S, Rathinam S, Harper L, Rajesh P, McAuley DF, et al. Soluble endostatin is a novel inhibitor of epithelial repair in idiopathic pulmonary fibrosis. Thorax. 2009;64(2):156.
88. Wu Y, Qin J, He J, Shen Y, Wang H, Li Y, et al. Serum Endostatin Is a Novel Marker for COPD Associated with Lower Lung Function, Exacerbation and Systemic Inflammation. International journal of chronic obstructive pulmonary disease. 2020;15:397-407.
89. Sand JMB, Tanino Y, Karsdal MA, Nikaido T, Misa K, Sato Y, et al. A Serological Biomarker of Versican Degradation is Associated with Mortality Following Acute Exacerbations of Idiopathic Interstitial Pneumonia. Respiratory research. 2018;19(1):82.

90. Lemaire F, Audonnet S, Perotin J-M, Gaudry P, Dury S, Ancel J, et al. The elastin peptide VGVAPG increases CD4+ T-cell IL-4 production in patients with chronic obstructive pulmonary disease. Respiratory research. 2021;22(1):14.
91. Patel DF, Snelgrove RJ. The multifaceted roles of the matrikine Pro-Gly-Pro in pulmonary health and disease. European Respiratory Review. 2018;27(148):180017.
92. Pehrsson M, Bager CL, Karsdal MA. Chapter 18 - Type XVIII collagen. In: Karsdal MA, editor. Biochemistry of Collagens, Laminins and Elastin (Second Edition): Academic Press; 2019. p. 149-62.
93. Mohajeri A, Sanaei S, Kiafar F, Fattahi A, Khalili M, Zarghami N. The Challenges of Recombinant Endostatin in Clinical Application: Focus on the Different Expression Systems and Molecular Bioengineering. Advanced pharmaceutical bulletin. 2017;7(1):21-34.
94. Jing Y, Lu H, Wu K, Subramanian IV, Ramakrishnan S. Inhibition of ovarian cancer by RGD-P125A-endostatin-Fc fusion proteins. International journal of cancer. 2011;129(3):751-61.
95. Yokoyama Y, Ramakrishnan S. Improved biological activity of a mutant endostatin containing a single amino-acid substitution. British Journal of Cancer. 2004;90(8):1627-35.
96. Ergün S, Kilic N, Wurmbach JH, Ebrahimnejad A, Fernando M, Sevinc S, et al. Endostatin inhibits angiogenesis by stabilization of newly formed endothelial tubes. Angiogenesis. 2001;4(3):193-206.
97. Voelkel NF, Gomez-Arroyo J. The role of vascular endothelial growth factor in pulmonary arterial hypertension. The angiogenesis paradox. American journal of respiratory cell and molecular biology. 2014;51(4):474-84.
98. Kim YM, Hwang S, Kim YM, Pyun BJ, Kim TY, Lee ST, et al. Endostatin blocks vascular endothelial growth factor-mediated signaling via direct interaction with KDR/Flk-1. The Journal of biological chemistry. 2002;277(31):27872-9.
99. Chang JH, Javier JA, Chang GY, Oliveira HB, Azar DT. Functional characterization of neostatins, the MMP-derived, enzymatic cleavage products of type XVIII collagen. FEBS letters. 2005;579(17):3601-6.
100. Goyanes AM, Moldobaeva A, Marimoutou M, Varela LC, Wang L, Johnston LF, et al. Functional Impact of Human Genetic Variants of COL18A1/Endostatin on Pulmonary Endothelium. American journal of respiratory cell and molecular biology. 2020;62(4):524-34.
101. Ling Y, Lu N, Gao Y, Chen Y, Wang S, Yang Y, et al. Endostar induces apoptotic effects in HUVECs through activation of caspase-3 and decrease of Bcl-2. Anticancer research. 2009;29(1):411-7.
102. Dhanabal M, Ramchandran R, Waterman MJ, Lu H, Knebelmann B, Segal M, et al. Endostatin induces endothelial cell apoptosis. The Journal of biological chemistry. 1999;274(17):11721-6.
103. Xu X, Mao W, Chen Q, Zhuang Q, Wang L, Dai J, et al. Endostar, a Modified Recombinant Human Endostatin, Suppresses Angiogenesis through Inhibition of Wnt/β-Catenin Signaling Pathway. PLOS ONE. 2014;9(9):e107463.
104. Dejana E. The role of wnt signaling in physiological and pathological angiogenesis. Circulation research. 2010;107(8):943-52.
105. Xu HL, Tan HN, Wang FS, Tang W. Research advances of endostatin and its short internal fragments. Current protein & peptide science. 2008;9(3):275-83.
106. Lee SJ, Jang JW, Kim YM, Lee HI, Jeon JY, Kwon YG, et al. Endostatin binds to the catalytic domain of matrix metalloproteinase-2. FEBS letters. 2002;519(1-3):147-52.
107. Frankish A, Diekhans M, Jungreis I, Lagarde J, Loveland JE, Mudge JM, et al. GENCODE 2021. Nucleic acids research. 2021;49(D1):D916-d23.
108. Ratti M, Lampis A, Ghidini M, Salati M, Mirchev MB, Valeri N, et al. MicroRNAs (miRNAs) and Long Non-Coding RNAs (lncRNAs) as New Tools for Cancer Therapy: First Steps from Bench to Bedside. Targeted oncology. 2020;15(3):261-78.

109. Lee S, Seo H-H, Lee CY, Lee J, Shin S, Kim SW, et al. Human Long Noncoding RNA Regulation of Stem Cell Potency and Differentiation. Stem Cells International. 2017;2017:6374504.
110. Zampetaki A, Albrecht A, Steinhofel K. Long Non-coding RNA Structure and Function: Is There a Link? Frontiers in Physiology. 2018;9(1201).
111. Zahid KR, Raza U, Chen J, Raj UJ, Gou D. Pathobiology of pulmonary artery hypertension: role of long non-coding RNAs. Cardiovascular Research. 2020;116(12):1937-47.
112. Willingham AT, Orth AP, Batalov S, Peters EC, Wen BG, Aza-Blanc P, et al. A strategy for probing the function of noncoding RNAs finds a repressor of NFAT. Science (New York, NY). 2005;309(5740):1570-3.
113. Chen L, Rao A, Harrison SC. Signal integration by transcription-factor assemblies: interactions of NF-AT1 and AP-1 on the IL-2 promoter. Cold Spring Harbor symposia on quantitative biology. 1999;64:527-31.
114. Tseng Y-Y, Moriarity BS, Gong W, Akiyama R, Tiwari A, Kawakami H, et al. PVT1 dependence in cancer with MYC copy-number increase. Nature. 2014;512(7512):82-6.
115. Mfossa ACM, Thekkekara Puthenparampil H, Inalegwu A, Coolkens A, Baatout S, Benotmane MA, et al. Exposure to Ionizing Radiation Triggers Prolonged Changes in Circular RNA Abundance in the Embryonic Mouse Brain and Primary Neurons. Cells. 2019;8(8).
116. Qin S, Zhao Y, Lim G, Lin H, Zhang X, Zhang X. Circular RNA PVT1 acts as a competing endogenous RNA for miR-497 in promoting non-small cell lung cancer progression. Biomedicine & Pharmacotherapy. 2019;111:244-50.
117. Wang Z, Zhang XJ, Ji YX, Zhang P, Deng KQ, Gong J, et al. The long noncoding RNA Chaer defines an epigenetic checkpoint in cardiac hypertrophy. Nature medicine. 2016;22(10):1131-9.
118. Rinn JL, Kertesz M, Wang JK, Squazzo SL, Xu X, Brugmann SA, et al. Functional demarcation of active and silent chromatin domains in human HOX loci by noncoding RNAs. Cell. 2007;129(7):1311-23.
119. Mondal T, Subhash S, Vaid R, Enroth S, Uday S, Reinius B, et al. MEG3 long noncoding RNA regulates the TGF-β pathway genes through formation of RNA–DNA triplex structures. Nature Communications. 2015;6(1):7743.
120. Paraskevopoulou MD, Hatzigeorgiou AG. Analyzing MiRNA-LncRNA Interactions. Methods in molecular biology (Clifton, NJ). 2016;1402:271-86.
121. Wang J, Liu X, Wu H, Ni P, Gu Z, Qiao Y, et al. CREB up-regulates long non-coding RNA, HULC expression through interaction with microRNA-372 in liver cancer. Nucleic acids research. 2010;38(16):5366-83.
122. Xia L, Nie D, Wang G, Sun C, Chen G. FER1L4/miR-372/E2F1 works as a ceRNA system to regulate the proliferation and cell cycle of glioma cells. Journal of cellular and molecular medicine. 2019;23(5):3224-33.
123. Kallen AN, Zhou XB, Xu J, Qiao C, Ma J, Yan L, et al. The imprinted H19 lncRNA antagonizes let-7 microRNAs. Molecular cell. 2013;52(1):101-12.
124. Piccoli M-T, Gupta SK, Viereck J, Foinquinos A, Samolovac S, Kramer FL, et al. Inhibition of the Cardiac Fibroblast–Enriched lncRNA Meg3 Prevents Cardiac Fibrosis and Diastolic Dysfunction. Circulation research. 2017;121(5):575-83.
125. Su H, Xu X, Yan C, Shi Y, Hu Y, Dong L, et al. LncRNA H19 promotes the proliferation of pulmonary artery smooth muscle cells through AT(1)R via sponging let-7b in monocrotaline-induced pulmonary arterial hypertension. Respiratory research. 2018;19(1):254.
126. Brock M, Schuoler C, Leuenberger C, Bühlmann C, Haider TJ, Vogel J, et al. Analysis of hypoxia-induced noncoding RNAs reveals metastasis-associated lung adenocarcinoma transcript 1 as an important regulator of vascular smooth muscle cell proliferation. Experimental biology and medicine (Maywood, NJ). 2017;242(5):487-96.
127. Wang D, Xu H, Wu B, Jiang S, Pan H, Wang R, et al. Long non-coding RNA MALAT1 sponges miR-124-3p.1/KLF5 to promote pulmonary vascular remodeling and cell cycle

progression of pulmonary artery hypertension. International journal of molecular medicine. 2019;44(3):871-84.
128. Wang H, Qin R, Cheng Y. LncRNA-Ang362 Promotes Pulmonary Arterial Hypertension by Regulating miR-221 and miR-222. Shock (Augusta, Ga). 2020;53(6):723-9.
129. Zehendner CM, Valasarajan C, Werner A, Boeckel JN, Bischoff FC, John D, et al. Long Noncoding RNA TYKRIL Plays a Role in Pulmonary Hypertension via the p53-mediated Regulation of PDGFRβ. American journal of respiratory and critical care medicine. 2020;202(10):1445-57.
130. Zhang H, Liu Y, Yan L, Wang S, Zhang M, Ma C, et al. Long noncoding RNA Hoxaas3 contributes to hypoxia-induced pulmonary artery smooth muscle cell proliferation. Cardiovasc Res. 2019;115(3):647-57.
131. Yang L, Liang H, Shen L, Guan Z, Meng X. LncRNA Tug1 involves in the pulmonary vascular remodeling in mice with hypoxic pulmonary hypertension via the microRNA-374c-mediated Foxc1. Life sciences. 2019;237:116769.
132. Xing Y, Zheng X, Fu Y, Qi J, Li M, Ma M, et al. Long Noncoding RNA-Maternally Expressed Gene 3 Contributes to Hypoxic Pulmonary Hypertension. Molecular therapy : the journal of the American Society of Gene Therapy. 2019;27(12):2166-81.
133. Liu Y, Sun Z, Zhu J, Xiao B, Dong J, Li X. LncRNA-TCONS_00034812 in cell proliferation and apoptosis of pulmonary artery smooth muscle cells and its mechanism. Journal of cellular physiology. 2018;233(6):4801-14.
134. Zhu TT, Sun RL, Yin YL, Quan JP, Song P, Xu J, et al. Long noncoding RNA UCA1 promotes the proliferation of hypoxic human pulmonary artery smooth muscle cells. Pflugers Archiv : European journal of physiology. 2019;471(2):347-55.
135. Gaggar A, Weathington N. Bioactive extracellular matrix fragments in lung health and disease. The Journal of clinical investigation. 2016;126(9):3176-84.
136. Wells JM, Gaggar A, Blalock JE. MMP generated matrikines. Matrix biology : journal of the International Society for Matrix Biology. 2015;44-46:122-9.
137. Chen J, Guo J, Cui X, Dai Y, Tang Z, Qu J, et al. The Long Noncoding RNA LnRPT Is Regulated by PDGF-BB and Modulates the Proliferation of Pulmonary Artery Smooth Muscle Cells. American journal of respiratory cell and molecular biology. 2018;58(2):181-93.
138. Han B, Bu P, Meng X, Hou X. Microarray profiling of long non-coding RNAs associated with idiopathic pulmonary arterial hypertension. Experimental and therapeutic medicine. 2017;13(6):2657-66.
139. Stulnig G, Frisch MT, Crnkovic S, Stiegler P, Sereinigg M, Stacher E, et al. Docosahexaenoic acid (DHA)-induced heme oxygenase-1 attenuates cytotoxic effects of DHA in vascular smooth muscle cells. Atherosclerosis. 2013;230(2):406-13.
140. Veith C, Zakrzewicz D, Dahal BK, Bálint Z, Murmann K, Wygrecka M, et al. Hypoxia- or PDGF-BB-dependent paxillin tyrosine phosphorylation in pulmonary hypertension is reversed by HIF-1α depletion or imatinib treatment. Thrombosis and haemostasis. 2014;112(6):1288-303.
141. Jandl K, Thekkekara Puthenparampil H, Marsh LM, Hoffmann J, Wilhelm J, Veith C, et al. Long non-coding RNAs influence the transcriptome in pulmonary arterial hypertension: the role of PAXIP1-AS1. The Journal of pathology. 2019;247(3):357-70.
142. Schmittgen TD, Livak KJ. Analyzing real-time PCR data by the comparative C(T) method. Nature protocols. 2008;3(6):1101-8.
143. Schiller HB, Fernandez IE, Burgstaller G, Schaab C, Scheltema RA, Schwarzmayr T, et al. Time- and compartment-resolved proteome profiling of the extracellular niche in lung injury and repair. Molecular Systems Biology. 2015;11(7):819.
144. Calvo A, Yokoyama Y, Smith LE, Ali I, Shih S-C, Feldman AL, et al. Inhibition of the mammary carcinoma angiogenic switch in C3(1)/SV40 transgenic mice by a mutated form of human endostatin. International Journal of Cancer. 2002;101(3):224-34.
145. Lowry OH, Rosebrough NJ, Farr AL, Randall RJ. Protein measurement with the Folin phenol reagent. The Journal of biological chemistry. 1951;193(1):265-75.

146. Cox J, Mann M. MaxQuant enables high peptide identification rates, individualized p.p.b.-range mass accuracies and proteome-wide protein quantification. Nature biotechnology. 2008;26(12):1367-72.
147. Mi H, Muruganujan A, Ebert D, Huang X, Thomas PD. PANTHER version 14: more genomes, a new PANTHER GO-slim and improvements in enrichment analysis tools. Nucleic acids research. 2018;47(D1):D419-D26.
148. Eden E, Navon R, Steinfeld I, Lipson D, Yakhini Z. GOrilla: a tool for discovery and visualization of enriched GO terms in ranked gene lists. BMC Bioinformatics. 2009;10(1):48.
149. Kanehisa M, Goto S. KEGG: kyoto encyclopedia of genes and genomes. Nucleic acids research. 2000;28(1):27-30.
150. Gillespie M, Jassal B, Stephan R, Milacic M, Rothfels K, Senff-Ribeiro A, et al. The reactome pathway knowledgebase 2022. Nucleic acids research. 2021;50(D1):D687-D92.
151. Szklarczyk D, Gable AL, Lyon D, Junge A, Wyder S, Huerta-Cepas J, et al. STRING v11: protein-protein association networks with increased coverage, supporting functional discovery in genome-wide experimental datasets. Nucleic acids research. 2019;47(D1):D607-d13.
152. Chen EY, Tan CM, Kou Y, Duan Q, Wang Z, Meirelles GV, et al. Enrichr: interactive and collaborative HTML5 gene list enrichment analysis tool. BMC Bioinformatics. 2013;14:128.
153. Shannon P, Markiel A, Ozier O, Baliga NS, Wang JT, Ramage D, et al. Cytoscape: a software environment for integrated models of biomolecular interaction networks. Genome research. 2003;13(11):2498-504.
154. Chang TH, Huang HY, Hsu JB, Weng SL, Horng JT, Huang HD. An enhanced computational platform for investigating the roles of regulatory RNA and for identifying functional RNA motifs. BMC Bioinformatics. 2013;14 Suppl 2(Suppl 2):S4.
155. Kong L, Zhang Y, Ye ZQ, Liu XQ, Zhao SQ, Wei L, et al. CPC: assess the protein-coding potential of transcripts using sequence features and support vector machine. Nucleic acids research. 2007;35(Web Server issue):W345-9.
156. Wang L, Park HJ, Dasari S, Wang S, Kocher JP, Li W. CPAT: Coding-Potential Assessment Tool using an alignment-free logistic regression model. Nucleic acids research. 2013;41(6):e74.
157. Gruber AR, Lorenz R, Bernhart SH, Neuböck R, Hofacker IL. The Vienna RNA websuite. Nucleic acids research. 2008;36(Web Server issue):W70-4.
158. Altschul SF, Gish W, Miller W, Myers EW, Lipman DJ. Basic local alignment search tool. Journal of molecular biology. 1990;215(3):403-10.
159. Morgulis A, Coulouris G, Raytselis Y, Madden TL, Agarwala R, Schaffer AA. Database indexing for production MegaBLAST searches. Bioinformatics. 2008;24(16):1757-64.
160. Coordinators NR. Database resources of the National Center for Biotechnology Information. Nucleic acids research. 2016;44(D1):D7-19.
161. Kreft L, Soete A, Hulpiau P, Botzki A, Saeys Y, De Bleser P. ConTra v3: a tool to identify transcription factor binding sites across species, update 2017. Nucleic acids research. 2017;45(W1):W490-w4.
162. Ritchie ME, Phipson B, Wu D, Hu Y, Law CW, Shi W, et al. limma powers differential expression analyses for RNA-sequencing and microarray studies. Nucleic acids research. 2015;43(7):e47.
163. Gentleman RC, Carey VJ, Bates DM, Bolstad B, Dettling M, Dudoit S, et al. Bioconductor: open software development for computational biology and bioinformatics. Genome biology. 2004;5(10):R80.
164. Hoffmann J, Wilhelm J, Olschewski A, Kwapiszewska G. Microarray analysis in pulmonary hypertension. European Respiratory Journal. 2016;48(1):229-41.
165. Xia J, Gill EE, Hancock RE. NetworkAnalyst for statistical, visual and network-based meta-analysis of gene expression data. Nature protocols. 2015;10(6):823-44.
166. Eden E, Lipson D, Yogev S, Yakhini Z. Discovering Motifs in Ranked Lists of DNA Sequences. PLOS Computational Biology. 2007;3(3):e39.

167. Jandl K, Marsh LM, Hoffmann J, Mutgan AC, Baum O, Bloch W, et al. Basement Membrane Remodeling Controls Endothelial Function in Idiopathic Pulmonary Arterial Hypertension. American journal of respiratory cell and molecular biology. 2020;63(1):104-17.
168. Cheetham SW, Faulkner GJ, Dinger ME. Overcoming challenges and dogmas to understand the functions of pseudogenes. Nature Reviews Genetics. 2020;21(3):191-201.
169. Katayama S, Tomaru Y, Kasukawa T, Waki K, Nakanishi M, Nakamura M, et al. Antisense transcription in the mammalian transcriptome. Science (New York, NY). 2005;309(5740):1564-6.
170. Fan H, Liu T, Tian H, Zhang S. [Corrigendum] TUSC8 inhibits the development of osteosarcoma by sponging miR-197-3p and targeting EHD2. International journal of molecular medicine. 2021;47(4).
171. Cong M, Li J, Jing R, Li Z. Long non-coding RNA tumor suppressor candidate 7 functions as a tumor suppressor and inhibits proliferation in osteosarcoma. Tumour biology : the journal of the International Society for Oncodevelopmental Biology and Medicine. 2016;37(7):9441-50.
172. Weirick T, Militello G, Ponomareva Y, John D, Döring C, Dimmeler S, et al. Logic programming to infer complex RNA expression patterns from RNA-seq data. Briefings in bioinformatics. 2018;19(2):199-209.
173. Altschul SF, Madden TL, Schäffer AA, Zhang J, Zhang Z, Miller W, et al. Gapped BLAST and PSI-BLAST: a new generation of protein database search programs. Nucleic acids research. 1997;25(17):3389-402.
174. Akan P, Deloukas P. DNA sequence and structural properties as predictors of human and mouse promoters. Gene. 2008;410(1):165-76.
175. Mathews DH, Disney MD, Childs JL, Schroeder SJ, Zuker M, Turner DH. Incorporating chemical modification constraints into a dynamic programming algorithm for prediction of RNA secondary structure. Proceedings of the National Academy of Sciences of the United States of America. 2004;101(19):7287-92.
176. Meng S, Zhou H, Feng Z, Xu Z, Tang Y, Li P, et al. CircRNA: functions and properties of a novel potential biomarker for cancer. Mol Cancer. 2017;16(1):94-.
177. Glažar P, Papavasileiou P, Rajewsky N. circBase: a database for circular RNAs. RNA. 2014.
178. Muñoz IM, Rouse J. Control of histone methylation and genome stability by PTIP. EMBO reports. 2009;10(3):239-45.
179. Archer SL. Pyruvate Kinase and Warburg Metabolism in Pulmonary Arterial Hypertension. Circulation. 2017;136(25):2486-90.
180. López-Colomé AM, Lee-Rivera I, Benavides-Hidalgo R, López E. Paxillin: a crossroad in pathological cell migration. Journal of Hematology & Oncology. 2017;10(1):50.
181. Li L, Huang L, Chen G, Huang S, Liu C, Wang H, et al. [Pathologic markers for evaluation of reversibility in pulmonary hypertension related to congenital heart disease]. Zhonghua bing li xue za zhi = Chinese journal of pathology. 2016;45(1):31-6.
182. Barnes EA, Chen CH, Sedan O, Cornfield DN. Loss of smooth muscle cell hypoxia inducible factor-1α underlies increased vascular contractility in pulmonary hypertension. FASEB journal : official publication of the Federation of American Societies for Experimental Biology. 2017;31(2):650-62.
183. Xie L, Palmsten K, MacDonald B, Kieran MW, Potenta S, Vong S, et al. Basement Membrane Derived Fibulin-1 and Fibulin-5 Function as Angiogenesis Inhibitors and Suppress Tumor Growth. Experimental Biology and Medicine. 2008;233(2):155-62.
184. Guo G, Booms P, Halushka M, Dietz HC, Ney A, Stricker S, et al. Induction of macrophage chemotaxis by aortic extracts of the mgR Marfan mouse model and a GxxPG-containing fibrillin-1 fragment. Circulation. 2006;114(17):1855-62.
185. Titz B, Dietrich S, Sadowski T, Beck C, Petersen A, Sedlacek R. Activity of MMP-19 inhibits capillary-like formation due to processing of nidogen-1. Cellular and Molecular Life Sciences CMLS. 2004;61(14):1826-33.

186. Ramchandran R, Dhanabal M, Volk R, Waterman MJ, Segal M, Lu H, et al. Antiangiogenic activity of restin, NC10 domain of human collagen XV: comparison to endostatin. Biochemical and biophysical research communications. 1999;255(3):735-9.
187. Karagiannis ED, Popel AS. Identification of novel short peptides derived from the alpha 4, alpha 5, and alpha 6 fibrils of type IV collagen with anti-angiogenic properties. Biochemical and biophysical research communications. 2007;354(2):434-9.
188. Bossard C, Van den Berghe L, Laurell H, Castano C, Cerutti M, Prats AC, et al. Antiangiogenic properties of fibstatin, an extracellular FGF-2-binding polypeptide. Cancer research. 2004;64(20):7507-12.
189. Ambesi A, McKeown-Longo PJ. Anastellin, the angiostatic fibronectin peptide, is a selective inhibitor of lysophospholipid signaling. Molecular cancer research : MCR. 2009;7(2):255-65.
190. Joshi R, Goihberg E, Ren W, Pilichowska M, Mathew P. Proteolytic fragments of fibronectin function as matrikines driving the chemotactic affinity of prostate cancer cells to human bone marrow mesenchymal stromal cells via the α5β1 integrin. Cell adhesion & migration. 2017;11(4):305-15.
191. Ma Y, Wu T, Zhou H, He G, Li Y, Wang B, et al. Canstatin represses glioma growth by inhibiting formation of VM-like structures. Translational neuroscience. 2021;12(1):309-19.
192. Aikio M, Alahuhta I, Nurmenniemi S, Suojanen J, Palovuori R, Teppo S, et al. Arresten, a collagen-derived angiogenesis inhibitor, suppresses invasion of squamous cell carcinoma. PLoS One. 2012;7(12):e51044.
193. Xu XM, Chen Y, Chen J, Yang S, Gao F, Underhill CB, et al. A peptide with three hyaluronan binding motifs inhibits tumor growth and induces apoptosis. Cancer research. 2003;63(18):5685-90.
194. Adair-Kirk TL, Atkinson JJ, Broekelmann TJ, Doi M, Tryggvason K, Miner JH, et al. A site on laminin alpha 5, AQARSAASKVKVSMKF, induces inflammatory cell production of matrix metalloproteinase-9 and chemotaxis. Journal of immunology (Baltimore, Md : 1950). 2003;171(1):398-406.
195. Giannelli G, Antonaci S. Biological and clinical relevance of Laminin-5 in cancer. Clinical & Experimental Metastasis. 2000;18(6):439-43.
196. Lin HC, Chang JH, Jain S, Gabison EE, Kure T, Kato T, et al. Matrilysin cleavage of corneal collagen type XVIII NC1 domain and generation of a 28-kDa fragment. Investigative ophthalmology & visual science. 2001;42(11):2517-24.
197. Game BA, Xu M, Lopes-Virella MF, Huang Y. Regulation of MMP-1 expression in vascular endothelial cells by insulin sensitizing thiazolidinediones. Atherosclerosis. 2003;169(2):235-43.
198. Galiè N, Channick RN, Frantz RP, Grünig E, Jing ZC, Moiseeva O, et al. Risk stratification and medical therapy of pulmonary arterial hypertension. European Respiratory Journal. 2019;53(1):1801889.
199. Geraci MW, Moore M, Gesell T, Yeager ME, Alger L, Golpon H, et al. Gene Expression Patterns in the Lungs of Patients With Primary Pulmonary Hypertension. Circulation research. 2001;88(6):555-62.
200. Rajkumar R, Konishi K, Richards TJ, Ishizawar DC, Wiechert AC, Kaminski N, et al. Genomewide RNA expression profiling in lung identifies distinct signatures in idiopathic pulmonary arterial hypertension and secondary pulmonary hypertension. American Journal of Physiology-Heart and Circulatory Physiology. 2010;298(4):H1235-H48.
201. Costello CM, Howell K, Cahill E, McBryan J, Konigshoff M, Eickelberg O, et al. Lung-selective gene responses to alveolar hypoxia: potential role for the bone morphogenetic antagonist gremlin in pulmonary hypertension. American Journal of Physiology-Lung Cellular and Molecular Physiology. 2008;295(2):L272-L84.
202. Rhodes CJ, Im H, Cao A, Hennigs JK, Wang L, Sa S, et al. RNA Sequencing Analysis Detection of a Novel Pathway of Endothelial Dysfunction in Pulmonary Arterial Hypertension. American journal of respiratory and critical care medicine. 2015;192(3):356-66.

203. Yu J, Wilson J, Taylor L, Polgar P. DNA microarray and signal transduction analysis in pulmonary artery smooth muscle cells from heritable and idiopathic pulmonary arterial hypertension subjects. Journal of cellular biochemistry. 2015;116(3):386-97.
204. Gou D, Ramchandran R, Peng X, Yao L, Kang K, Sarkar J, et al. miR-210 has an antiapoptotic effect in pulmonary artery smooth muscle cells during hypoxia. American Journal of Physiology-Lung Cellular and Molecular Physiology. 2012;303(8):L682-L91.
205. Laumanns IP, Fink L, Wilhelm J, Wolff JC, Mitnacht-Kraus R, Graef-Hoechst S, et al. The noncanonical WNT pathway is operative in idiopathic pulmonary arterial hypertension. American journal of respiratory cell and molecular biology. 2009;40(6):683-91.
206. Barnes JW, Tian L, Heresi GA, Farver CF, Asosingh K, Comhair SAA, et al. O-linked β-N-acetylglucosamine transferase directs cell proliferation in idiopathic pulmonary arterial hypertension. Circulation. 2015;131(14):1260-8.
207. Song M, Finley SD. Mechanistic insight into activation of MAPK signaling by pro-angiogenic factors. BMC Systems Biology. 2018;12(1):145.
208. Siekmann AF, Lawson ND. Notch signalling and the regulation of angiogenesis. Cell adhesion & migration. 2007;1(2):104-6.
209. Boopathy GTK, Hong W. Role of Hippo Pathway-YAP/TAZ Signaling in Angiogenesis. Frontiers in cell and developmental biology. 2019;7:49.
210. Valkovic AL, Bathgate RA, Samuel CS, Kocan M. Understanding relaxin signalling at the cellular level. Molecular and cellular endocrinology. 2019;487:24-33.
211. Yung L-M, Nikolic I, Cavallo J, Chain D, Dwyer SC, Southwood MR, et al. Abstract 20479: Relaxin Inhibits TGFβ-induced Pulmonary Artery Smooth Muscle Cell Fibrogenic Differentiation Via Modulation Of SMAD-ERK Signaling. Circulation. 2016;134(suppl_1):A20479-A.
212. Stearman RS, Bui QM, Speyer G, Handen A, Cornelius AR, Graham BB, et al. Systems Analysis of the Human Pulmonary Arterial Hypertension Lung Transcriptome. American journal of respiratory cell and molecular biology. 2019;60(6):637-49.
213. Saygin D, Tabib T, Bittar HET, Valenzi E, Sembrat J, Chan SY, et al. Transcriptional profiling of lung cell populations in idiopathic pulmonary arterial hypertension. Pulmonary circulation. 2020;10(1):???
214. Chang Y-C, Hsu B-G, Liou H-H, Lee C-J, Wang J-H. Serum levels of sclerostin as a potential biomarker in central arterial stiffness among hypertensive patients. BMC Cardiovasc Disord. 2018;18(1):214-.
215. Hao S, Jiang P, Xie L, Xiang G, Liu Z, Hu W, et al. Essential Genes and MiRNA-mRNA Network Contributing to the Pathogenesis of Idiopathic Pulmonary Arterial Hypertension. Frontiers in cardiovascular medicine. 2021;8:627873.
216. Bumgarner R. Overview of DNA microarrays: types, applications, and their future. Current protocols in molecular biology. 2013;Chapter 22:Unit 22.1.
217. Lepetit H, Eddahibi S, Fadel E, Frisdal E, Munaut C, Noel A, et al. Smooth muscle cell matrix metalloproteinases in idiopathic pulmonary arterial hypertension. European Respiratory Journal. 2005;25(5):834-42.
218. Calvier L, Xian X, Lee RG, Sacharidou A, Mineo C, Shaul PW, et al. Reelin Depletion Protects Against Atherosclerosis by Decreasing Vascular Adhesion of Leukocytes. Arteriosclerosis, Thrombosis, and Vascular Biology. 2021;41(4):1309-18.
219. Capuano A, Pivetta E, Baldissera F, Bosisio G, Wassermann B, Bucciotti F, et al. Integrin binding site within the gC1q domain orchestrates EMILIN-1-induced lymphangiogenesis. Matrix biology : journal of the International Society for Matrix Biology. 2019;81:34-49.
220. Rabajdova M, Urban P, Spakova I, Saksun L, Dudic R, Ostro A, et al. The crucial role of emilin 1 gene expression during progression of tumor growth. Journal of cancer research and clinical oncology. 2016;142(11):2397-402.

221. Schiavinato A, Keene DR, Wohl AP, Corallo D, Colombatti A, Wagener R, et al. Targeting of EMILIN-1 and EMILIN-2 to Fibrillin Microfibrils Facilitates their Incorporation into the Extracellular Matrix. The Journal of investigative dermatology. 2016;136(6):1150-60.
222. Zimmer J, Takahashi T, Hofmann AD, Puri P. Downregulated Elastin Microfibril Interfacer 1 Expression in the Pulmonary Vasculature of Experimental Congenital Diaphragmatic Hernia. European journal of pediatric surgery : official journal of Austrian Association of Pediatric Surgery [et al] = Zeitschrift fur Kinderchirurgie. 2018;28(1):115-9.
223. Oh S, Jang AY, Chae S, Choi S, Moon J, Kim M, et al. Comparative analysis on the anti-inflammatory/immune effect of mesenchymal stem cell therapy for the treatment of pulmonary arterial hypertension. Scientific reports. 2021;11(1):2012.
224. Yurchenco PD, McKee KK. Linker Protein Repair of LAMA2 Dystrophic Neuromuscular Basement Membranes. Frontiers in Molecular Neuroscience. 2019;12.
225. Jones LK, Lam R, McKee KK, Aleksandrova M, Dowling J, Alexander SI, et al. A mutation affecting laminin alpha 5 polymerisation gives rise to a syndromic developmental disorder. Development (Cambridge, England). 2020;147(21).
226. Meyrick B, Clarke SW, Symons C, Woodgate DJ, Reid L. Primary pulmonary hypertension a case report including electronmicroscopic study. British Journal of Diseases of the Chest. 1974;68:11-20.
227. Franks A, Airoldi E, Slavov N. Post-transcriptional regulation across human tissues. PLOS Computational Biology. 2017;13(5):e1005535.
228. Koussounadis A, Langdon SP, Um IH, Harrison DJ, Smith VA. Relationship between differentially expressed mRNA and mRNA-protein correlations in a xenograft model system. Scientific reports. 2015;5(1):10775.
229. Yu M, Wang XX, Zhang FR, Shang YP, Du YX, Chen HJ, et al. Proteomic analysis of the serum in patients with idiopathic pulmonary arterial hypertension. Journal of Zhejiang University Science B. 2007;8(4):221-7.
230. Abdul-Salam VB, Paul GA, Ali JO, Gibbs SR, Rahman D, Taylor GW, et al. Identification of plasma protein biomarkers associated with idiopathic pulmonary arterial hypertension. Proteomics. 2006;6(7):2286-94.
231. Huang L, Li L, Hu E, Chen G, Meng X, Xiong C, et al. Potential biomarkers and targets in reversibility of pulmonary arterial hypertension secondary to congenital heart disease: an explorative study. Pulmonary circulation. 2018;8(2):2045893218755987.
232. Rice LM, Mantero JC, Stratton EA, Warburton R, Roberts K, Hill N, et al. Serum biomarker for diagnostic evaluation of pulmonary arterial hypertension in systemic sclerosis. Arthritis research & therapy. 2018;20(1):185.
233. Sandqvist A, Schneede J, Kylhammar D, Henrohn D, Lundgren J, Hedeland M, et al. Plasma L-arginine levels distinguish pulmonary arterial hypertension from left ventricular systolic dysfunction. Heart and vessels. 2018;33(3):255-63.
234. Zhang J, Zhang Y, Li N, Liu Z, Xiong C, Ni X, et al. Potential diagnostic biomarkers in serum of idiopathic pulmonary arterial hypertension. Respiratory medicine. 2009;103(12):1801-6.
235. Wu D, Talbot CC, Jr., Liu Q, Jing ZC, Damico RL, Tuder R, et al. Identifying microRNAs targeting Wnt/β-catenin pathway in end-stage idiopathic pulmonary arterial hypertension. Journal of molecular medicine (Berlin, Germany). 2016;94(8):875-85.
236. Sarrion I, Milian L, Juan G, Ramon M, Furest I, Carda C, et al. Role of circulating miRNAs as biomarkers in idiopathic pulmonary arterial hypertension: possible relevance of miR-23a. Oxidative medicine and cellular longevity. 2015;2015:792846.
237. Rhodes CJ, Otero-Núñez P, Wharton J, Swietlik EM, Kariotis S, Harbaum L, et al. Whole-Blood RNA Profiles Associated with Pulmonary Arterial Hypertension and Clinical Outcome. American journal of respiratory and critical care medicine. 2020;202(4):586-94.
238. Han Y, Ali MK, Dua K, Spiekerkoetter E, Mao Y. Role of Long Non-Coding RNAs in Pulmonary Arterial Hypertension. Cells. 2021;10(8):1892.

239. Michalik KM, You X, Manavski Y, Doddaballapur A, Zörnig M, Braun T, et al. Long noncoding RNA MALAT1 regulates endothelial cell function and vessel growth. Circulation research. 2014;114(9):1389-97.
240. Han B, Bu P, Meng X, Hou X. Microarray profiling of long non-coding RNAs associated with idiopathic pulmonary arterial hypertension. Experimental and therapeutic medicine. 2017;13.
241. Wang S, Cao W, Gao S, Nie X, Zheng X, Xing Y, et al. TUG1 Regulates Pulmonary Arterial Smooth Muscle Cell Proliferation in Pulmonary Arterial Hypertension. The Canadian journal of cardiology. 2019;35(11):1534-45.
242. He M, Shen J, Zhang C, Chen Y, Wang W, Tao K. Long-Chain Non-Coding RNA Metastasis-Related Lung Adenocarcinoma Transcript 1 (MALAT1) Promotes the Proliferation and Migration of Human Pulmonary Artery Smooth Muscle Cells (hPASMCs) by Regulating the MicroRNA-503 (miR-503)/Toll-Like Receptor 4 (TLR4) Signal Axis. Medical science monitor : international medical journal of experimental and clinical research. 2020;26:e923123.
243. Arun G, Aggarwal D, Spector DL. MALAT1 Long Non-Coding RNA: Functional Implications. Noncoding RNA. 2020;6(2):22.
244. Johnsson P, Lipovich L, Grandér D, Morris KV. Evolutionary conservation of long non-coding RNAs; sequence, structure, function. Biochimica et biophysica acta. 2014;1840(3):1063-71.
245. Carlevaro-Fita J, Johnson R. Global Positioning System: Understanding Long Noncoding RNAs through Subcellular Localization. Molecular cell. 2019;73(5):869-83.
246. Smyth RP, Negroni M, Lever AM, Mak J, Kenyon JC. RNA Structure-A Neglected Puppet Master for the Evolution of Virus and Host Immunity. Frontiers in immunology. 2018;9:2097.
247. Li J, Zhang J, Wang J, Li W, Wang W. Structure Prediction of RNA Loops with a Probabilistic Approach. PLOS Computational Biology. 2016;12(8):e1005032.
248. Kim EZ, Wespiser AR, Caffrey DR. The domain structure and distribution of Alu elements in long noncoding RNAs and mRNAs. Rna. 2016;22(2):254-64.
249. Ricci EP, Kucukural A, Cenik C, Mercier BC, Singh G, Heyer EE, et al. Staufen1 senses overall transcript secondary structure to regulate translation. Nat Struct Mol Biol. 2014;21(1):26-35.
250. Rashid F, Shah A, Shan G. Long Non-coding RNAs in the Cytoplasm. Genomics Proteomics Bioinformatics. 2016;14(2):73-80.
251. Otsuka H, Fukao A, Funakami Y, Duncan KE, Fujiwara T. Emerging Evidence of Translational Control by AU-Rich Element-Binding Proteins. Front Genet. 2019;10:332.
252. Chen J, Liu L, Wei G, Wu W, Luo H, Yuan J, et al. The long noncoding RNA ASNR regulates degradation of Bcl-2 mRNA through its interaction with AUF1. Scientific reports. 2016;6(1):32189.
253. Pullamsetti SS, Perros F, Chelladurai P, Yuan J, Stenmark K. Transcription factors, transcriptional coregulators, and epigenetic modulation in the control of pulmonary vascular cell phenotype: therapeutic implications for pulmonary hypertension (2015 Grover Conference series). Pulmonary circulation. 2016;6(4):448-64.
254. Leisegang MS, Fork C, Josipovic I, Richter FM, Preussner J, Hu J, et al. Long Noncoding RNA MANTIS Facilitates Endothelial Angiogenic Function. Circulation. 2017;136(1):65-79.
255. Göhler T, Munoz IM, Rouse J, Blow JJ. PTIP/Swift is required for efficient PCNA ubiquitination in response to DNA damage. DNA repair. 2008;7(5):775-87.
256. Cho EA, Prindle MJ, Dressler GR. BRCT domain-containing protein PTIP is essential for progression through mitosis. Molecular and cellular biology. 2003;23(5):1666-73.
257. Wang R, Xu J, Wu J, Gao S, Wang Z. Angiotensin-converting enzyme 2 alleviates pulmonary artery hypertension through inhibition of focal adhesion kinase expression. Experimental and therapeutic medicine. 2021;22(4):1165.

258. Dixelius J, Cross M, Matsumoto T, Sasaki T, Timpl R, Claesson-Welsh L. Endostatin regulates endothelial cell adhesion and cytoskeletal organization. Cancer research. 2002;62(7):1944-7.
259. Schlosser K, Hanson J, Villeneuve PJ, Dimitroulakos J, McIntyre L, Pilote L, et al. Assessment of Circulating LncRNAs Under Physiologic and Pathologic Conditions in Humans Reveals Potential Limitations as Biomarkers. Scientific reports. 2016;6:36596.
260. Zhang Y, Chen Y, Yao H, Lie Z, Chen G, Tan H, et al. Elevated serum circ_0068481 levels as a potential diagnostic and prognostic indicator in idiopathic pulmonary arterial hypertension. Pulmonary circulation. 2019;9(4):2045894019888416.
261. Arita T, Ichikawa D, Konishi H, Komatsu S, Shiozaki A, Shoda K, et al. Circulating long non-coding RNAs in plasma of patients with gastric cancer. Anticancer research. 2013;33(8):3185-93.
262. Moonmuang S, Chaiyawat P, Jantrapirom S, Pruksakorn D, Lo Piccolo L. Circulating Long Non-Coding RNAs as Novel Potential Biomarkers for Osteogenic Sarcoma. Cancers. 2021;13(16):4214.
263. Huo Y, Li Q, Wang X, Jiao X, Zheng J, Li Z, et al. MALAT1 predicts poor survival in osteosarcoma patients and promotes cell metastasis through associating with EZH2. Oncotarget. 2017;8(29):46993-7006.
264. Xu H, Zhao G, Zhang Y, Jiang H, Wang W, Zhao D, et al. Long non-coding RNA PAXIP1-AS1 facilitates cell invasion and angiogenesis of glioma by recruiting transcription factor ETS1 to upregulate KIF14 expression. Journal of Experimental & Clinical Cancer Research. 2019;38(1):486.
265. Nogueira-Ferreira R, Vitorino R, Ferreira R, Henriques-Coelho T. Exploring the monocrotaline animal model for the study of pulmonary arterial hypertension: A network approach. Pulmonary Pharmacology & Therapeutics. 2015;35:8-16.
266. Fujiwara S. Humanized mice: A brief overview on their diverse applications in biomedical research. Journal of cellular physiology. 2018;233(4):2889-901.